Stephen, R.A., Kasahara, J., Acton, G.D., et al., 2003
Proceedings of the Ocean Drilling Program, Initial Reports Volume 200

1. Leg 200 Summary[1]

Shipboard Scientific Party[2]

ABSTRACT

During Leg 200, we completed drilling operations for two distinct projects: (1) the Hawaii-2 Observatory (H2O), where we established a cased reentry borehole at Site 1224 and sampled the upper oceanic crust; and (2) the Nuuanu Landslide, where we recovered deposits at Site 1223 that were derived from the Hawaiian Islands. The primary focus of the cruise was drilling at H2O, with Nuuanu Landslide drilling only being added to the Ocean Drilling Program (ODP) operations schedule ~3 months prior to the cruise and consuming only 2 days of operations. Below, we describe each project separately, focusing first on the H2O results and then the Nuuanu Landslide results.

The long-term H2O site satisfies three scientific objectives of crustal drilling: (1) it is located in one of the high-priority regions for the Ocean Seismic Network; (2) its proximity to the Hawaii-2 cable and the H2O junction box makes it a unique site for real-time, continuous monitoring of geophysical, microbiological, and geochemical experiments in the crust; and (3) it is on fast-spreading Pacific crust (71 mm/yr half-rate), which represents one end-member for models of crustal generation and evolution and crust/mantle interaction. The H2O junction box is in the eastern Pacific at 27°52.916′N, 141°59.504′W at a water depth of 4979 m, roughly halfway between California and Hawaii. The primary goal of the leg was to drill a suitable hole for a borehole seismometer that will be installed later. This was accomplished in Hole 1224D, where we installed a reentry cone and cemented casing 30 m into basaltic basement 1.48 km northeast of the H2O junction box. Above basement there was 28 m of soft, red clay. The cased basement interval, in which the instrument will be installed, consisted of massive basalt flows that had been cemented by calcite. We also drilled a second single-bit hole, which was cored and logged, within 20 m of the first to a depth of 145 m into basement. The second hole was left with a free-

[1]Examples of how to reference the whole or part of this volume.
[2]Shipboard Scientific Party addresses.

Ms 200IR-101

fall funnel so that it also could be reentered using the wireline reentry technology to carry out other borehole experiments at the site. In addition to a suite of shipboard physical and chemical analyses that can be used to characterize the crust surrounding the observatory, we also conducted microbiological analyses of the recovered sediments and basalts. As a general trend, bacterial population numbers decreased with increasing depth, although the amount of metabolically active bacteria remained remarkably high at 41%–62% of the total cell counts. The successful cultivation of lithotrophic oxidizing bacteria and the microscopic indication of further microbial structures within the basaltic rock confirm the presence and even activity of microbial life not only in deep marine sediments, but also in the Paleogene oceanic crust from the North Pacific.

During Leg 200, we also cored the Nuuanu Landslide site on the Hawaiian Arch, ~300 km northeast of Honolulu. The upper 100 m of sediment at this site was thought to contain a record of the Nuuanu Landslide, a catastrophic event or series of events that removed ~40% (3000 to 4000 km^3) of the Koolau Volcano on the island of Oahu. We recovered several lithologic units that were transported to the site by a number of distinct depositional events, some of which may have been initiated by landslides. The origin of the deposits, as indicated by petrographic inspection and geochemistry, is the Hawaiian Islands. Two pyroclastic events, similar to the 1980 Mount Saint Helens' eruption but an order of magnitude larger, occurred on Koolau at ~2 Ma. These events may correlate with the collapse of the flank of the volcano and the formation of the Nuuanu debris field. The turbidites and pyroclastic material are similar in age to the Nuuanu Landslide (1.8–2.4 Ma) and are >38 m thick at Site 1223, >300 km from Oahu. We did not core to the bottom of the postulated Nuuanu-related sequence. Thus the Nuuanu-related deposits may be thicker, and additional landslide events may have occurred.

HAWAII-2 OBSERVATORY

The use of submarine cables provides a tremendous opportunity for real-time data acquisition from permanent broadband seismometers on the seafloor. Programs to use retired submarine cables for this purpose have been initiated in the United States (e.g., Butler et al., 1995a) and Japan (e.g., Kasahara et al., 1998).

The Hawaii-2 submarine cable system is a retired American Telephone and Telegraph (AT&T) telephone cable system that originally connected San Luis Obispo, California, and Makaha, on Oahu, Hawaii (Fig. **F1**). The cable system was originally laid in 1964. In 1998, Incorporated Research Institutions for Seismology (IRIS) and scientists from the University of Hawaii and Woods Hole Oceanographic Institution installed a long-term seafloor observatory about halfway along the cable (~140°W, 28°N). The cable was cut and terminated with a seafloor junction box (Fig. **F2**). The location of the junction box on the seafloor defines the location of the Hawaii-2 Observatory (H2O), which was named after the original AT&T cable.

The junction box has eight underwater make-break connections. About 500 W of power is available from the junction box, and there is ample capacity for two-way, real-time communications with seafloor instruments. Data channels from the seafloor can be monitored continuously via the Oahu end of the cable to any laboratory in the world.

F1. Locations of Sites 1223 and 1224 (H2O), p. 35.

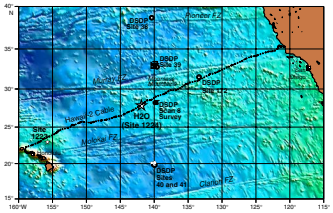

F2. Artist's conception of the H2O, p. 36.

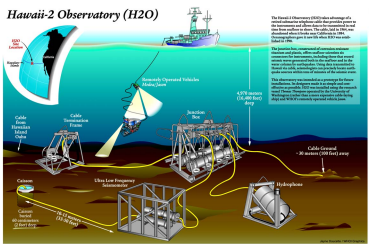

The California end of the cable cannot be used because it was cut and removed from the continental shelf.

There is a shallow buried broadband seismometer operating at the site that monitored noise from the *JOIDES Resolution* during our cruise. The sensor consists of a modified Guralp CMG-3T broadband seismometer and a conventional 4.5-Hz three-component geophone, and it is buried in a caisson ~1 m below the seafloor (mbsf) (Duennebier et al., 2000, 2002). This sensor has been transmitting seismic data to shore continuously and in real time for >2 yr. The seismic data are forwarded to the IRIS Data Management Center in Seattle and are included in the Global Seismic Network database for use in global and regional earthquake studies. Other seafloor observatories, such as a geomagnetic observatory (Chave et al., 1995), a hydrothermal observatory (Davis et al., 1992; Foucher et al., 1995), or a broadband borehole seismic observatory (Orcutt and Stephen, 1993), can be installed at the site as funding becomes available.

Within the Ocean Drilling Program (ODP) and marine geology and geophysics communities, there has been considerable interest in the past few years in long-term seafloor observatories that include a borehole installation. Prototype long-term borehole and seafloor experiments almost exclusively use battery power and internal recording. The data are only available after a recovery cruise. One exception to this is the Columbia-Point Arena ocean-bottom seismic station (OBSS), which was deployed on an offshore cable by Sutton and others in the 1960s (Sutton et al., 1965; Sutton and Barstow, 1990). For the foreseeable future, the most practical method for acquiring real-time, continuous data from the seafloor will be over cables (Chave et al., 1990). The H2O project provides this opportunity.

Geological Setting

The Hawaii-2 cable runs south of the Moonless Mountains between the Murray and Molokai Fracture Zones (Fig. **F1**) (Mammerickx, 1989). Between 140°and 143°W, water depths along the cable track are typical for the deep ocean (4250–5000 m); the crustal age varies from 45 to 50 Ma (Eocene); and the sediment thickness to within the available resolution is ~100 m or less. Prior to the cable survey cruise in August 1997 (Stephen et al., 1997), sediment thickness was not well resolved along the track (Winterer, 1989).

Tectonically, the cable runs across the "disturbed zone" south of the Murray Fracture Zone, between magnetic isochrons 13 and 19 (Atwater, 1989; Atwater and Severinghaus, 1989). In the disturbed zone, substantial pieces of the Farallon plate were captured by the Pacific plate in three discrete ridge jumps and several propagating rifts. To avoid this tectonically complicated region and to be well away from the fracture zone south of the disturbed zone, the H2O was situated west of isochron 20 (45 Ma) at ~140°W. The crust west of 140°W was formed between the Pacific and Farallon plates under "normal" spreading conditions at a "fast" half-rate of ~71 mm/yr (Atwater, 1989; Cande and Kent, 1992). At the time this crust was formed, the Farallon plate had not split into the Cocos and Nazca plates, and the ridge that formed this crust was the same as the present-day East Pacific Rise.

Between 140° and 143°W, the Hawaii-2 cable lies in the pelagic clay province of the North Pacific (Leinen, 1989). The sediments in this part of the Pacific are eolian in origin, consisting primarily of dust blown

eastward from the arid regions of central Asia. This region of the Pacific is below the calcite compensation depth (~3500 m), and little or no biogenic calcite is thought to reach the seafloor (Leinen, 1989). Siliceous biogenic material is rapidly dissolved by the silica-poor bottom waters. At the seafloor, the sediments are unfossiliferous red clays.

The H2O site lies in a smooth abyssal plain environment. The drill site, identified as Site H2O-5 during planning and now identified as ODP Site 1224, is on the same crustal block as the H2O junction box (Table T1; Figs. F3, F4).

T1. Operations summary, p. 66.

F3. Location of the H2O junction box, p. 37.

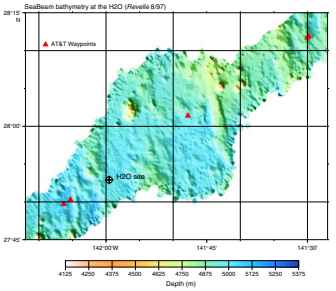

F4. A 3.5-kHz echo sounder record, p. 38.

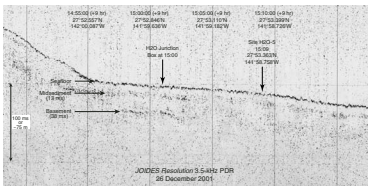

Scientific Objectives

Drilling at the H2O site was proposed to accomplish two main objectives:

1. Drill and case a reentry hole into basement near the existing Hawaii-2 cable and the H2O junction box in order to establish a long-term borehole geophysical observatory for continuous real-time seismic monitoring, as well as other geophysical experiments.
2. Sample a section of normal, fast-spreading ocean crust for use in constraining geochemical and hydrothermal models of crustal evolution.

Ocean Seismic Network

Establishing a borehole seismometer in the H2O area is valuable for addressing both teleseismic (whole Earth) and regional seismic studies. For uniform coverage of seismic stations on the surface of the planet, which is necessary for whole-Earth tomographic studies, seafloor seismic observatories are required. This site, where there is no land within a 1700-km radius, is one of three high-priority prototype observatories for the Ocean Seismic Network (OSN) (Butler, 1995a, 1995b; Purdy, 1995). Global seismic tomography (GST) provides three-dimensional images of the lateral heterogeneity in the mantle and is essential in addressing fundamental problems in subdisciplines of geodynamics such as mantle convection, mineral physics, long-wavelength gravimetry, geochemistry of ridge systems, geomagnetism, and geodesy. Specific problems include the characteristic spectrum of lateral heterogeneity as a function of depth, the anisotropy of the inner core, the structure of the core/mantle boundary, the role of oceanic plates and plumes in deep mantle circulation, and the source rupture processes of Southern Hemisphere earthquakes, which are among the world's largest (Forsyth et al., 1995).

The culturally important earthquakes in California are only observed at regional distances on land stations in North America, which restrict the azimuthal information to an arc spanning ~180°. To observe California earthquakes at regional distances to the west requires seafloor stations. Regional observations are used in constraining earthquake source mechanisms. Since the H2O data will be available in real time, data could be incorporated into focal mechanism determinations within minutes of California earthquake events. Other problems that can be addressed with regional data from Californian and Hawaiian earthquakes are the structure of the 410-, 525-, and 670-km discontinuities in the northeastern Pacific and the variability of elastic and anelas-

tic structure in the Pacific lithosphere from P_o and S_o (Butler 1995a, 1995b).

In 1998 at the OSN pilot experiment site established in seafloor west of Hawaii, we deployed seafloor, buried, and borehole broadband seismometers to compare the performance of three different styles of installation. Figures F5 and F6 summarize for vertical and horizontal component data, respectively, the improvement that we expect to see in ambient seismic noise on placing a sensor in basement rather than on or in the sediments. Above the microseism peak at 0.3 Hz, the seafloor, buried, and borehole spectra at the OSN-1 site show the borehole to be 10 dB quieter on vertical components and 30 dB quieter on horizontal components (Collins et al., 2001). Shear wave resonances (or Scholte modes) are the physical mechanism responsible for the higher noise levels in or on the sediment. The resonance peaks are particularly distinct and strong at the H2O site. Note the 15-dB peak on the vertical component and the 35-dB peak on the horizontal components near 1 Hz on the H2O spectra. By placing a borehole seismometer in basement at the H2O site, we expect to eliminate these high ambient noise levels.

F5. Vertical component spectra, p. 39.

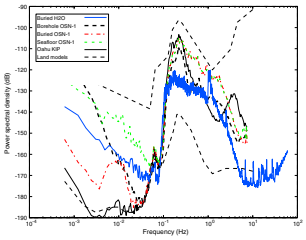

F6. Horizontal component spectra, p. 40.

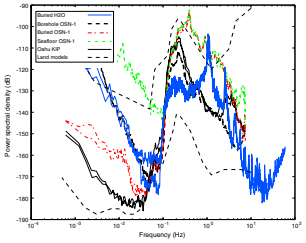

Basement Drilling on the Pacific Plate

In >30 yr of deep ocean drilling prior to ODP Leg 200 at more than 1200 sites worldwide, there have been only 13 holes with >10 m penetration into "normal" igneous Pacific plate: only one hole during ODP, only one hole with >100 m penetration, and no holes in crust with ages between 29 and 72 Ma. Table T2 summarizes the boreholes drilled on "normal" crust on the Pacific plate that have >10 m of basement penetration and crustal ages <100 Ma. Holes in seamounts, plateaus, aseismic ridges, and fracture zones were not included. Holes with crustal ages >100 Ma are not included because they would be affected by the mid-Cretaceous superplume (Pringle et al., 1993).

Besides the general sparsity of sampling of oceanic crust, there are no boreholes off-axis in "very fast" spreading crust. Although fast-spreading ridges represent only ~20% of the global ridge system, they produce more than one-half of the ocean crust on the surface of the planet, almost all of it along the East Pacific Rise. Most ocean crust currently being recycled back into the mantle at subduction zones was produced at a fast-spreading ridge. If we wish to understand the Wilson cycle in its most typical and geodynamically significant form, we need to examine ocean crust produced at fast-spreading ridges. We have also known for >40 yr that crust generated by fast spreading is both simple and uniform, certainly so in terms of seismic structure (Raitt, 1963; Menard, 1964). Successful deep drilling of such crust at any single location is thus likely to provide fundamental information that can be extrapolated to a significant fraction of the Earth's surface. Seafloor spreading that generated the ~45 Ma crust at the H2O was fast, with the full rate averaging 142 mm/yr. Thus, one objective of Leg 200 was to provide a reference station in "normal" fast-spreading ocean crust for use in constraining geochemical and hydrothermal models of crustal evolution.

T2. Summary of holes drilled, p. 67.

Operations

A synopsis of the Leg 200 operations is given in Table T3. A summary of the time spent on various activities is given in Figure F7, and the operations summary is given in Table T1. The coring summary for Site

T3. Time distribution, p. 68.

F7. Operations time distribution, p. 41.

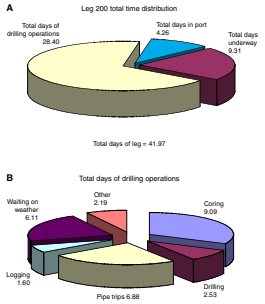

1224 is given in Table T4. We departed Site 1223 at 0130 hr on 23 December 2001 and arrived in the vicinity of the H2O junction box (27°52.916′N, 141°59.504′W) at 0000 hr on 26 December to begin a seismic and 3.5-kHz echo sounder survey. All times are reported in ship local time, which is Universal Time Coordinated (UTC) – 9 hr at Site 1224. The 766-nmi voyage took 2.9 days at an average speed of 10.9 kt.

Following completion of the surveying at 0745 hr on 26 December, the *JOIDES Resolution* returned and positioned on proposed Site H2O-5 (Fig. F8) with Global Positioning System (GPS) navigation at 0845 hr on 26 December. Operations were suspended while waiting on weather (WOW) because of heave, pitch, roll, and wind up to 7.7 m, 5.2°, 4.5°, and 29 kt, respectively. A total of 13.25 hr of WOW time occurred before drilling operations could proceed.

Prior to conducting drilling operations, the vibration isolated television (VIT) camera was launched to conduct a camera survey of the site for debris, while also conducting a survey with an echo sounder attached to the VIT frame to further delineate subsurface layers. The survey covered a 30 m × 30 m area, took 2.0 hr, and showed the site was flat, undisturbed, and free of debris and cables.

T4. Coring summary, Site 1224, p. 69.

F8. Location of H2O and proposed drilling sites, p. 42.

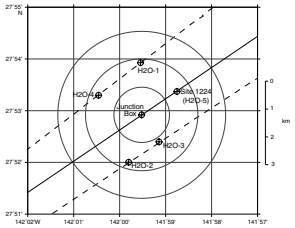

First Jet-In Test

Drilling operations began when seafloor was tagged at 4966.1 meters below sea level (mbsl), or 4977 meters below rig floor (mbrf), at 1525 hr on 27 December. The jet-in test was performed to confirm a refusal depth for jetting in the reentry cone with 20-in casing. At 12 to 13 mbsf a hard layer was encountered, although the test was suspect as the ship was experiencing 4- to 5-m heave at the time of the test. Following the test, we were again forced to WOW, this time for 13.75 hr.

Hole 1224A

Hole 1224A was spudded at 1455 hr on 28 December at 4977 mbrf. Core 200-1224A-1X was advanced 6 m downhole with no recovery; hence, we could not establish a precise mudline (Table T4). On Core 200-1224A-4X, drilling progress was slow when we got to hard rock, which at the time was thought to be chert or basaltic basement. Recovery of 1.24 m of red clay and pieces of basalt confirmed that we had penetrated basement near the bottom of the 5.5-m interval cored or at ~28 mbsf. We attempted one more extended core barrel (XCB) core (200-1224A-5X), before switching to the motor-driven core barrel (MDCB) for one last short core. We pulled out of the hole and cleared the seafloor at 0530 hr on 29 December, ending Hole 1224A.

Overall we cored 32.2 m in Hole 1224A and recovered 1.67 m of core (5.19% recovery), with 32 m cored and 1.45 m recovered (4.53% recovery) with the XCB, and 0.2 m cored and 0.22 m recovered (110% recovery) with the MDCB (Table T4).

Hole 1224B

Hole 1224B was spudded with the advanced piston corer (APC) at 0650 hr on 29 December, but only 0.2 m of core was recovered. The primary goal of APC coring was to establish the mudline; therefore, we offset to spud Hole 1224C. Hole 1224B officially ended at 0745 hr on 29 December after we pulled the bit up to clear the seafloor.

Hole 1224C

The bit was positioned at 4964.1 mbsl (4975 mbrf), and Hole 1224C was spudded with the APC at 0820 hr on 29 December. We recovered 6.53 m of core and established the mudline at 4967.1 mbsl (4978.0 mbrf). Having successfully determined the mudline, the bit was pulled clear of the seafloor at 0915 hr on 29 December, marking the end of Hole 1224C.

Second Jet-In Test

Operations were delayed by bad weather, which included maximum heave, pitch, and roll of 6.3 m, 2.4°, and 8.1°, respectively, with winds up to 44 kt. Total time WOW was 16.0 hr, with operations beginning again at 0115 hr on 30 December.

A second jet-in test was deemed necessary to confirm the depth of penetration for the 20-in surface casing, which would be run with the reentry cone. A wash barrel was dropped, and the bottom-hole assembly (BHA) was jetted in to 4996.1 mbsl (5007 mbrf), ~29 mbsf, with no obstructions encountered, unlike the first jet-in test. The drill string was pulled out of the hole, with the bit clearing the rotary table at 1430 hr on 30 December.

Hole 1224D

The reentry cone was positioned over the moonpool doors, and the casing string was partially assembled at 1830 hr on 30 December 2001. Poor weather conditions and the associated large heave, roll, and pitch forced us to delay operations until 1715 hr on 1 January 2002, a loss of 46.75 hr.

With weather conditions improving, the reentry cone and ~25 m of 20-in casing were assembled and lowered through the moonpool at 2335 hr on 1 January. Hole 1224D was spudded at 1220 hr on 2 January. It took only 24 min to jet the 20-in casing string down to 5003.47 mbrf (25.47 mbsf) and set the reentry cone. VIT observation of the reentry cone confirmed that it was in a satisfactory position. The bit cleared the seafloor at 1315 hr on 2 January, and the pipe was tripped back to the rig floor, with the jet-in BHA and bit clearing the rotary table at 0200 hr on 3 January.

Hole 1224D was reentered with an RCB bit at 1837 hr on 3 January, with coring beginning at 25.5 mbsf. Coring progressed down to 59 mbsf, with several delays caused by the poor weather conditions, adding up to another 26.0 hr of WOW. The marine forecast was for continued poor weather for our operating area, with very strong low-pressure systems to the west and north and large swells. It was therefore decided to prepare to take advantage of any weather window by tripping the drill string and changing to the 14¾-in bit and BHA. This would allow us to open the cored hole when a more appropriate weather window was available and be in position to run 10¾-in casing. At 0045 hr on 7 January we started to trip the pipe, with the bit clearing the rotary at 1100 hr on 7 January.

Overall we cored 33.5 m in Hole 1224D and recovered 15.65 m of core (46.72% recovery) with the RCB coring system (Table **T4**).

Reaming the Hole

After tripping the pipe with the 14¾-in bit to 4790 mbrf at 2345 hr on 7 January, operations were again put on hold while WOW for 19.0 hr. Operations resumed at 1845 hr on 8 January after Hole 1224D was reentered.

We reamed the hole to 64.7 mbsf before drilling difficulties halted penetration. This was sufficiently close to the planned drilling depth of 67 mbsf, so we ceased drilling at 0730 hr on 11 January, for a total depth in Hole 1224D of 64.7 mbsf. When the drill string was pulled to the surface, to the surprise of all, the bit had been left in the hole, thus explaining the drilling difficulties. The bit appeared to have been sheared off.

Installation of 10¾-in Casing

Starting at 2030 hr on 11 January, the drill crew began assembling the 10¾-in casing string, which consisted of five joints of 10¾-in (40.5 lb/ft) casing. Hole 1224D was reentered by the casing string at 1336 hr on 12 January. We noted during reentry that the reentry cone and skirt had settled by ~1.7 m below the original mudline. The casing string was run down and landed with the base at 5036.47 mbrf (58.47 mbsf) on 1515 hr on 12 January. The casing was cemented with 18.8 bbl of 15.5 ppg Class G cement. The first attempt to release from the casing hanger failed and resulted in the 10¾-in casing hanger being pulled up above the reentry cone. The casing hanger was landed again in the 20-in casing hanger, and this time the 10¾-in hanger released at 1715 hr on 12 January. The pipe was tripped up, with the running tool clearing the rotary table at 0530 hr on 13 January.

The BHA was assembled with a RCB bit and run down to 4388.89 mbrf in preparation for coring in Hole 1224E. Before starting Hole 1224E, we reentered Hole 1224D to ensure that the casing and cement were properly installed.

Hole 1224E

The *JOIDES Resolution* was offset 15 m to the southwest, and Hole 1224E was spudded at 1840 hr on 13 January at 4978 mbrf. We washed down the first 8 m and then took two punch, or push, cores (200-1224E-1R and 2R), which were acquired by lowering the RCB bit through the soft sediments without rotating the bit. Both cores sustained substantial drilling disturbance, but we were able to recover 10.52 m of sediment core in a 19.2-m-long interval from 8.0 to 27.1 mbsf, where recovery was virtually absent in the other holes.

Coring penetrated from 27.1 to 36.7 mbsf for Core 200-1224E-3R. Basement was tagged at 27.7 mbsf during coring. Recovery consisted of basaltic basement underlying a 5-cm-thick piece of hyaloclastite, into which basalt glass and clay pieces had been incorporated. This likely is the top few centimeters of the basement. After completing coring on Core 200-1224E-3R, the bit was pulled up by one stand of drill pipe to connect another joint of pipe. This placed the bit above the sediment/basement contact. After making the connection, the driller was unable to reenter the basement hole. After 1 hr of attempting to find the hole by rotating the bit on bottom, a new hole (1224F) was started.

Overall we cored 28.7 m in Hole 1224E and recovered 14.91 m of core (51.95% recovery) with the RCB coring system (Table T4).

Hole 1224F

The start of Hole 1224F is somewhat of an anomaly in the ODP nomenclature, since the bit never pulled totally out of Hole 1224E, but it did pull out of the basement portion of Hole 1224E. The distance between Holes 1224E and 1224F is likely no more than ~1 m. In any case, we began penetrating basement again at 1630 hr on 14 January in Hole 1224F.

For all the bad weather we had previously endured, we were due a good spell. Thus, coring proceeded without interruption except for the occasional wiper trip and one trip to replace the knobby joints with drill pipe. During the latter trip, which started at 2315 hr on 17 January after recovery of Core 200-1224F-11R, the bit was inadvertently pulled above the basement/sediment contact. The driller worked the drill string up and down with rotation in an attempt to reenter Hole 1224F. Instead, Hole 1224E was reentered five times before finally the bit went back into Hole 1224F. RCB coring proceeded after washing ~11 m of soft fill from the bottom of hole. Cores continued to be cut at a rate of ~6–8 hr/core, which was roughly twice as fast as cores cut from near the top of the basement. No core was recovered in Core 200-1224F-16R. The bit deplugger was run to remove potential obstructions, but Core 200-1224F-17R also had no recovery. Owing to time limitation, coring in Hole 1224F ended and preparations for logging began.

Overall in Hole 1224F, we penetrated 174.5 m, cored 146.8 m, and recovered 37.7 m of core (25.68% recovery) with the RCB coring system (Table T4).

Logging

The bit was released in the bottom of the hole at 2320 hr on 19 January. The hole was then displaced with 75 bbl of sepiolite mud. A free-fall funnel (FFF) was launched at 0442 hr on 20 January to facilitate reentries into Hole 1224F during future scientific experiments.

At 0730 hr on 20 January, the triple combination (triple combo) tool was prepared to run downhole (see "Logging," p. 9, in "Operations" in the "Site 1224" chapter). The tool reached 5152 mbrf, which is only 0.5 m off the bottom of the hole. The first logging run was completed, and the tool was through the rotary table at 1520 hr on 20 January. For each logging run, the base of the pipe was lowered to 49.9 mbsf initially. As each run was made uphole, the pipe was pulled up from 49.9 to 34.5 mbsf to increase the open-hole interval for logging.

The second logging run was with the Formation MicroScanner/dipole sonic imager (FMS/DSI) tool. Three passes of this string were run uphole at 275 m/hr from the bottom of the hole to the basement contact (27.7 mbsf). The second logging run was completed, and the tool cleared the rotary table at 0525 on 21 January.

We had planned to test the three-component well seismic tool (WST-3) if time and weather conditions permitted. While testing the tool and air gun, three problems were found: a faulty circuit in the blast hydrophone of the air gun, an air leak from the air gun, and the WST-3 telemetry worked intermittently. The experiment was thus terminated because there was insufficient time to attempt to fix the problems and

complete the planned shooting program to the WST-3. The time constraint on the logging program was determined by the departure time required to make the San Diego port call. The WST was back through the rotary table at 0945 hr on 21 January.

The VIT was launched starting at 1030 hr 21 January to observe the FFF at the top of Hole 1224. A large hole was observed in the seafloor from circulating the cuttings out of the hole. As a result the top of the FFF was observed at ~4980.5 mbrf (2.5 mbsf) with the three buoys just below the mudline, secured to the FFF by a $^{5}/_{32}$-in steel cable. The end of the casing on the FFF is estimated to be at 6.2 mbsf.

The open end of the drill pipe cleared the seafloor and FFF at 1238 hr on 21 January. The VIT was recovered at 1445 hr, and the BHA cleared the rotary table at 2355 hr on 21 January, completing activity at Site 1224.

Principal Results

Borehole Seismic Installation

The primary objective of the cruise was to prepare a borehole in basaltic crust for the installation of a broadband borehole seismometer that will be connected to the Hawaii-2 Observatory (H2O) for continuous, real-time data transmission to the University of Hawaii. From Hawaii the data will be made available to seismologists worldwide through the IRIS Data Management Center in Seattle.

Proposed Site H2O-5 (27°53.363′N, 141°58.758′W) (Fig. **F8**) was selected for the seismometer installation. This is 1.48 km northeast (a bearing of 056°) of the H2O junction box location. The bearing was chosen so that regional earthquake events from the Island of Hawaii would be on the same great circle path to both the shallow buried seismometer at the junction box and to the borehole seismometer to be installed at Site 1224. The range was chosen as a compromise between being sufficiently far away to not disturb other experiments at the junction box but still close enough to conveniently run a cable from the borehole to the junction box. The bathymetry slopes smoothly downward ~6 m from the junction box to Site 1224, and the two sites appear to be on the same crustal block in a relatively flat abyssal plain environment.

Hole 1224D (27°53.370′N, 141°58.753′W; 4967 m water depth) has a reentry cone and 58.5 m of 10¾-in casing, which was cemented into a 30-m-thick well-consolidated massive basalt flow underlying 28 m of soft, red clay (Figs. **F9, F10**). After cementing, the hole was washed to a depth of 5036 mbrf (58 mbsf or 30 m into basaltic basement). On reentering for the wiper trip, we noticed that the cone had settled ~1.7 m into the sediment.

After setting the reentry cone and casing in Hole 1224D, we drilled a single-bit hole (1224F) to 174.5 mbsf to acquire sediment and basalt samples for shipboard and shore-based analysis as well as to run a logging program. Hole 1224F is <20 m southeast of Hole 1224D, and measurements in Hole 1224F can be used to infer the structure surrounding the seismometer hole. We dropped a FFF in Hole 1224F so that future borehole experiments using wireline reentry technology can be conducted (Figs. **F11, F12**). For example, this would be a good site to compare measurements in a sealed hole in basement (1224D) with measurements in an open hole in basement (1224F).

F9. Summary of the critical dimensions of the reentry cone and casing deployed, Hole 1224D, p. 43.

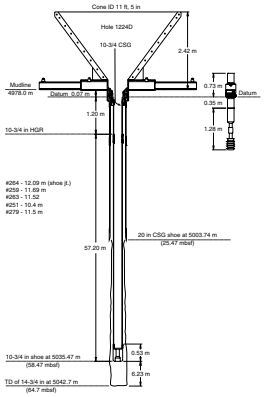

F10. Reentry cone, Hole 1224D, p. 44.

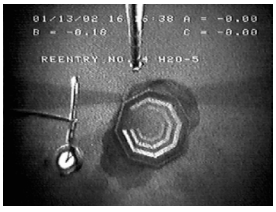

F11. Summary of the critical dimensions of the FFF deployed, Hole 1224F, p. 45.

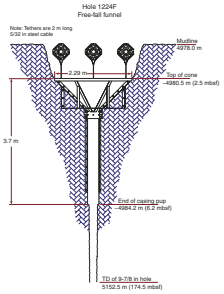

F12. Free-fall funnel, Hole 1224F, p. 46.

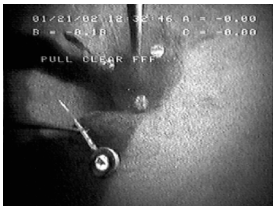

Lithology

Sedimentary Section

Sediments were obtained from parts of Holes 1224A, 1224B, 1224C, and 1224E. The sediments consist mostly of abyssal clays of varying color. Occasional coarser horizons are present as are horizons with varying densities of microfossils, both siliceous (radiolarians and sponge spicules) and calcareous (coccoliths and discoasters) (Fig. F13).

Core recovery from Holes 1224A and 1224B was not significant enough to characterize the sediments. One significant discovery, however, was the recovery of light-colored noneffervescing granules and pebbles from a depth of between 6 and 15.6 mbsf from Hole 1224A. These were found to be zeolite deposits that were interpreted to have infilled burrows.

The total sediment depth at Site 1224 is 28 m. The top 6.53 m, as characterized by a single piston core in Hole 1224C, is massive brown clay that gradually changes color to very dark brown. Radiolarian spicules are present throughout the section, but they increase with depth and are common at the bottom of the unit. Sponge spicules are not found near the top of the section but are common below 4.50 m.

In Hole 1224E, we recovered 10.52 m of clay in the interval from 8.0 to 27.1 mbsf, in which two punch cores were collected with the RCB coring system by pushing through the sediment without rotating. The clay varies in color between dark brown, very dark brown, black, and dark yellowish brown. The high disturbance due to the punch coring process causes the colors to be streaked and mottled throughout the hole. Most color changes are gradual. Light-colored granules and pebbles are found in the top few centimeters of Core 200-1224E-1R (~8 mbsf). Like the burrows in Hole 1224A, they do not effervesce and are thought to be infilled burrows. These sediments also contain small manganese nodules. They are up to 2 mm in width and may be irregular or elongated in shape. Coccoliths and discoasters are present below 17.5 m.

We did not have a paleontologist on board, but Bob Goll and John Firth from ODP-TAMU (Texas A&M University) examined the radiolarians and calcareous nannofossils, respectively, postcruise. Paleontological analysis of the calcareous nannofossils indicates that essentially the whole sedimentary sequence was deposited within a few million years of the crustal age of ~46 Ma.

F13. Coccoliths and discoasters, p. 47.

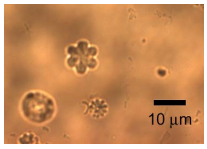

Hard Rock Section

The basalt stratigraphy at the site is summarized in Figure F14. In this figure, the depth for the top of each core, except for the topmost cores into basement, is taken as the top of the cored interval, as is the ODP convention. The cored interval is determined from the drill string length, which is entered into the ODP database. The topmost basement cores in all four holes, however, assume that the top of basaltic basement lies at a constant depth of 28 mbsf, which was our best estimate based on all drill holes and jet-in tests. For these cores only, the recovered basalt is placed below this fixed depth, rather than at the top of the cored intervals. The basement depth of 28 mbsf is probably uncertain by about a meter, and there may be some slight relief to the top of basalts as well. This approach avoids assigning basalt recovery to depths that actually are above the point where basement was touched by the drill string.

F14. Lithologic summary of basalts cored at Site 1224, p. 48.

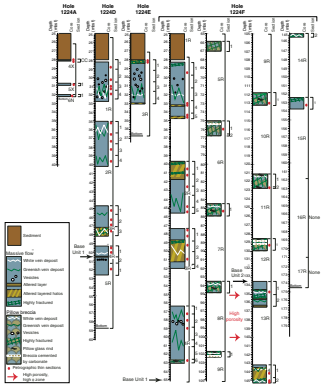

The lithostratigraphy of basalts at Site 1224 is divided into three units. Unit 3, the deepest unit, is intermixed pillows and flows of no more that a few meters thickness each. At least two, and probably more, eruptive events are represented. Overlying Unit 3, Unit 2 is a succession of thin flows and pillows. Chemical analyses of these rocks are very similar, indicating that they are one eruptive composition. Two thick lava flows from Unit 1 cap the underlying units. The lower of these has the same composition as the basalts of Unit 2. These two flows may have accumulated in a structural depression or pond that formed, probably by faulting, after eruption of the last thin flows or pillows of Unit 2.

Apart from the interiors of the massive flows, the lava sequence was pervasively altered under conditions with variable oxygen fugacity. Hydrous fluids carrying dissolved metals flowed through cracks, cavities, and fractures in the formation and deposited iron oxyhydroxides and sulfide minerals in this porosity structure. The fluids penetrated several centimeters into the rock adjacent to the fractures and impregnated microfractures with the same material that was deposited in the larger veins. Later, carbonate-saturated fluids coursed through the same fractures depositing calcite (Fig. F15). Except for the interiors of the two upper massive lavas, most of the rock was at least partially transformed to secondary minerals by this process. Eventually, enough calcite precipitated to cement the originally fragile iron oxyhydroxides and sulfide minerals. The calcite cementing is the principal reason why the coring of basalts above ~60 mbsf at Site 1224 was so successful.

It is too early to say how warm the fluids might have been, although calcite and aragonite are the ideal minerals to use for oxygen isotope determinations and to estimate temperature for the cementation portion of these processes. Iron oxyhydroxides are a principal component of hydrothermal sediments deposited on volcanically active ridge axes near, but not at, high-temperature vents. Elsewhere on the flanks of the East Pacific Rise, basalt coring has not been successful in crust as old as Miocene, largely because of the absence of calcite vein cement. Thus the carbonate-lined veins in the Eocene rocks at Site 1224 may be evidence for sustained fluid flow at low temperature and far off-axis. There is only a thin layer of sediment at Site 1224, insufficient to seal off fluids circulating in the crust. Interaction of those fluids with oxygenated bottom water may be why most of the section cored exhibits mainly oxidative alteration. The exception to this is the massive basalts at the top. In those, fractures may have been so few and widely spaced that fluid flow was restricted. The oxygen fugacity of the small quantity of fluids moving along them was consequently reduced by reaction with adjacent wall rocks, allowing pyrite to precipitate.

F15. Flow-top hyaloclastite cemented by calcite, p. 49.

Petrography

Thin section examination of volcanic basement at Site 1224 (Holes 1224A, 1224D, 1224E, and 1224F) evidenced a relatively homogeneous mineral paragenesis. The main phases are plagioclase, clinopyroxene, opaque minerals, and rare pigeonite; therefore, the rocks can be classified as tholeiitic basalts. Olivine is rare and only a few small iddingsitized euhedral to anhedral groundmass crystals were found. Iddingsite is a typical alteration of olivine and is made up by a mixture of goethite and layer silicates (e.g., smectite). The majority of the basalt is holocrystalline (almost 100% crystals) to hypocrystalline (glass concentration <50%) and can be ascribed to lava flows. With increasing depth of cor-

ing, hypohyaline textures and volcanic glass contents >90% become common and indicate the presence of pillow fragments with chilled margins. The deepest samples recovered (~153 mbsf) also show textural features of holocrystalline massive lava flows. With regard to their granularity, the basalts range from aphanitic (difficult to distinguish the crystals in the groundmass with the naked eye) to aphyric (absence of phenocrysts), though rare plagioclase or plagioclase-clinopyroxene sparsely phyric basalts (phenocryst content <2%) have been also found. The relative size of the crystals in the groundmass is equigranular, and their distribution is isotropic. The groundmass is hypidiomorphic with the presence of euhedral- to anhedral-shaped crystals. The texture of the massive lava flow basalts is intergranular (with clinopyroxene in interstitial relationships with plagioclase) to subophitic (with plagioclase laths partially enclosed in clinopyroxene) and, more rarely, intersertal (with microcrystalline to glassy material between plagioclase). Hyalopilitic (with plagioclase laths and clinopyroxene crystals in a glassy matrix) to, more rarely, intersertal textures have been found in the pillow lavas. The grain size of the groundmass ranges from very fine grained (0.001–0.5 mm) to fine grained (0.5–1 mm).

Geochemistry

Inductively coupled plasma–atomic emission spectroscopy (ICP-AES) data for K_2O, TiO_2, MgO, Ba, and Zr were obtained on samples from Site 1224. These were supplemented in the site report by shore-based X-ray fluorescence data kindly provided by S. Haraguchi. The rocks recovered at the top of the hole (28–62.7 mbsf) consist of massive fresh basalt, with only widely spaced and narrow veins containing carbonate minerals, clays, and pyrite. From 62.7 to 133.5 mbsf, the basalts are thin sheet flows and pillows. From 133.5 to 161.7 mbsf, they are somewhat more massive pillows and flows.

The basalts are differentiated normal mid-ocean-ridge basalt (N-MORB) with 2–3.5 wt% TiO_2. The samples selected for analysis from Hole 1224D are scarcely altered, with loss on ignition (LOI) values ranging from 0 to 0.45 wt%. Concentrations of K_2O (0.11–0.27 wt%) may be slightly elevated in three of ten samples analyzed from this hole, but most values and all those for Ba (9 to 18 ppm) are consistently lower than in many comparably differentiated MORB glasses from the East Pacific Rise. This may indicate a greater-than-average depletion of the mantle sources of basalts obtained at depths shallower than 60 mbsf from Hole 1224D. Alternatively, the rocks may have experienced a slight nonoxidative alteration in which these components were partially removed from the rock. This seems unlikely, however, given the more extensive oxidative alteration observed in rocks from Holes 1224E and 1224F, obtained only a few meters away.

Both TiO_2 contents and Zr concentrations are determined precisely enough, and they are so little affected by alteration that they can be used to define a chemical stratigraphy (Fig. F16). Most of the basalts from Hole 1224D belong to one chemically uniform, extensively differentiated basalt flow >20 m thick. This overlies a second flow that is not quite so differentiated. This in turn overlies pillows that are geochemically similar. Below 133.5 mbsf, strongly differentiated ferrobasalts were recovered.

X-ray diffraction (XRD) analysis was carried out on one clayey pebble from the sediment and twenty-five vein materials within the basalt.

F16. Chemical compositions for basalts, Hole 1224D, p. 50.

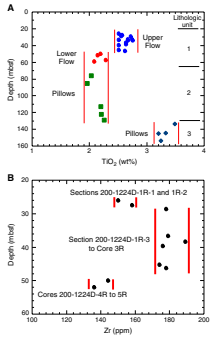

Five distinct vein types were documented by XRD analysis: clay, carbonate, zeolite, quartz, and calcite/smectite (Fig. F17). Many vein minerals in the basement at Site 1224 are stable at low temperature and pressure (i.e., zeolite). Phillipsite, the principal zeolite present at Site 1224, is a low-temperature member of the zeolite group (Miyashiro, 1973). Smectite is also commonly found as a product of the alteration of volcanic ash and rocks from the seafloor and is present in most of the low-grade metamorphic terranes in the world.

Four of the vein types observed at Site 1224, clay (smectite-illite), carbonate (calcite-aragonite), quartz, and zeolite, are similar to veins observed at Sites 896 and 504 near the Costa Rica Rift (Alt, Kinoshita, Stokking, et al., 1993). These minerals are present in relatively lower temperature hydrothermal assemblages (probably <100°C) at these sites (Laverne et al., 1996). Truly high-temperature vein assemblages, such as the actinolite and epidote veins found below 2000 mbsf at Site 504, were not found at Site 1224. The mineral laumontite in the illite veins indicates a high-temperature zeolite facies assemblage (Miyashiro, 1973). Aragonite generally forms at a higher temperature than calcite. These minerals indicate the local influence of warm hydrothermal fluids.

F17. Identification of main secondary minerals in basement, p. 51.

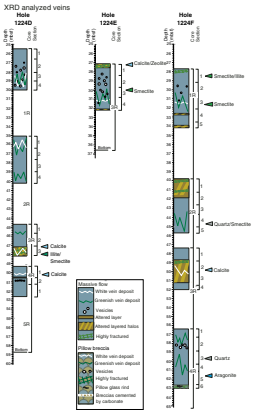

Paleomagnetism

We used progressive alternating-field (AF) demagnetization of archive-half sections, one whole-core section, one working-half section, and discrete samples to characterize the paleomagnetic signal and resolve the magnetization components recorded in the recovered core. An unambiguous magnetostratigraphy could not be obtained from the only undisturbed core (Core 200-1224C-1H) that was recovered in the sedimentary section; the other sediment cores were extremely disturbed by drilling. In addition, we only had time for a cursory interpretation of the magnetization of the basaltic units, although fairly detailed demagnetization experiments were conducted on split cores and discrete samples.

The magnetization of the basalts should provide a valuable paleolatitude estimate for the Pacific plate at ~45 Ma. This age corresponds to the Pacific plate's abrupt change in motion relative to the hotspots as marked by the kink in the Hawaiian-Emperor hotspot track. A cusp in the Pacific plate apparent polar wander path (APWP) may also occur at this age, marking a change in the motion of the Pacific plate relative to the spin axis. The Pacific APWP and hotspot tracks together provide key constraints on estimates of the size of motions between hotspots, ultimately extending our understanding of mantle dynamics (Acton and Gordon, 1994). Additionally, the age also lies within the period (39–57 Ma) when the Hawaiian hotspot has been shown to have moved rapidly southward relative to the spin axis (Petronotis et al., 1994). If geomagnetic secular variation has been averaged by the basalt units and if secondary overprints caused by alteration do not mask the primary magnetization, then we should be able to obtain an accurate paleolatitude. Finally, rock magnetic studies of the basalts should help refine our understanding of the magnetization of the upper oceanic crust and its role in generating lineated marine magnetic anomalies.

Microbiology

Samples of different sediment types and from basaltic rock were collected at Site 1224 for aerobic and anaerobic cultivation, for deoxyribonucleic acid (DNA) extraction and analysis, for phylogenetic characterization, for total cell counts, and for determination of the live/dead ratio of indigenous microbial communities. Sediment suspensions and ground basalt material were used under oxygen-depleted conditions in the anaerobic chamber for the establishment of enrichment cultures. Aerobic cultivation was conducted using both seawater-based media and commercial Zobell's medium. Anaerobic cultures were based on reduced mineral media.

To evaluate the microbial background at Site 1224, ambient seawater samples were collected at 1 m below sea surface upwind of the *JOIDES Resolution*. The microscopically enumerated total cell counts in the surface water at Site 1224 were 1.4×10^4 cells/mL.

Sediment samples from Holes 1224C, 1224D, and 1224E were obtained from different depths ranging from the near-surface layer down to 24.9 mbsf. Bacteria were present in all sediment samples taken to 24.9 mbsf.

The amount of active bacteria was assessed in two representative sediment samples taken from the near-surface layer (Sample 200-1224C-1H-1, 0–5 cm) and from a depth of 25 mbsf (Sample 200-1224E-2R-5, 143–150 cm). As indicated by fluorescent signals after hybridization with the Bacteria-specific probe EUB338, the amount of metabolically active bacteria ranged in these sediment layers from 62% to 41% of the total cell counts, respectively (Fig. **F18**).

Microscopic investigation of thin sections revealed the first survey of the presence of eukaryotic microorganisms within the basement of the North Pacific Ocean, which are counted among the kingdom of fungi. Hyphae have been found within cavities, small fractures, and veins filled with $CaCO_3$. These fungal structures were viewed by transmitted light microscopy, in which they appear with a brownish tinge. The net of fungal hyphae shown in Figure **F19** filled the complete space spanning from the basalt/calcite boundary to the center of the cavity. The cross-sectional dimension of the hyphal network is 5–10 µm with a length ranging from 50 to several hundred micrometers. The hyphae are typically interrupted at irregular intervals by cross-walls, so-called septa, which divide the entire fungal hyphae into single distinctive cells. Our results provide strong evidence for eukaryotic life in addition to bacteria in deep subsurface environments.

F18. Bacterial cells from an upper sediment layer, p. 53.

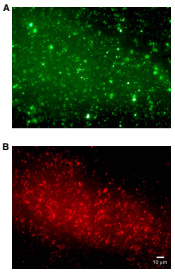

F19. Fungal hyphae in a $CaCO_3$-filled cavity in a massive lava flow unit, p. 54.

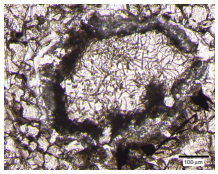

Physical Properties

In Hole 1224A, *P*-wave velocities of aphyric basalt from Cores 200-1224A-5X and 6N are ~5900 m/s and ~5800 m/s, respectively.

In Hole 1224C, the gamma ray attenuation (GRA) densities of sediments gradually decrease with increasing depth between 0 and 6.4 mbsf, corresponding to a color change from light brown to dark brown. Similarly we observed an unusual trend for bulk and dry densities in Hole 1224C, which decreases from ~1.52 to ~1.36 g/cm³ and from ~0.8 to 0.54 g/cm³, respectively. Porosities in Hole 1224C gradually increase from 71% to 80%. *P*-wave velocities from the *P*-wave logger (PWL), however, show a small increase from 1460 to 1500 m/s with depth between 0 and 6.4 mbsf. *P*-wave velocities from PWS3 contact probe mea-

surements from Core 200-1224C-1H to 4H (between 0 and ~5.70 mbsf) range from 1525 to 1535 m/s. The *P*-wave velocity in Core 200-1224C-5H is ~1555 m/s, which is greater than other sections. Grain densities in Hole 1224C show a small increase from 2.782 to 2.831 g/cm³ for depths shallower than 2 mbsf. Between 2 and 6 mbsf, grain densities remain fairly constant between ~2.70 and ~2.74 g/cm³.

In Hole 1224D, bulk and dry densities increase from 2.7 to 2.9 g/cm³ and 2.6 to 2.8 g/cm³, respectively, in Core 200-1224D-2R. In Core 200-1224D-3R, bulk and dry densities decrease from 2.9 to 2.8 g/cm³ and from 2.8 to 2.7 g/cm³, respectively. In Cores 200-1224D-4R and 5R, they also decrease from 2.85 to 2.80 g/cm³ and from 2.8 to 2.7 g/cm³, respectively. Porosities remain at low values ranging from 4% to 9%. PWS velocities range from 4200 to 6500 m/s. Compressional wave velocity anisotropies for each sample are ~2%–10%. PWS velocities have a sinusoidal depth variation. They decrease between 25 and 35 mbsf, increase between 35 and 45 mbsf, and decrease again between 45 and 55 mbsf. This sinusoidal depth variation is also identified for Hole 1224F.

Between 25 and 60 mbsf, PWS velocities in Holes 1224E and 1224F have a similar trend to Hole 1224D. PWS velocities have a strong depth dependence. Compressional velocities separate into seven depth zones (Fig. **F20**):

1. 30–38 mbsf: 5500–6000 m/s,
2. 38–41 mbsf: 4200–5500 m/s,
3. 41–61 mbsf: 5000–6000 m/s,
4. 61–100 mbsf: 4500–5000 m/s,
5. 100–138 mbsf: 4700–6000 m/s,
6. 138–147 mbsf: 4000–4700 m/s, and
7. >147 mbsf: 5500 m/s.

Zones 1–3 may be characterized as rather uniform basalt flow zones with a thin low-velocity (fractured) layer. Zone 4 is characterized as a slightly low velocity zone. Velocities of zone 5 are higher than those for zones 4 and 6. Zone 6 is highly fractured, characterized by the lowest velocities. Zone 7 corresponds to more uniform basalt layers.

P-wave velocities are scattered with increasing bulk density. *P*-wave velocity vs. porosity, however, has a good inverse correlation, as *P*-wave velocity decreases with increasing porosity. These two relations imply that *P*-wave velocities are not controlled by bulk densities, but are well controlled by porosities. Large porosities are associated with more fractured zones. If this is true, zones 2 and 6 are intensively fractured.

Logging and Correlation to Other Data

Based on shipboard preliminary log analysis at this site during Leg 200, we conclude that basement in Hole 1224F consists of at least five distinctive units (Figs. **F21, F22**):

Sediments: 0–28 mbsf,
Unit I: 28–45 mbsf,
Unit II: 45–63 mbsf,
Unit III: 63–103 mbsf,
Unit IV: 103–142 mbsf, and
Unit V: Deeper than 142 mbsf.

F20. Compressional wave velocities, p. 55.

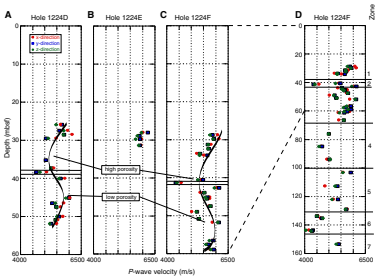

F21. Temperature, SP, and electrical resistivity logs, p. 56.

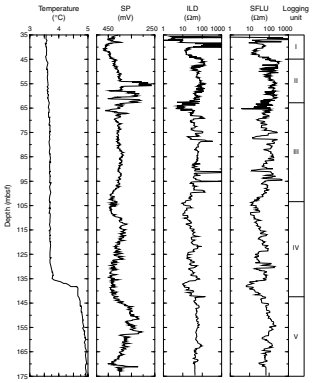

F22. Logging data, Hole 1224F, p. 57.

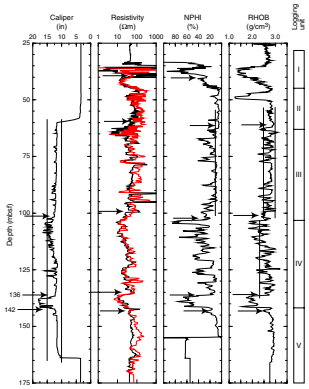

These layered formations can be distinguished using the continuous electrical resistivity, density, sonic, neutron porosity, magnetic field, and possibly spectral gamma ray logs. The existence of a conduit or large-scale fracture between 138 and 142 mbsf was detected by all the log tools including the temperature tool. In addition, the temperature tool reveals that the "warmer" fluid had a temperature of 4.6°C at the time of the logging. The vicinity of the 138- to 162-mbsf zone is much more highly altered than other rocks penetrated by the hole, as indicated by the gamma ray logs. Because of the relative position of the tools located in the tool strings, some tools can resolve the top logged intervals like gamma ray, porosity, density, and sonic logs. On the other hand, the resistivity tools and FMS placed at the bottom of the tool string can resolve the formation properties near the bottom of the hole. The values of the magnetic fields calculated from the three-component inclinometer tool are invalid near the bottom of the pipe (~35 mbsf). In the logged intervals where all the tools overlapped, they provide consistent information to support the layered structural units based on these geophysical properties.

Core lithology, physical properties, well logs, and seismic reflection data from the site were compared. The upper sediment unit (0–28 mbsf) is a brown clay layer with radiolarians at shallow depth. The mean velocities by physical properties measurements are ~1500 m/s. Logging Units I and II, between 28 and 63 mbsf, are two massive basalt flows with fractures at roughly 45 mbsf. These two logging units combined thus correspond to lithologic Unit 1. The compressional wave velocities in logging Units I and II based on core measurements are ~5500 m/s. Smecite veins were found in these units. Logging Unit III (63–103 mbsf) is characterized by fractured basalt layers both in core recovered and in data collected by the FMS/DSI logging tool. Calcite veins were found in this unit. The compressional velocity is ~5000 m/s. Logging Unit IV (103–142 mbsf) is characterized by stacks of small pieces of pillow lavas. This layer has compressional velocities slightly higher than 5.0 km/s as measured on discrete core samples. Logging data, however, indicate that this unit is highly porous. Logging Unit IV also contains smectite veins. At the base of logging Unit IV, large variations are present on the caliper log, resistivity log, compressional and shear velocity logs, U and Th content, and the temperature log. Physical properties measurements also indicate that this unit is highly fractured. The presence of high U and Th contents suggests that this unit is a highly altered zone. Logging Units III and IV combined correspond to lithologic Unit 2. In logging Unit V, below ~142 mbsf, basalt sheet flows were found. This logging unit corresponds to lithologic Unit 3. The single-channel seismic (SCS) data suggest that this is the top of a massive basalt unit that extends deeper than our deepest drilling depth (174.5 mbsf). In comparing the above units with the SCS records, these unit boundaries extend many kilometers away from the site. With further analysis it should be possible to understand the nature of oceanic Layers 2A and 2B and their relationship to lithologic boundaries in ~45-Ma fast-spreading oceanic crust.

3.5-kHz Deep-Source Experiment

A long-standing problem in the red clay province of the eastern Pacific Ocean is to adequately resolve chert layers and basement in the presence of sediments <50 m thick. By lowering a battery-powered, free-running 3.5-kHz pinger to the seafloor on the VIT sled and recording

the pulse on the ship's 3.5-kHz acquisition system, we hoped to increase the sound level incident on the seafloor, to improve the penetration into the subbottom, to reduce the footprint of the sound on the seafloor, and to increase the received signal levels. The deep-source 3.5-kHz experiment was carried out whenever the VIT camera was lowered to the seafloor either for reconnaissance surveys or reentries.

Examination of the deep-source 3.5-kHz records shows two prominent reflections at 13 and 38 ms below the seafloor (Fig. F23). Depending on the sound velocity in the seabed, these reflectors would be 10 to 13 m and 28 to 38 m deep. The continuity of these reflectors varies with time throughout the survey, whereas the ship moves only a few meters.

Our preliminary interpretation had been that the 13-ms reflection is present at an intermittent chert layer. The first jet-in test stopped abruptly at 13 m. Although chert layers within the sediments have been encountered at other drill sites in the eastern Pacific, nowhere at Site 1224 did we sample chert. The 13-ms reflection may correlate with a radiolarian-rich layer that was cored. Basalt cores were regularly acquired at 28–30 m depth, corresponding to the 38-ms reflector.

In summary, the deep-source 3.5-kHz experiment identified a previously unrecorded reflector at 38 ms below the seafloor that corresponded to basaltic basement. This reflector was not observed in the traditional 3.5-kHz survey conducted in 1997 or in the shipboard 3.5-kHz survey acquired while we came on site (Fig. F4). The 38-ms reflector, however, was observed beneath the H2O junction box.

F23. Installation of the reentry cone and steel casing in Hole 1224D as observed on deep-source records, p. 58.

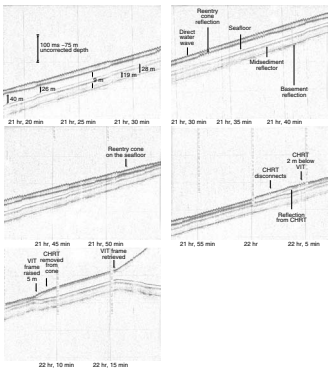

Broadband Seismic Observations during the Leg

Drilling at the H2O provides a unique opportunity to observe drilling related noise from the *JOIDES Resolution* on a seafloor seismometer in the 0.1- to 80-Hz frequency band. The University of Hawaii operates a Guralp CMG-3T three-component broadband seafloor seismometer and a conventional three-axis geophone at the H2O. Data are acquired continuously and are made available to scientists worldwide through the IRIS Data Management Center in Seattle. During the cruise, Jim Jolly and Fred Duennebier at the University of Hawaii relayed sample data files to the *JOIDES Resolution* by file transfer protocol (FTP) over the shipboard telephone. We were then able to process data and study correlations with on-site activities and weather. The University of Hawaii also maintained a Web site showing H2O seismic data collected during the cruise (**www.soest.Hawaii.edu/H2O/**).

Seismic activity could be associated with wind speed, sea state, shear resonance effects in the sediments, whales, water gun shooting, earthquakes, passing ships, and drilling-related activities such as bit noise and running pipe (Fig. F24).

F24. Energy levels on the H2O seafloor seismometer, p. 59.

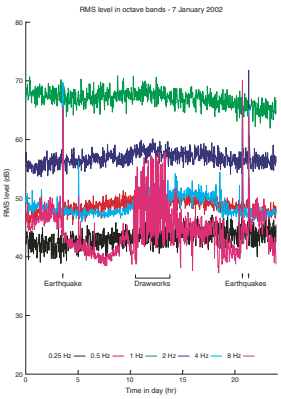

Summary

1. Site 1224 (27°53.367′N, 141°58.755′W) was selected for the seismometer installation (Fig. F8). This is 1.48 km northeast (a bearing of 056°) of the H2O junction box location. Hole 1224D (27°53.370′N, 141°58.753′W; 4967 m water depth) has a reentry cone and 58.5 m of 10¾-in casing that was cemented into 30 m of well-consolidated, massive basalt underlying 28–30 m of soft, red clay.

2. A single-bit hole (1224F) was drilled to 174.5 mbsf, and we sampled a 146.5-m-thick section of basaltic oceanic crust. Hole 1224F is <20 m to the southeast of Hole 1224D. Cores and well logs were acquired to characterize the site. The physical properties measured from well logs indicate that the basaltic basement can be divided into five distinct units at 28–45 mbsf, 45–63 mbsf, 63–103 mbsf, 103–142 mbsf, and below 142 mbsf. This hole was equipped with a FFF so that it also could potentially be used for long-term borehole seismic experiments in the future.
3. A suite of experiments and observations was conducted to investigate the role of microbial life in the deep biosphere. As a general trend, bacterial population numbers decreased with increasing depth, though the amount of metabolically active bacteria remained remarkably high at 41% to 62% of the total cell counts. Both the high total cell counts as well as the amount of bacteria with apparent physiological potential within the sediment layers suggest a higher contribution of sediment bacteria than has been previously assumed. The successful cultivation of lithotrophic oxidizing bacteria and the microscopic indication of further microbial structures within a cavity of basaltic rock confirm the presence and even activity of microbial life not only in deep marine sediments, but also in the Paleogene oceanic crust from the North Pacific.
4. We tested a deep 3.5-kHz source that could be deployed on the VIT frame to inspect the shallow structure of the seafloor at a higher spatial resolution than conventional echo sounding.
5. The total sediment depth at Site 1224 is 28 m. Paleontological analysis of the calcareous nannofossils indicates that essentially the whole sedimentary sequence was deposited within a few million years of the crustal age of ~46 Ma.
6. The basalts are differentiated N-MORB with 2–3.5 wt% TiO_2.
7. The lithostratigraphy of basalts at Site 1224 breaks down in a straightforward manner into three categories of extrusive basalt. The deepest rocks cored (Unit 3) are intermixed pillows and flows of no more than a few meters thickness each. At least two, and probably more, eruptive events are represented. These were followed by a succession of thin flows and pillows (Unit 2). Chemical analyses of these rocks are very similar, indicating that they are one eruptive composition. The whole sequence is capped by two thick lava flows (Unit 1). The lower of these has the same composition as the basalts of Unit 2. These two flows may have accumulated in a structural depression or pond that probably formed by faulting after eruption of the last thin flows or pillows of Unit 2.
8. Apart from the interiors of the massive flows, the lava sequence was pervasively altered under oxidizing conditions. Hydrous fluids carrying dissolved metals flowed through cracks, cavities, and fractures in the formation and deposited iron oxyhydroxides in this porosity structure. The fluids penetrated several centimeters into rock adjacent to fractures, impregnating microfractures with the same material that was deposited in the larger veins. Later, carbonate-saturated fluids coursed through the same fractures and additional new ones, depositing calcite. Except for the interiors of the two upper massive ponded lavas, most of the rock was at least partially transformed into secondary minerals by this process. Eventually, enough calcite precipi-

tated to cement the originally fragile iron oxyhydroxides, and this is the principal reason why the coring of basalts at Site 1224 was successful.

NUUANU LANDSLIDE

Recent studies have shown that the collapse of large volcanoes due to gravitational instability plays an important role in shaping volcanic environments. Detailed offshore bathymetric surveys of the Hawaiian Ridge (Moore et al., 1994), Reunion Island (Lenat et al., 1989), and the Canary Islands (Masson et al., 2002) reveal extremely large landslides. In the case of Hawaii, one of the Nuuanu Landslides caused by the collapse of Koolau Volcano on Oahu extends more than 200 km from the island. In the Canary Islands, the debris extends to 30 km. Landslides on both island chains might have generated huge tsunamis (Moore, 1964; Moore and Moore, 1988; Moore et al., 1989). Herrero-Bervera et al. (2002) estimated the age of Nuuanu Landslides at 2.1–1.8 Ma. However, the size, the age, and the number of Nuuanu Landslides are still in question. Site 1223 is ~300 km from Oahu and ~100 km to the northeast of the presently defined Nuuanu Wailau debris field (Figs. **F1, F25**).

F25. Location of Site 1223 and the Nuuanu Landslides, p. 60.

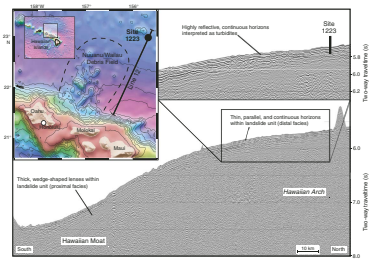

Geological Setting

The Nuuanu Landslide, which broke away from the northeast flank of Koolau Volcano on the island of Oahu, is the largest Hawaiian landslide. It is a debris avalanche that contains enormous blocks such as the Tuscaloosa Seamount, which is ~30 km long, 17 km wide, and at least 2 km tall. The landslide is spread over a 23,000-km² area (Normark et al., 1993; Naka et al., 2000), with distal portions extending up the Hawaiian Arch. To reach the upper portion of the arch, the target site for drilling, the landslide would have had to traverse the deep moat on the northeast side of Oahu and travel over 100 km uphill.

Reaching the landslide deposit by gravity or piston coring has proven difficult because the deposit is overlain by a carapace of younger debris such as turbidites and associated deposits. Thus, the thickness and depositional history of the landslide are poorly known. Prior to drilling, the thickness of the distal portion of the landslide was estimated to be from 1 to 100 m (Rees et al., 1993; Naka et al., 2000). Similarly, the age of the landslide is poorly constrained, although it apparently occurred near the end or after the formation of the Koolau Volcano, which has surface flows with ages 1.8–2.6 Ma based on K-Ar dating by Doell and Dalrymple (1973).

Scientific Objectives

The objectives of drilling at the Nuuanu Landslide site are

1. To resolve whether the Nuuanu Landslide occurred as a single distinct event or as multiple collapses;
2. To determine the age of the landslide(s);
3. To determine the thickness of the landslide deposit at the distal site and to obtain ground truth for the available seismic data in order to estimate the volume of the slide;
4. To study the deposition history of the landslide(s); and

5. To gain insight into potential hazards related to giant landslides on the flanks of ocean island volcanoes.

Operations

The *JOIDES Resolution* departed from the Honolulu Harbor at 1404 hr on 20 December for the Nuuanu Landslide Site NU-1 (ODP Site 1223). The 170-nmi voyage to Site 1223 required 17.0 hr at an average speed of 10.0 kt.

Hole 1223A

Hole 1223A was spudded with the APC at 2030 hr on 21 December at a depth of 4235.1 m (4245.8 mbrf). We took two APC and four XCB cores. We cored 41 m and recovered 23.54 m of core (57.4% recovery), with 12.7 m cored and 10.87 m recovered (85.6% recovery) with the APC and 28.3 m cored and 12.67 m recovered (44.8% recovery) with the XCB (Table T5). After two APC cores, we switched to XCB coring. The use of the XCB system at these shallow depths and the long time needed for coring was unexpected, as was the presence of lithified volcanic rocks. Core 200-1223A-5X was advanced only 1.0 m when it was recovered because there were indications of jamming. Core 200-1223A-6X was advanced 8.0 m to a depth of 41.0 mbsf when it was recovered because the time on site had expired. The drill bit cleared the rig floor at 0130 hr on 23 December, and we departed for Site 1224 (H2O).

T5. Coring summary, Site 1223, p. 72.

Principal Results

Major Discoveries

The core recovered from Hole 1223A (Fig. F26) answered several of the questions posed precruise, but also resulted in some unexpected discoveries. One of the objectives of coring at this site was to determine if the Nuuanu Landslide occurred as a single or as a multistage event as indicated by the number of turbidites recovered. Several unconsolidated volcaniclastic turbidites of varying thickness were recovered in the first two cores in Hole 1223A. At least seven of these were >10 cm thick at 0.86–1.01, 2.11–2.53, and 3.76–3.99 mbsf in lithologic Unit 1 and the four or more turbidites that comprise nearly all of lithologic Unit 2, spanning the interval from 5.11 to 7.32 mbsf. Other turbidites that were <1 cm thick were also recovered. Paleomagnetic data indicate that all but the uppermost turbidite have an age between 1.77 and 1.95 Ma. The top turbidite has an estimated age between 0.99 and 1.07 Ma.

A surprising discovery was the recovery of two crystal vitric tuff layers. Preliminary geochemical analyses indicate these tuffs are geochemically similar to Hawaiian tholeiitic basalts. Olivine in the vitric tuff is fresh. Kink banding and fibrous structures were observed in some olivine. The fibrous structure may have been caused by crystallization of hematite. The kink banding and fibrous olivine may have been derived from deformed dunite cumulates from deep in the lower crust or upper mantle. Paleomagnetic data indicate that the vitric tuffs are older than 1.95 Ma.

Another important result is the identification of the minerals anhydrite, paragonite, and wairakite in sediments just below the deeper vitric tuff. These are hydrothermal minerals and are stable at a tempera-

F26. Lithologic units of Site 1223, p. 61.

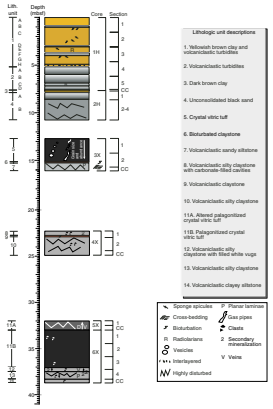

ture range from 150° to 350°C. This suggests that considerable heat was involved when the crystal vitric tuff was deposited. Tentative interpretations for the origin of crystal vitric tuffs are given in "Lithology," p. 22.

Lithology

We identified 14 distinct lithologic units (Fig. F26):

Unit 1 (0–5.11 mbsf) contains yellowish brown clay and volcaniclastic turbidites.
Unit 2 (5.11–7.32 mbsf) consists of volcaniclastic turbidites only.
Unit 3 (7.32–7.90 mbsf) is a thin layer of dark-brown clay.
Unit 4 (7.90–10.78 mbsf) is unconsolidated black sand.
Unit 5 (12.70–15.06 mbsf) is a crystal vitric tuff.
Unit 6 (15.06–15.29 mbsf) is bioturbated claystone.
Unit 7 (15.29–16.10 mbsf) is volcaniclastic sandy siltstone.
Unit 8 (22.30–22.80 mbsf) is volcaniclastic silty claystone with carbonate granules.
Unit 9 (22.80–22.91 mbsf) is volcaniclastic claystone.
Unit 10 (22.91–24.92 mbsf) is volcaniclastic silty claystone.
Subunit 11A (32.00–33.00 mbsf) is altered vitric tuff, highly disturbed by drilling.
Subunit 11B (33.00–36.99 mbsf) is palagonatized crystal vitric tuff.
Unit 12 (36.99–37.47) is volcaniclastic silty claystone with scapolite amygdules.
Unit 13 (37.47–38.31 mbsf) is volcaniclastic silty claystone.
Unit 14 (38.31–38.70 mbsf) is volcaniclastic clayey siltstone.

Coring gaps of several meters exist between some of the cores, so additional units may exist or those identified may be thicker by several meters.

Volcanic material is present throughout the stratigraphic column. Although we identified 14 distinct lithologic units, they may be grouped into three main types of lithologies:

1. Unconsolidated clay and volcanic sediments,
2. Weakly consolidated claystones and siltstones, and
3. Crystal vitric tuffs.

The turbidites are concentrated in the upper 12.7 m of the core. They are dominated by a volcanic fraction that varies from 45% to 100%. The main constituents are, in order of increasing abundance, glassy shards, vitric fragments, olivine phenocrysts and clasts, plagioclase, palagonitized glass, lithic fragments, and clinopyroxene clasts. An MgO-rich olivine and Ca-rich plagioclase composition indicates equilibrium with mafic magmas. The mudstones and siltstones are found both in the middle and the bottom of the sections cored; they have high contents of clay, indicating detrital sources, and they have a low but variable volcanic fraction (~1%–25%). The silty claystone at the bottom of the deepest crystal vitric tuff (Subunit 11B) is characterized by the presence of relatively large (up to 3.5 mm) amygdules filled by anhydrite, a sulfate associated with hydrothermally altered basic rocks. The vitric tuffs were found just below the sand and at the top and in the middle of the mudstones and siltstones cored. The "nonvolcanic" fraction is made up of

claystone clasts, micritic clasts, and, more rarely, radiolarians (generally <1%).

Whole-rock ICP-AES analyses were conducted on the two vitric tuffs, as well as several of the siltstones and claystones. They have high MgO concentrations (12.4–15.8 wt%), which are not surprising because of the high percentage of olivine present. The tuff's major elements are SiO_2 (47.6–49.6 wt%), TiO_2 (~2 wt%), Al_2O_3 (11.3–11.9 wt%), Fe_2O_3 (11.3–12.7 wt%), MgO (12.4–15.8 wt%), CaO (6.74–7.17 wt%), Na_2O (2.19–3.07 wt%), K_2O (0.47–0.83 wt%), and P_2O_3 (0.16–0.23 wt%). Their trace elements are Ba (50–70 ppm), Sr (22–330 ppm), Y (~20 ppm), Zr (~120 ppm), and Ni (~430–580 ppm). Siltstones and claystones show similar values to those of the tuffs. The geochemistries of whole-rock crystal vitric tuff, siltstone, and claystone were compared with the basalt glass geochemistry of MORB, Kilauea tholeiitic basalt, Haleakala alkali basalt, North Arch alkali basalt, and Koolau tholeiitic basalt. The crystal vitric tuff, siltstones, and claystones have the most in common, geochemically, with the Hawaiian tholeiitic lavas. There are some ambiguities in the measurements and samples, however, because the tuff contains clay minerals, which may affect the chemical compositions.

Several of the claystones and siltstones contain effervescing white amygdules. XRD analysis of the filling from interval 200-1223A-6X-4, 0–20 cm, gave a complex spectrum. The major components of the material are anhydrite and paragonite. Additional components include wairakite and possibly pumpellyite of varying compositions as a minor component. Grains from two intervals in the turbidite were analyzed by XRD (intervals 200-1223A-1H-5, 94–95 and 114–115 cm). The upper interval has brown grains with dominant XRD peaks at wavelengths consistent with phillipsite. In addition, some of the smaller peaks have spectra consistent with clay minerals, mainly smectite and illite and minor plagioclase. Therefore, the composition of the material analyzed is mainly phillipsite with clay minerals and minor plagioclase. The lower interval has white granules identified as calcite by XRD analysis.

Wairakite was originally found in hot springs in the geothermal fields of Wairakei in New Zealand and of Onikobe in Japan (Miyashiro, 1973). It has also been found in hydrothermal areas in the Mariana Trough (Natland and Hekinian, 1982). Wairakite is stable at a temperature range from 200° to 300°C. This suggests that considerable heat was involved when the crystal vitric tuff was deposited sometime thereafter. Anhydrite and paragonite are found together in altered basalts in the stockwork of the Trans-Atlantic Geotraverse (TAG) hydrothermal mound on the Mid-Atlantic Ridge where they formed at temperatures from 210° to 390°C (Honnorez et al., 1983).

Some of the olivine clasts in the tuffaceous layers show kink banding. Many mantle rocks such as lehrzolites and dunites show kink banding in olivine crystals. Also, tectonized peridotites often show such microstructures (e.g., Ishii et al., 1992). The kink bands are formed where shear is applied to the olivine (e.g., Kirby, 1983). Dislocations by shear stress in the olivine crystals generate the kink bands. Another interesting feature is masses of fibrous lines seen in some olivine crystals. Iron oxide exsolution may be the cause of this structure. The presence of kink bands and fibrous structures indicates that olivine crystals in the crystal vitric tuffs were subjected to tectonic deformation.

Other Observations

We measured bulk density using GRA, magnetic susceptibility, natural gamma ray (NGR), and compressional velocity (V_P) on whole-core sections with the multisensor track (MST). Moisture and density and compressional wave velocities were also measured on selected individual samples. The yellowish brown clay in Core 200-1223A-1H has 83% porosity and a compressional velocity of 1.5 km/s. GRA density values from 0 to 10 mbsf gradually increase downhole from 1.2 to 2.2 g/cm^3. The GRA densities agree with the bulk densities of the individual measurements, except for Core 200-1223A-3X, where GRA densities of the vitric tuff in Core 200-1223A-3X average 1.8 g/cm^3, but bulk densities are slightly higher. Corresponding compressional velocity values for the vitric tuff in Core 200-1223A-3X average ~3.3 km/s. Bulk density, grain density, and compressional velocity for the siltstone in Core 200-1223A-4X are 1.6–2.0 g/cm^3, 2.8 g/cm^3, and 1.8–3.3 km/s, respectively. The vitric tuff in Core 200-1223A-6X has a 2.1 g/cm^3 bulk density, a 2.6 g/cm^3 grain density, and a 4.0 km/s compressional velocity. Grain densities of vitric tuff in Core 200-1223A-6X are lower than those in Core 200-1223A-3X. This is caused by the higher levels of alteration in Core 200-1223A-6X. The compressional wave velocities of the crystal vitric tuffs in lithologic Unit 5 (just below sand) and lithologic Unit 11 are ~3 and ~4 km/s, respectively. However, the bulk densities for both are similar, at ~2.2 g/cm^3. The compressional wave velocity for the upper crystal vitric tuff deviates from the generally expected compressional velocity-density relationship (e.g., Johnston and Christensen, 1997), possibly because of the weak consolidation of lithologic Unit 5. Compressional velocity and density increase with depth within the turbidites of lithologic Units 1 and 2, and the gradients can be associated with the graded bedding in the turbidites. Using this velocity and density increase with depth, we can identify the presence of the turbidite layers.

The magnetostratigraphy for Hole 1223A appears to record all the major chrons and subchrons from Chron C1n (the Brunhes Chron; 0.0–0.780 Ma) through Chron 2r (1.95–2.581 Ma). The Brunhes normal polarity interval spans only the top 14 cm of Core 200-1223A-1H, which is thinner than expected by ~1 m based on prior piston coring in the vicinity. Thus, we may not have recovered the very upper meter or so of the sedimentary section, or sedimentation rates may vary locally. The top and base of the normal polarity interval interpreted as Subchron C1r.1n (Jaramillo Subchron; 0.99–1.07 Ma) are at 0.79 and 1.23 mbsf, respectively. The top and base of the normal polarity interval interpreted as Chron C2n (the Olduvai Chron; 1.77–1.95 Ma) are at 2.02 and ~7 mbsf, respectively. All recovered core below ~7 mbsf appears to be of reversed polarity, which is interpreted to be the upper part of Chron C2r, possibly with the entire interval lying within Subchron C2r.1r (1.95–2.14 Ma).

We did not have a paleontologist on board, but Bob Goll and John Firth from ODP-TAMU did postcruise examinations of sediment samples for radiolarians and calcareous nannofossils, respectively. No calcareous nannofossils were found. Of six samples that were examined for radiolarians, two could be used for dating and indicate an early Eocene age. This conflicts with the magnetostratigraphic dates. We consider that reworking is likely in these landslide deposits and that the early Eocene age is not representative of the depositional age of the units.

Microbiological analyses from Site 1223 were conducted on sediments and tuffs. Most probable number (MPN) series were prepared from all samples in order to determine the concentration of sulfate-reducing as well as fermentative bacteria. From Site 1223, 25 distinct microbial colonies could be isolated to pure cultures and could be further characterized as facultatively anaerobic organisms forming stable cell aggregates under appropriate conditions.

Interpretation

As noted above, three types of material—unconsolidated clay and volcanic sediments, weakly consolidated claystones and siltstones, and crystal vitric tuffs—were recovered in the cores from Hole 1223A. The first type consists of interbedded layers of pelagic clays and volcaniclastic sediments thought to be turbidites. These turbidites potentially originated from one of the Hawaiian Islands. The sand, which is present in the upper 15 m of the section, has a high vitric component suggesting a volcanic source. The claystones and siltstones, on the other hand, which are present in both the middle and the bottom of the section cored, have a lower percentage of coarse volcanic material.

We considered two hypotheses for the origin of these claystones and siltstones. The first describes them as sedimentary rocks derived from detrital material from the Hawaiian Islands and emplaced by turbidity currents. The second hypothesis describes them as volcanic tuffs derived from submarine pyroclastic flows either from the Hawaiian Islands or from a local vent. Unwelded submarine pyroclastics in general tend to have a massive to poorly bedded and poorly sorted lower unit and an upper thinly bedded unit (Fiske and Matsuda, 1964; Bond, 1973; Niem, 1977). Fisher and Schmincke (1984) state that it is very difficult to distinguish between the deposits of these two types of events.

The vitric tuffs that are present below the sands and at the top and in the middle of the claystones and siltstones are also problematic. Hypotheses for their origin must address the following questions:

1. Why are they indurated at such a shallow depth?
2. Why are they so glass rich?
3. Why do they have so much fresh olivine?
4. Why is their general character tholeiitic?
5. Were they warm to fairly hot at, or shortly after, deposition?

Alteration and cementation in the lower tuff and the transformations in sediments at its lower contact probably occurred at a high temperature, perhaps 150°–320°C, consistent with zeolite metamorphic conditions and the occurrences of wairakite/analcime, paragonite, and anhydrite described above.

Formation of palagonite was not isochemical. In this case, it involved loss of both CaO and Sr and addition of K_2O to the bulk compositions of the rocks (see **"Geochemistry,"** p. 13, in "Principal Results" in "Hawaii-2 Observatory"). These exchanges required substantial flow of fluids derived from seawater through the porous tuffs. The presence of anhydrite and paragonite, a sodic mica, suggests that some of the fluids were brines.

We consider two origins for the crystal vitric tuffs, a Hawaiian Island source and a local source. If the source of the tuffs was local, they were presumably produced by igneous activity, either intrusion or extrusion, that has not yet been documented for this part of the Hawaiian Arch.

Neither lava fields nor fissures associated with such hypothetical volcanism are evident in seismic data of the smoothly sedimented crest of the arch near Site 1223, but no high-resolution bathymetry data have been taken of the surrounding area. The nearest known young volcanism on the arch occurred at the North Arch volcanic field, some 200 km to the northwest. There, lavas and tuffs are alkalic olivine basalts, basanites, and olivine nephelinites (Dixon et al., 1997), very unlike the tholeiitic precursors to the indurated tuffs and other sedimentary rocks of Hole 1223A. Similar volcanism near the drill site thus would only coincidentally have driven hydrothermal fluids through the sediments that we cored.

A possible scenario for a Hawaiian source is that a very large eruption of Hawaiian tholeiite occurred when a deep magma reservoir was breached by catastrophic failure of the flank of a volcano, similar to the 1980 eruption of Mount Saint Helens (Fig. **F27**) (Moore and Albee, 1981). This may have occurred on Oahu when the northeast flank of Koolau Volcano collapsed, producing the giant Nuuanu debris avalanche. Sudden decompression caused pressure release, vesiculation, and expansion of the magma. The magma erupted as a directed blast and passed over the collapsing blocks now strewn on the seafloor as a submarine pyroclastic debris flow that reached over the Hawaiian Arch. In this scenario, if the material reached the area of Site 1223 (300 km away) quickly enough in a bottom-hugging density flow, it may have retained enough heat to cause the alteration and induration of the two crystal vitric tuffs. Water surrounding a hot pyroclastic flow may become vaporized, creating a water vapor barrier around the flow which helps to insulate the flow and prevent mixing (Kato et al., 1971; Yamazaki et al., 1973).

F27. Schematic drawing of a landslide and the resulting eruption, p. 62.

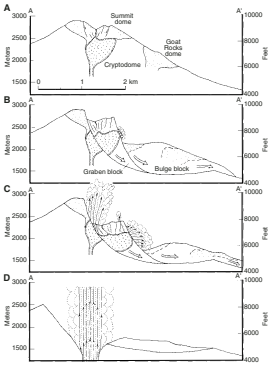

Subaerial pyroclastic flows have been observed with velocities ranging from 14 km/hr (Tsuya, 1930) to 230 km/hr (Moore and Melson, 1969). They have traveled great distances (>100 km) and surmounted obstacles >600 m high (Fisher and Schmincke, 1984). Their mobility has been attributed to several factors, namely exsolution of gas from glassy particles, gas being released when particles are broken, and the heating of the medium causing thermal expansion (e.g., Sparks, 1979). The gas reduces the friction between particles, allowing the flow to travel faster. In addition to moving at tremendous speeds, pyroclastic flows are very good at retaining heat. Boyd (1961) calculated that cold air has a minimal effect on a hot pyroclastic flow. Therefore, a hot pyroclastic flow may remain at almost magmatic temperatures during transport and even after deposition.

The above applies to subaerial pyroclastic eruptions; subaqueous pyroclastic flows are less well understood. A massive, coarse-grained, subaqueous pyroclastic flow deposit over 4.5 m thick and extending up to 250 km from its source was recovered in the Grenada Basin, Lesser Antilles. Carey and Sigurdsson (1980) interpreted the deposit to be a debris flow that originated when a hot subaerially erupted pyroclastic flow entered the ocean. The debris flow incorporated pelagic sediment and seawater, decreasing internal friction, giving the flow great mobility and the ability to suspend large fragments. Thermal remanent magnetism of a similar deposit (Pliocene–Miocene in age) was interpreted by Kato et al. (1971) to have been deposited at temperatures of ~500°C.

An alternative is that the tuffs were deposited containing some heat. Nevertheless, the amount of heat in a few meters of such materials is unlikely to have driven fluid flow for very long, at least if the deposit was small. On the other hand, a widespread blanket of hot material de-

posited suddenly might have acted as a compressive load on uncompacted surface sediments and, where sufficiently thick, as an impermeable barrier to fluids mobilized by sudden compaction. The fluids, thus forced to flow laterally, may have sustained high temperatures at the base of the tuff for some time and there produced the most concentrated effects of alteration and contact metamorphism. A somewhat similar effect was postulated for the pattern of fluid flow at the top of basaltic basement, beneath ~100 m of volcaniclastic turbidites in the eastern Mariana Trough at Deep Sea Drilling Project Site 456 (Natland and Hekinian, 1982). Greenschist facies hydrothermal conditions were reached, and both wairakite and cristobalite formed in the sediments at the contact.

This hypothesis provides a mechanism for directing fluid flow and thus concentrating the most pronounced alteration effects in the tuff beds themselves, rather than in adjacent sediments. This probably would not have been the case if hydrothermal flow was directed along vertical fissures associated with local igneous action. Admittedly, the geometry of fluid flow in variably permeable sediments is difficult to extrapolate over long distances from the vantage of a single hole.

At Site 1223, the two tuffs, although about equally indurated, experienced alteration that was different either in type or in degree. The upper tuff is not palagonitized, although it is cemented by clay minerals and zeolites, and almost all of its original glass is still fresh. Probably the essential difference was temperature—lower for the upper tuff—although the upper tuff may have experienced less fluid flow as well. Lower temperature and reduced fluid flow should mean the same thing, less heat was available to drive fluids, whether or not it was derived locally or from a more distant source.

Both the whole-rock ICP-AES analyses and the preliminary electron microprobe analyses of individual glass fragments within both crystal vitric tuffs (Unit 5 and Subunit 11B) support a Hawaiian Islands source. Unlike the whole-rock ICP-AES analyses, the effects of olivine accumulation and alteration do not complicate the glass geochemistry. Therefore, it is easier to compare the glass geochemistry from the tuffs with the geochemistry from other potential sources (i.e., Hawaiian Islands and North Arch volcanic field). The glass geochemistry suggests that the tuffs have tholeiitic basalt compositions and are similar to Hawaiian tholeiitic basalts.

Futhermore, the glasses in both tuffs have low S concentrations (majority <300 ppm) (S.B. Sherman, unpubl. data). Sulfur concentrations can be used to estimate depths of eruption (e.g., Moore and Fabbi, 1971; Dixon et al., 1991). Low S concentrations (<200 ppm) are indicative of significant degassing and predominantly result from subaerial eruptions. Deep submarine glasses with low S contents were recovered from Puna Ridge, which is a submarine extension of Kilauea Volcano. The low S abundances for these glasses were attributed to mixing between lavas that had degassed at or near the subaerial surface with the rift lavas that were erupted underwater (Clague et al., 1995). Therefore, the low S concentrations in the glasses in the tuffs suggest that they were erupted subaerially or at least mixed with subaerial lavas. A subaerial eruption supports a Hawaiian rather than a North Arch source for the tuffs. Not only is the North Arch volcanic field submarine, the majority of the glasses from the North Arch volcanic field have S contents >300 ppm (Dixon et al., 1997). It may be difficult to imagine the source for the tuffs from Site 1223 as one of the Hawaiian Islands, but the geochemical evidence indicates it is the most likely option.

Further discussion of the provenance of the Site 1223 materials is given in "Provenance and Petrogenesis," p. 28.

Provenance and Petrogenesis

It is necessary to determine the provenance of the Site 1223 materials in order to confirm whether these materials did or did not originate in the Nuuanu Landslide event(s). An island provenance would be a prerequisite if this were indeed the case. On the other hand, a local source of heat seemed required to explain the induration of the two welded tuffs so near the seafloor. A local provenance for the tuffs, perhaps a nearby seamount, would be consistent with this hypothesis. Accordingly, we compared bulk compositions of samples from Hole 1223A with varieties of Hawaiian basaltic rocks, with lavas of the North Arch volcanic field, some 200 km to the northwest, and with both normal and enriched abyssal basalts (N-MORB and E-MORB). Our initial petrographic interpretation was that the olivine-bearing glass shards in the tuffs resembled types of Hawaiian picritic tholeiite, but the issue still remained whether tholeiite itself might have erupted recently along the Hawaiian Arch and provided a local source for the tuffs essentially identical to the islands.

Existence of a significant component of aluminous detrital clay, produced ultimately by subaerial erosion, confirmed by chemical analyses, sets most of these issues at rest. The source of the aluminous component in all of the sediments and tuffs was clearly the islands, making it extremely unlikely that a separate local source provided the volcanic glass shards and associated minerals and lithic fragments. But what can now be said in more detail about the composition of source materials? Tholeiitic basalt is, of course, the most voluminous of Hawaiian lava types (e.g., Macdonald and Katsura, 1964; Clague and Dalrymple, 1987). However, alkalic olivine basalts, basanites, and olivine nephelinites erupted during both the earliest and latest stages of Hawaiian volcanism, and it is possible that these at least contributed volcaniclastic materials to the sedimentary succession at Site 1223.

Major oxide discriminant diagrams (Fig. F28A, F28B) show the similarity of analyzed samples from Hole 1223A to Hawaiian tholeiite, represented by basalt glasses from Kilauea Volcano and its undersea extension, Puna Ridge (Clague et al., 1995). The diagrams also show strong differences between our samples (as well as Kilauea tholeiites) and Hawaiian alkalic olivine basalts, basanites, and olivine nephelinites from three localities—the North Arch volcanic field (Dixon et al., 1997), the Honolulu Volcanic Series of Oahu (Jackson and Wright, 1970; Clague and Frey, 1982), and the Hana Volcanic Series of Haleakala Volcano on the island of Maui (Chen et al., 1991). Data are also plotted for a representative suite of abyssal tholeiites from the East Pacific Rise (J. Natland, Y. Niu, and P. Castillo, unpubl. data). This suite includes a wide range of primitive and differentiated abyssal tholeiites (N-MORB). Samples from Site 1223 clearly differ from these as well.

Because we compare bulk sediment compositions with compositions of glasses from Kilauea and the East Pacific Rise, the effects of abundant olivine in Site 1223 samples need to be taken into account. Olivine forms 9–13 wt% of the mode of the vitric tuffs. If its composition is about Fo_{85}, the effect of subtracting 13 wt% of olivine from the bulk composition of a tuff with 10.5 wt% Al_2O_3, 47.5 wt% SiO_2, and 11 wt% iron as Fe_2O_3 is shown by the arrows in Figure F28A and F28B. This is

F28. Major oxide discriminant diagrams, p. 63.

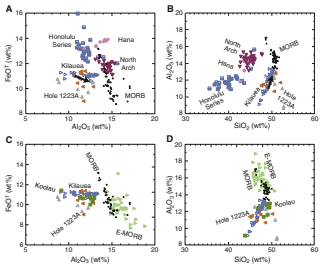

about the composition of Group 1 tuff in Figure F29 with the least amount of detrital clay in its makeup. The tip of the arrows in Figure F28 therefore is approximately that of an aphyric basalt or basalt glass still very closely resembling the composition of Kilauea tholeiite. In amounts of these oxides, it is far from the compositions of Hawaiian alkalic basaltic lavas and from MORB.

In Figure F28C and F28D, compositions of samples from Hole 1223A are explicitly compared with E-MORB glasses, using a compilation drawn from the literature, and with eight analyses of magnesian tholeiites and tholeiitic picrites from Koolau Volcano (Frey et al., 1994). E-MORB resembles N-MORB, except in being slightly more aluminous. Most of the several Koolau lavas have slightly higher SiO_2 contents and lower iron as Fe_2O_3 than Kilauea tholeiitic glasses. In these diagrams, the effects of the addition of detrital clays and of authigenesis make it difficult to describe samples from Hole 1223A as more like one of the Hawaiian volcanoes than the other.

Figure F30 provides additional hints about the particular Hawaiian provenance of samples from Hole 1223A. Again, data for MORB, E-MORB, Kilauea-Puna Ridge, and Koolau Volcano are plotted for comparison. Again, samples from Hole 1223A resemble Hawaiian tholeiites rather than MORB or E-MORB. Several of the tuff samples from Hole 1223A, including those falling in Group 1 in Figure F29A and F29B, have higher SiO_2, lower Ba, and lower Zr than Kilauea glasses at given MgO content (Fig. F30). In all these respects, they more closely resemble Koolau. For SiO_2 and Ba, these estimations may be complicated by the presence of some detrital clay, and in two samples, Ba clearly is too high. However, the comparison holds for those samples with the least amounts of clay or, that is, highest CaO contents. In addition, Zr is an element that is usually unaffected by alteration. It is also usually precisely and consistently measured from one laboratory to the next. The measurements should give a relatively solid estimation of its original concentration in volcanic glass and lithic fragments in the sediments and tuffs, diluted by up to 13% with olivine and only small amounts of clay in several of the tuffs. The effect of subtraction of olivine with ~45 wt% MgO and no Zr is given by the arrow in Figure F30C. Addition or subtraction of olivine cannot direct residual liquid compositions from Koolau into the field of Kilauea tholeiites. Dilution by clays in samples of Hole 1223A will draw compositions nearly toward the origin (no Zr and <1 wt% MgO), but in several samples, this effect should not be too important. The diagram suggests, then, a Koolau provenance for the vitric tuffs. The higher SiO_2, lower Ba, and lower iron as Fe_2O_3 (Fig. F28C) of the same samples support this contention.

A great number of glass shards in the vitric tuffs have olivine phenocrysts that enclose small Cr spinel crystals. The bulk samples are fairly olivine rich, approaching the bulk compositions of Hawaiian tholeiitic picrites in many respects. The high Ni, Cr, and MgO contents of all the samples indicate the importance of olivine tholeiite, and perhaps even picrite, in their provenance. Olivine tholeiite is not atypical of Hawaiian volcanoes at the shield-building stage, but many Hawaiian tholeiites are far more differentiated than this and either have no olivine on the liquidus or very little olivine in their general petrography. Average Hawaiian tholeiite has ~7.5–8 wt% MgO (Engel and Engel, 1970).

Picritic Hawaiian tholeiite is thought to reside at deep levels in the conduit-reservoir systems of Kilauea and Mauna Loa Volcanoes, where it crystallized to produce abundant dunite, a common type of xenolith

F29. Ternary diagrams showing effects of adding detrital and authigenic clays to basaltic volcaniclastic material, p. 64.

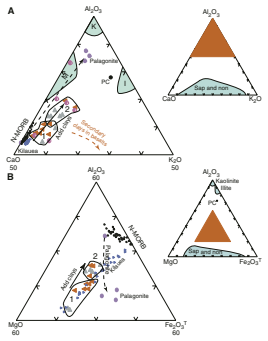

F30. Comparison of analyses of samples from Hole 1223A, p. 65.

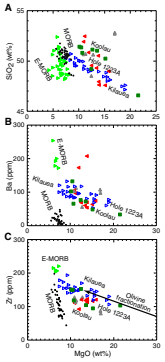

in late-stage Hawaiian basalts (Jackson, 1968). More differentiated lavas develop in the shallow reaches of rift zones, where they mix with more primitive lavas during eruptive cycles (e.g., Wright and Fiske, 1971). If the magmas that supplied most of the glass in the two vitric tuffs of Hole 1223A are truly primitive with, for example, high MgO in the glasses; if, in addition, the associated olivines are also forsteritic; and if, in particular, the tuffs each have a restricted range of primitive glass compositions; this evidence together would indicate that the sources were very large eruptions of tholeiitic magma, dwarfing the volume of any eruptions known from the islands themselves. Such a quantity of magma could only be derived from the deep, high-temperature reaches of Hawaiian magma reservoirs during the main shield-building stage. To reach into the main reservoir, below the shallow active rift system, would require one or more massive failures of the flank of the volcano of the type inferred for the Nuuanu Landslide.

Summary

One of the objectives of coring at this site was to try to determine if the Nuuanu Landslide occurred as a single or as a multistage event by inference from the number of turbidites recovered. Several unconsolidated volcaniclastic turbidites of varying thickness were recovered. Paleomagnetic data indicate that the uppermost turbidite has an estimated age between 0.99 and 1.07 Ma, that the other turbidites have an age between 1.77 and 1.95 Ma, and that other underlying units are older than 1.95 Ma. A surprising discovery was the recovery of the two crystal vitric tuff layers. Preliminary geochemical analyses indicate these tuffs are MgO-rich tholeiitic basalts and have geochemical similarities to Hawaiian tholeiites. However, there remain some other possibilities for the sources of crystal vitric tuffs, such as a part of the Hawaiian Arch or a nearby seamount. The genesis of crystal vitric tuffs can be complicated. Questions arise about why they are indurated so close to the seafloor, why they are so glassy, why they are so rich in fresh olivine, why they include kink banding and fibrous structures in the olivine crystals, and why they were warm or even hot when emplaced.

Preliminary results are summarized below:

1. We recovered several lithologic units that were transported to the site most likely by a number of distinct landslide events. The origin of the deposits, as indicated by petrographic inspection and geochemistry, is the Hawaiian Islands. Furthermore, the age of the transported units is coeval with the age estimate for the Nuuanu Landslides. The turbidites associated with the landslides were also identified by physical properties changes.
2. Two pyroclastic events similar to the 1980 Mount Saint Helens' eruption but an order of magnitude larger occurred on Koolau Volcano at ~2 Ma. These events may correlate with the collapse of the flank of the volcano and the formation of the Nuuanu debris field.
3. The thickness of turbidites and pyroclastic material corresponding in age to the Nuuanu Landslide (1.8–2.4 Ma) is >38 m at Site 1223, over 300 km from Oahu. We did not core to the bottom of this sequence; thus, the related deposits may be thicker, and additional landslide events may have occurred.

REFERENCES

Acton, G.D., and Gordon, R.G., 1994. Paleomagnetic tests of Pacific plate reconstructions and implications for motion between hotspots. *Science,* 263:1246–1254.

Alt, J.C., Kinoshita, H., Stokking, L.B., et al., 1993. *Proc. ODP, Init. Repts.,* 148: College Station, TX (Ocean Drilling Program).

Atwater, T., 1989. Plate tectonic history of the northeast Pacific and western North America. *In* Winterer, E.L., Hussong, D.M., and Decker, R.W. (Eds.), *The Eastern Pacific Ocean and Hawaii*. Geol. Soc. Am., Geol. of North America Ser., N:21–72.

Atwater, T., and Severinghaus, J., 1989. Tectonic maps of the northeast Pacific. *In* Winterer, E.L., Hussong, D.M., and Decker, R.W. (Eds.), *The Eastern Pacific Ocean and Hawaii*. Geol. Soc. Am., Geol. of North America Ser., N:15–20.

Bond, G.C., 1973. A late Paleozoic volcanic arc in the eastern Alaska Range, Alaska. *J. Geol.,* 81:557–575.

Boyd, F.R., 1961. Welded tuff and flows in the rhyolite plateau of Yellowstone Park, Wyoming. *Geol. Soc. Am. Bull.,* 72:387–426.

Butler, R., 1995a. The Hawaii-2 Observatory: a deep-ocean geoscience facility reusing the Hawaii-2 telephone cable. *In* Purdy, G.M., and Orcutt, J.A. (Eds.), *Broadband Seismology in the Oceans—Towards a Five-Year Plan:* Washington, D.C. (Joint Oceanographic Institutions), 50–58.

————, 1995b. Proposed station locations and rationale for the OSN component of GSN. *In* Purdy, G.M., and Orcutt, J.A. (Eds.), *Broadband Seismology in the Oceans—Towards a Five-Year Plan:* Washington, D.C. (Joint Oceanographic Institutions), 20–25.

Cande, S.C., and Kent, D.V., 1992. A new geomagnetic polarity time scale for the Late Cretaceous and Cenozoic. *J. Geophys. Res.,* 97:13917–13951.

Carey, S.N., and Sigurdsson, H., 1980. The Roseau ash: deep-sea tephra deposits from a major eruption on Dominica, Lesser Antilles arc. *J. Volcanol. Geotherm. Res.,* 7:67–86.

Chave, A.D., Butler, R., Pyle, T.E. (Eds.), 1990. *Workshop on Scientific Uses of Undersea Cables*. Washington, D.C. (Joint Oceanographic Institutions).

Chave, A.D., Green, A.W. Jr., Evans, R.L., Filloux, J.H., Law, L.K., Petitt, R.A. Jr., Rasson, J.L., Schultz, A., Spiess, F.N., Tarits, P., Tivey, M., and Webb, S.C., 1995. *Report of a Workshop on Technical Approaches to Construction of a Seafloor Geomagnetic Observatory:* Woods Hole, MA (Woods Hole Oceanographic Institution).

Chen, C.-Y., Frey, F.A., Garcia, M.O., Dalrymple, G.B., and Hart, S.R., 1991. The tholeiite to alkalic basalt transition at Haleakala Volcano, Maui, Hawaii. *Contrib. Mineral. Petrol.,* 106:183–200.

Clague, D.A., and Dalrymple, G.B., 1987. The Hawaiian-Emperor volcanic chain, Part I. Geologic evolution. *In* Decker, R.W., Wright, T.L., and Stauffer, P.H. (Eds.), *Volcanism in Hawaii*. U.S. Geol. Surv. Prof. Pap., 5–73.

Clague, D.A., and Frey, F.A., 1982. Petrology and trace element chemistry of the Honolulu volcanics, Oahu: implications for the oceanic mantle below Hawaii. *J. Petrol.,* 23:447–504.

Clague, D.A., Moore, J.G., Dixon, J.E., and Friesen, W.B., 1995. Petrology of submarine lavas from Kilauea's Puna Ridge, Hawaii. *J. Petrol.,* 36:299–349.

Collins, J.A., Vernon, F.L., Orcutt, J.A., Stephen, R.A., Peal, K.R., Wooding, F.B., Spiess, F.N., and Hildebrand, J.A., 2001. Broadband seismology in the oceans: lessons from the Ocean Seismic Network pilot experiment. *Geophys. Res. Lett.,* 28:49–52.

Cronan, D.S., and Toombs, J.S., 1969. The geochemistry of manganese nodules and associated pelagic deposits from the Pacific and Indian Oceans. *Deep-Sea Res.,* 16:335–339.

Davis, E.E., Becker, K., Pettigrew, T., Carson, B., and MacDonald, R., 1992. CORK: a hydrologic seal and downhole observatory for deep-ocean boreholes. *In* Davis,

E.E., Mottl, M.J., Fisher, A.T., et al., *Proc. ODP, Init. Repts.,* 139: College Station, TX (Ocean Drilling Program), 43–53.

Dixon, J.E., Clague, D.A., and Stolper, E.M., 1991. Degassing history of water, sulfur, and carbon in submarine lavas from Kilauea Volcano, Hawaii. *J. Geol.,* 99:371–394.

Dixon, J.E., Clague, D.A., Wallace, P., and Poreda, R., 1997. Volatiles in alkalic basalts from the North Arch volcanic field, Hawaii: extensive degassing of deep submarine-erupted alkalic series lavas. *J. Petrol.,* 38:911–939.

Doell, R.R., and Dalrymple, G.B., 1973. Potassium-argon ages and paleomagnetism of the Waianae and Koolau Volcanic Series, Oahu, Hawaii. *Geol. Soc. Am. Bull.,* 84:1217–1242.

Duennebier, F.K., Butler, R., Chave, A., Harris, D., Jolly, J., and Babinec, J., 2000. Broadband seismograms from the Hawaii-2 Observatory [paper presented at Am. Geophys. Union Mtg., San Francisco, Fall 2000].

Duennebier, F.K., Harris, D.W., Jolly, J., Babinec, J., Copson, D., and Stiffel, K., 2002. The Hawaii-2 Observatory seismic system. *IEEE J. Oceanic Eng.,* 27:212–217.

Engel, A.E.J., and Engel, C.G., 1970. Mafic and ultramafic rocks. *In* Maxwell, A.E. (Ed.), *The Sea* (Vol. 4, Part 1): New York (Wiley-Interscience), 465–519.

Fisher, R.F., and Schmincke, H.-U., 1984. *Pyroclastic Rocks:* New York (Springer Verlag), 400–407.

Fiske, R.S., and Matsuda, T., 1964. Submarine equivalents of ash flows in the Tokiwa Formation, Japan. *Am. J. Sci.,* 262:76–106.

Forsyth, D., Dziewonski, A., and Romanowicz, B., 1995. Scientific objectives and required instrumentation. *In* Purdy, G.M., and Orcutt, J.A. (Eds.), *Broadband Seismology in the Oceans—Towards a Five-Year Plan:* Washington, D.C. (Joint Oceanographic Institutions), 8–18.

Foucher, J.-P., Harmegnies, F., Floury, L., Lanteri, N., and Henry, P., 1995. Long-term observation and testing in boreholes: the ODP Leg 156 experiment. *In* Montagner J.-P., and Lancelot, Y. (Eds.), *Multidisciplinary Observatories on the Deep Seafloor:* Marseille (INSU/CNRS), 109–110.

Frey, F.A, Garcia, M.O., and Roden, M., 1994. Geochemical characteristics of Koolau Volcano: implications of intershield geochemical differences among Hawaiian volcanoes. *Geochim. Cosmochim. Acta,* 58:1441–1462.

Grim, R.E., 1964. *Clay Mineralogy:* New York (McGraw-Hill).

Herrero-Bervera, E., Cañon-Tapia, E., Walker, G.P.L., Guerrero-Garcia, J.C., 2002. The Nuuanu and Wailau giant landslides: insights from paleomagnetic and anisotropy of magnetic susceptibility (AMS) studies. *Phys. Earth Planet. Inter.,* 129:83–98.

Honnorez, J., Laverne, C., Hubberten, H.-W., Emmermann, R., and Muehlenbachs, K., 1983. Alteration processes in Layer 2 basalts from Deep Sea Drilling Project Hole 504B, Costa Rica Rift. *In* Cann, J.R., Langseth, M.G., Honnorez, J., Von Herzen, R.P., White, S.M., et al., *Init. Repts. DSDP,* 69: Washington (U.S. Govt. Printing Office), 509–546.

Ishii, T., Robinson, P.T., Maekawa, H., and Fiske, R., 1992. Petrological studies of peridotites from diapiric serpentinite seamounts in the Izu-Ogasawara-Mariana forearc, Leg 125. *In* Fryer, P., Pearce, J.A., Stokking, L.B., et al., *Proc. ODP, Sci. Results,* 125: College Station, TX (Ocean Drilling Program), 445–485.

Jackson, E.D., 1968. The character of the lower crust and upper mantle beneath the Hawaiian Islands. *Proc. 23rd Int. Geol. Conf.,* 1:135–150.

Jackson, E.D., and Wright, T.L., 1970. Xenoliths in the Honolulu Volcanic Series, Hawaii. *J. Petrol.,* 11:405–430.

Johnston, J.E., and Christensen, N.I., 1997. Seismic properties of Layer 2 basalts. *Geophys. J. Intr.,* 128:285–300.

Kasahara, J., Uada, H., Sato, T., and Kinoshita, H., 1998. Submarine cable OBS using a retired submarine telecommunication cable: GeO-TOC program. *Phys. Earth Planet. Inter.,* 108:113–127.

Kato, I., Murai, I., Yamazaki, T. and Abe, M., 1971. Subaqueous pyroclastic flow deposits in the upper Donzurubo Formation, Nijo-san District, Osaka, Japan. *J. Geol. Soc. Jpn.,* 77:193–296.

Kirby, S.H., 1983. Rheology of the lithosphere. *Rev. Geophys.,* 21:1458–1487.

Laverne, C., Belarouchi, A., and Honnorez, J., 1996. Alteration mineralogy and chemistry of the upper oceanic crust from Hole 896A, Costa Rica Rift. *In* Alt, J.C., Kinoshita, H., Stokking, L.B., and Michael, P.J. (Eds.), *Proc. ODP, Sci. Results,* 148: College Station, TX (Ocean Drilling Program), 151–170.

Leinen, M., 1989. The pelagic clay province of the North Pacific Ocean. *In* Winterer, E.L., Hussong, D.M., and Decker, R.W. (Eds.), *The Geology of North America* (Vol. N): *The Eastern Pacific Ocean and Hawaii.* Geol. Soc. Am., 323–335.

Lenat, J.-F., Vincent, P., and Bachelaery, P., 1989. The offshore continuation of an active basaltic volcano: Piton de la Fournaise. *J. Volcanol. Geotherm. Res.,* 36:1–36.

Macdonald, G.A., and Katsura, T., 1964. Chemical composition of Hawaiian lavas. *J. Petrol.,* 5:82–133.

Mammerickx, J., 1989. Large-scale undersea features of the northeast Pacific. *In* Winterer, E.L., Hussong, D.M., Decker, R.W. (Eds.), *The Eastern Pacific Ocean and Hawaii.* Geol. Soc. Am., Geol. of North Am. Ser., N:5–13.

Masson, D.G., Watts, A.B., Gee, M.J.R., Urgeles, R., Mitchell, N.C., Le Bas, T.P., Canals, M., 2002. Slope failures on the flanks of the western Canary Islands. *Earth Sci Rev.* 57:1–35.

Menard, H.W., 1964. *Marine Geology of the Pacific:* New York (McGraw-Hill).

Miyashiro, A., 1973. *Metamorphism and Metamorphic Belts:* London (George Allen and Unwin).

Moore, G.W., and Moore, J.G., 1988. Large scale bedforms in boulder gravel produced by giant waves in Hawaii. *In* Clifton, H.E. (Ed.), *Sedimentologic Consequences of Convulsive Geologic Events.* Spec. Pap.—Geol. Soc. Am., 229:101–109.

Moore, J.G., 1964. Giant submarine landslides on the Hawaiian Ridge. *Geological Survey Research 1964.* U.S. Geol. Surv. Prof. Pap., 95–98.

Moore, J.G., and Albee, W.C., 1981. Topographic and structural changes, March–July 1980; photogrammetric data. *In* Lipman, P.W., and Mullineaux, D.R. (Eds.), *The 1980 Eruptions of Mount St. Helens, Washington.* U.S. Geol. Surv. Prof. Pap., 1250.

Moore, J.G., Clague, D.A., Holcomb, R.T., Lipman, P.W., Normark, W.R., and Torresan, M.E., 1989. Prodigious submarine landslides on the Hawaiian Ridge. *J. Geophys. Res.,* 94:17,465–17,484.

Moore, J.G., and Fabbi, B.P., 1971. An estimate of the juvenile sulfur content of basalt. *Contrib. Mineral. Petrol.,* 33:118–127.

Moore, J.G., and Melson, W.G., 1969. Nuees ardentes of the 1968 eruption of Mayon Volcano, Philippines. *Bull. Volcanol.,* 33:600–620.

Moore, J.G., Normark, W.R., and Holcomb, R.T., 1994. Giant Hawaiian landslides. *Annu. Rev. Earth Planet. Sci.,* 22:119–144.

Naka, J., Takahashi, E., Clague, D., Garcia, M., Hanyu, T., et al., 2000. Tectono-magmatic processes investigated at deep-water flanks of Hawaiian volcanoes. *Eos, Trans. Am. Geophys. Union.,* 81:227–230.

Natland, J., and Hekinian, R., 1982. Hydrothermal alternation of basalts and sediments at Deep Sea Drilling Project Site 456, Mariana Trough. *In* Hussong, D.M., Uyeda, S., et al., *Init. Repts., DSDP,* 60: Washington (U.S. Govt. Printing Office), 759–767.

Niem, A.R., 1977. Mississippian pyroclastic flow and ash-fall deposits in the deep-marine Ouachita flysch basin, Oklahoma and Arkansas. *Geol. Soc. Am. Bull.,* 88:49–61.

Noack, Y., Emmermann, R., and Hubberten, H.-W., 1983. Alteration in Site 501 (Leg 68) and Site 504 (Leg 69) basalts: preliminary results. *In* Cann, J.R., Langseth, M.G., Honnorez, J., Von Herzen, R.P., White, S.M., et al., *Init. Repts. DSDP,* 69: Washington (U.S. Govt. Printing Office), 497–508.

Normark, W.R., Moore, J.G., and Torresan, M.E., 1993. Giant volcano-related landslides and the development of the Hawaiian Islands. *In* Schwab, W.C., Lee, H.J., Twichell, D.C. (Eds.), *Submarine Landslides: Selected Studies in the U.S. Exclusive Economic Zone*. U.S. Geol. Surv. Bull., 2002:184–196.

Orcutt, J.A,. and Stephen, R.A., 1993. OSN seismograph system is underway. *Seismic Waves,* 2:3–5.

Petronotis, K.E., Gordon, R.G., and Acton, G.D., 1994. A 57 Ma Pacific plate paleomagnetic pole determined from a skewness analysis of crossings of marine magnetic Anomaly 25r. *Geophys. J. Int.,* 118:529–554.

Pringle, M.S., Sager, W.W., Sliter, W.V., and Stein, S. (Eds.), 1993. *The Mesozoic Pacific: Geology, Tectonics, and Volcanism*. Geophys. Monogr., Am. Geophys. Union, 77.

Purdy, G.M., 1995. A five year plan. *In* Purdy, G.M., and Orcutt, J.A. (Eds.), *Broadband Seismology in the Oceans—Towards a Five-Year Plan:* Washington, D.C. (Joint Oceanographic Institutions), 68–75.

Raitt, R.W., 1963. The crustal rocks. *In* Hill, M.N. (Ed.), *The Sea—Ideas and Observations on Progress in the Study of the Seas* (Vol. 3): *The Earth Beneath the Sea:* New York (Wiley-Interscience), 85–102.

Rees, B.A., Detrick, R.S., and Coakley, B.J., 1993. Seismic stratigraphy of the Hawaiian flexural moat. *Geol. Soc. Am. Bull.,* 105:189–205.

Sparks, R.S.J., 1979. Gas release rates from pyroclastic flows: an assessment of the role of fluidization in their emplacement. *Bull Volcanol.,* 41:1–9.

Stephen, R.A., Swift, S.A., and Greaves, R.J,. 1997. *Bathymetry and Sediment Thickness Survey of the Hawaii-2 Cable.* Woods Hole, MA (Woods Hole Oceanographic Institution), WHOI-03-97.

Sutton, G.H., and Barstow, N., 1990. Ocean-bottom ultralow-frequency (ULF) seismoacoustic ambient noise: 0.002 to 0.4 Hz. *J. Acoustical Soc. Am.,* 87:2005–2012.

Sutton, G.H., McDonald, W.G., Prentiss, D.D., and Thanos, S.N., 1965. Ocean-bottom seismic observatories. *Proc. IEEE,* 53:1909–1921.

Tsuya, H., 1930. The eruption of Komagatake, Hokkaido, in 1929. *Bull. Earthquake Res. Inst., Univ. Tokyo,* 8:238–270.

Winterer, E.L., 1989. Sediment thickness map of the Northeast Pacific. *In* Winterer, E.L., Hussong, D.M., and Decker, R.W. (Eds.), *The Eastern Pacific Ocean and Hawaii*. Geol. Soc. Am., Geol. of North America Ser., N:307–310.

Wright, T.L., and Fiske, R.S., 1971. Origin of the differentiated and hybrid lavas of Kilauea Volcano, Hawaii. *J. Petrol.* 12:1–65.

Yamazaki, T., Kato, I., Muroi, I., and Abe, M., 1973. Textural analysis and flow mechanism of the Donzurubo subaqueous pyroclastic flow deposits. *Bull. Volcanol.,* 37:231–244.

Figure F1. Locations are shown of Site 1224 and the Hawaii-2 Observatory (H2O) junction box (large star), Site 1223 (small star), repeater locations along the Hawaii-2 cable (crosses), major fracture zones (FZ), and previous drill sites (circles) from DSDP Legs 5 (Sites 38, 39, 40, and 41) and 18 (Site 172). Superimposed on the map is the satellite-derived bathymetry.

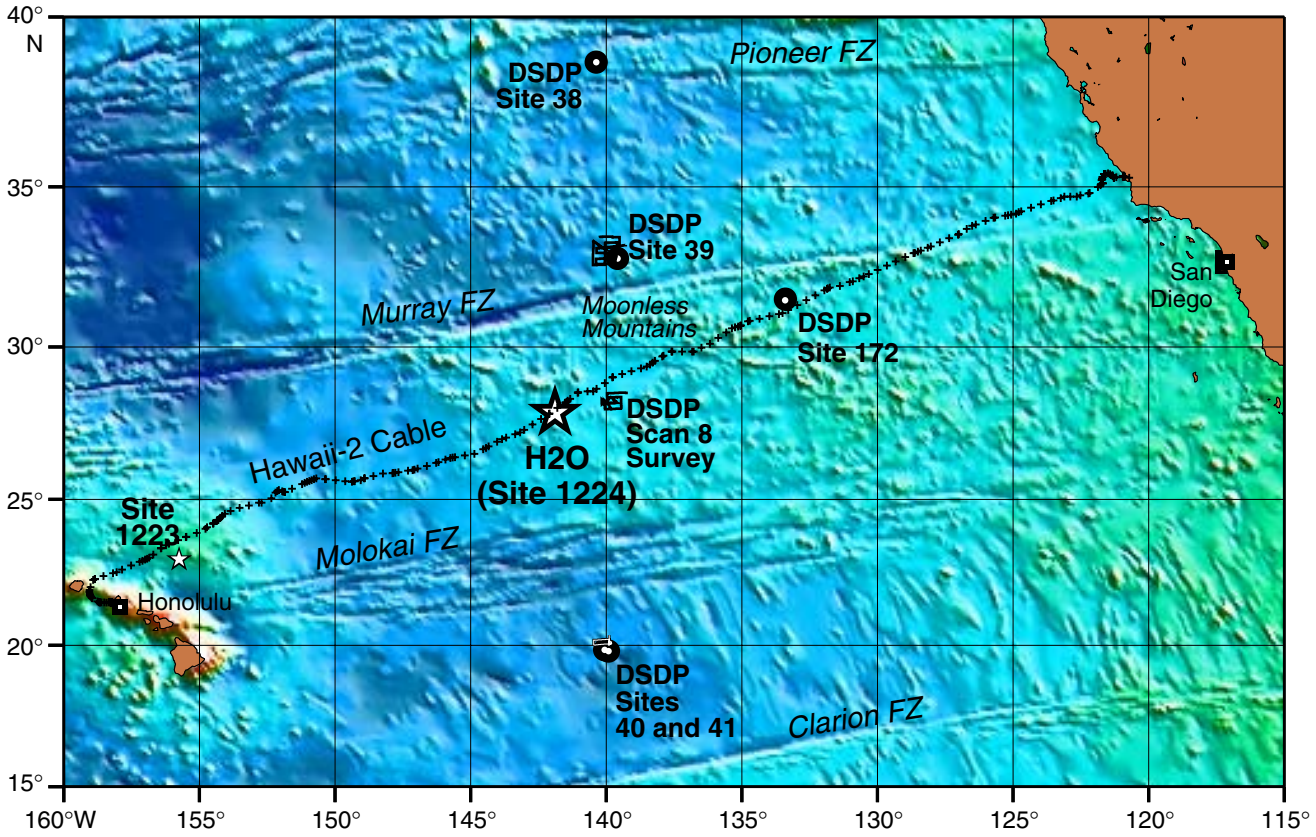

Figure F2. This artist's conception of the Hawaii-2 Observatory (H2O) summarizes some of the important components of the installation (© copyright Jayne Doucette, Woods Hole Oceanographic Institution [WHOI]. Reproduced with permission of WHOI).

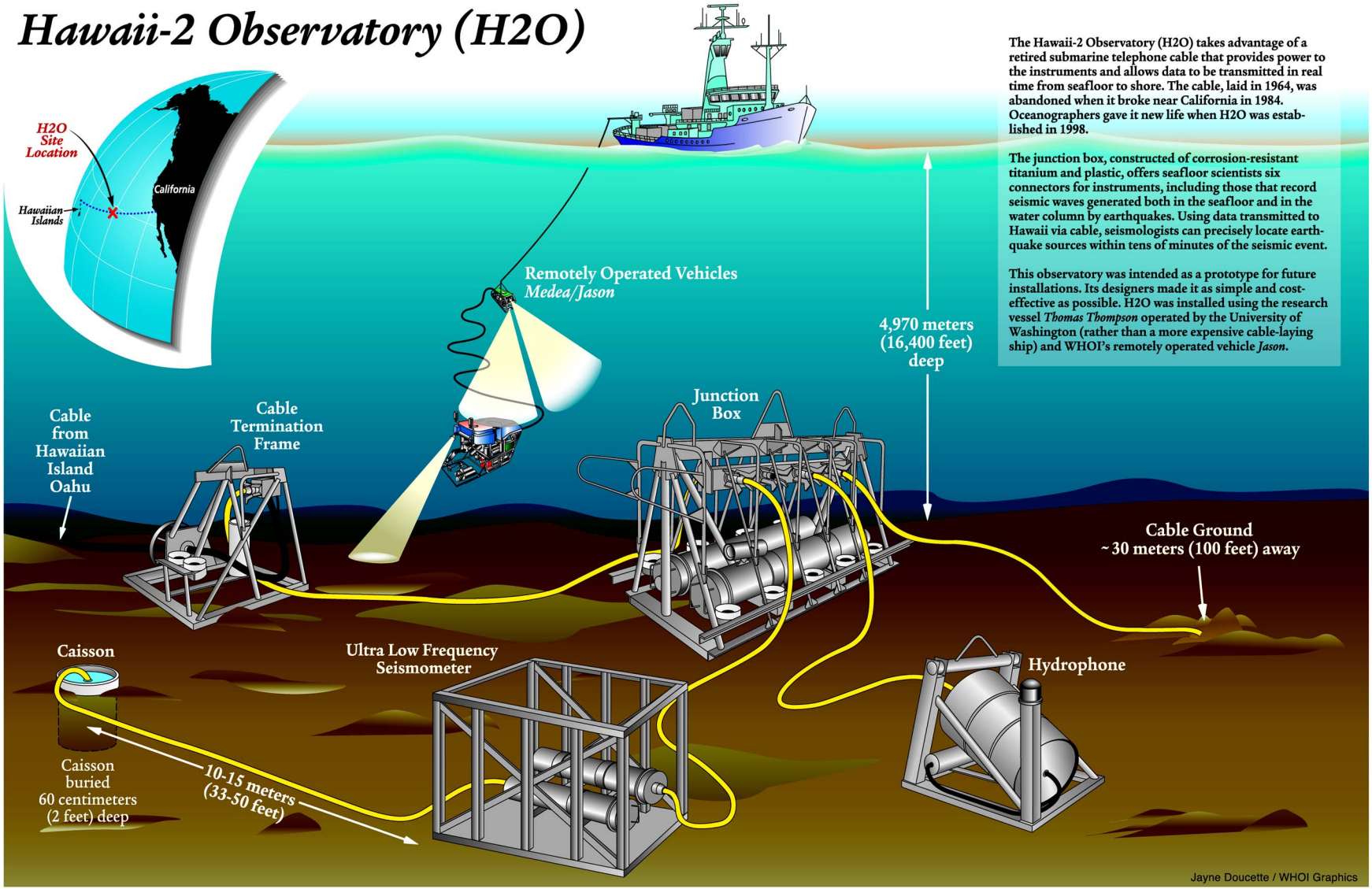

Figure F3. The location of the Hawaii-2 Observatory (H2O) junction box is shown on the SeaBeam bathymetry acquired during the site survey in August 1997 (Stephen et al., 1997). The locations of the repeaters (AT&T waypoints) on the cable are also shown (solid triangles).

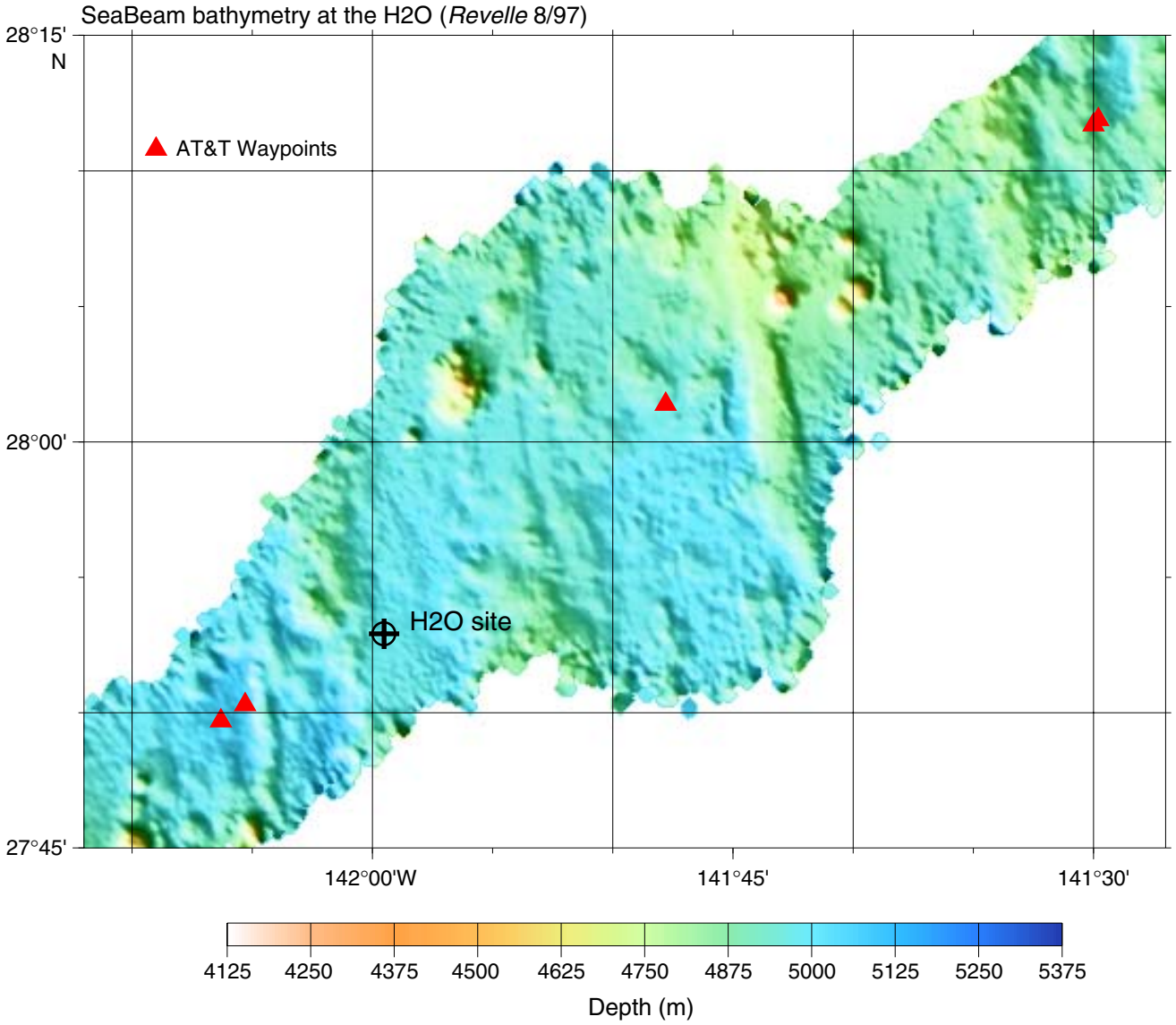

Figure F4. A 3.5-kHz echo sounder record showing that the seafloor dips smoothly ~6 m from the H2O junction box to Site 1224 (proposed Site H2O-5). One subbottom horizon at ~9 m is fairly uniform throughout the area. Based on drilling results, this is a midsediment reflector. A second reflector at ~30 m below the junction box can be associated with basaltic basement, although it appears only occasionally in the record. PDR = precision depth recorder.

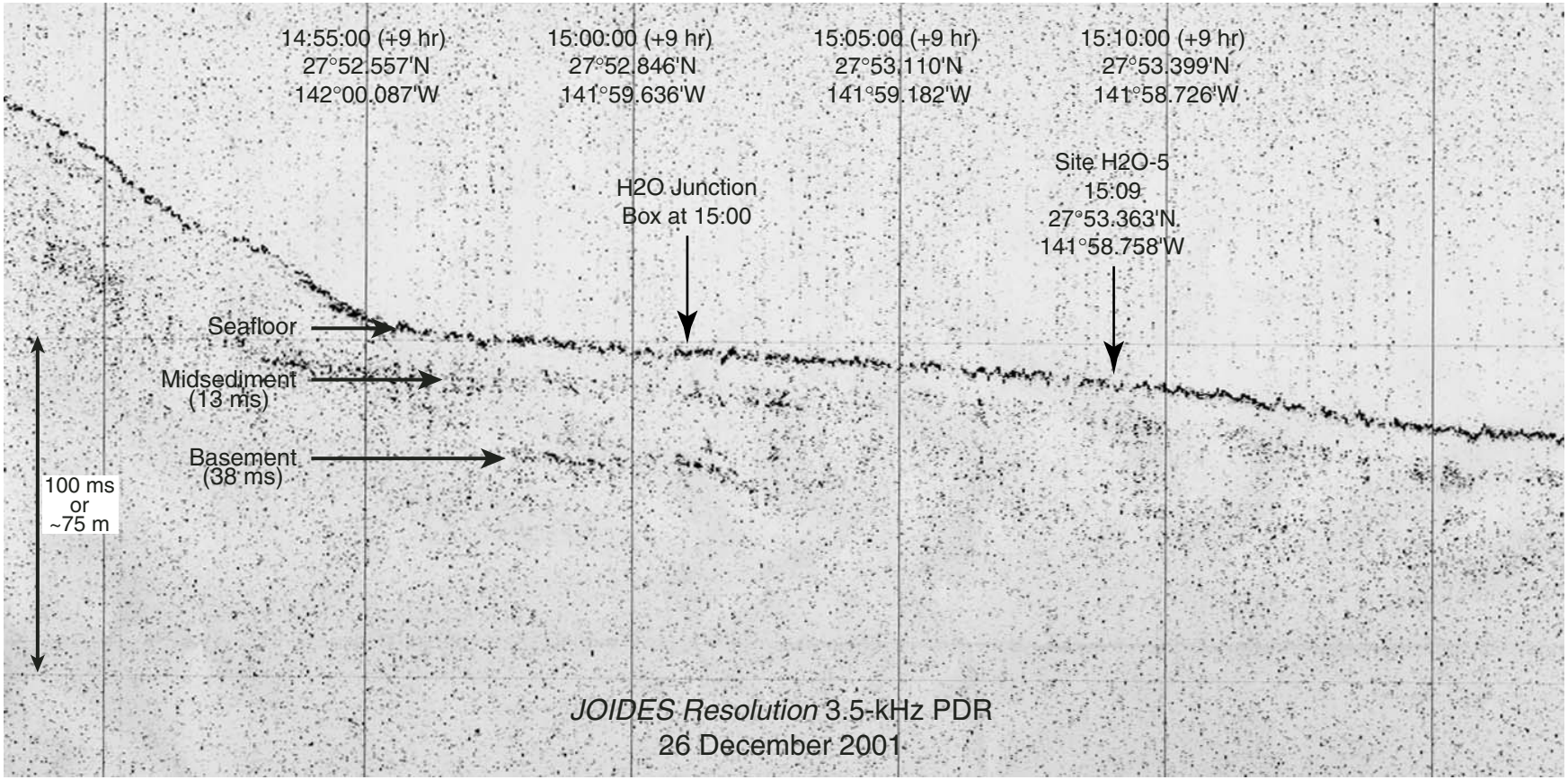

Figure F5. Vertical component spectra from the seafloor, buried, and borehole installations at the OSN-1 (Ocean Seismic Network) are compared with the spectra from the buried installation at the H2O and from the KIP GSN station on Oahu. The H2O has extremely low noise levels above 5 Hz and near the microseism peak from 0.1 to 0.3 Hz. The H2O has high noise levels below 50 mHz. Otherwise, the H2O levels are comparable to the OSN borehole and KIP levels. The sediment resonances at the H2O near 1.1 and 2.3 Hz are very prominent. Power spectral density is given in decibels relative to 1 $(m/s^2)^2$/Hz.

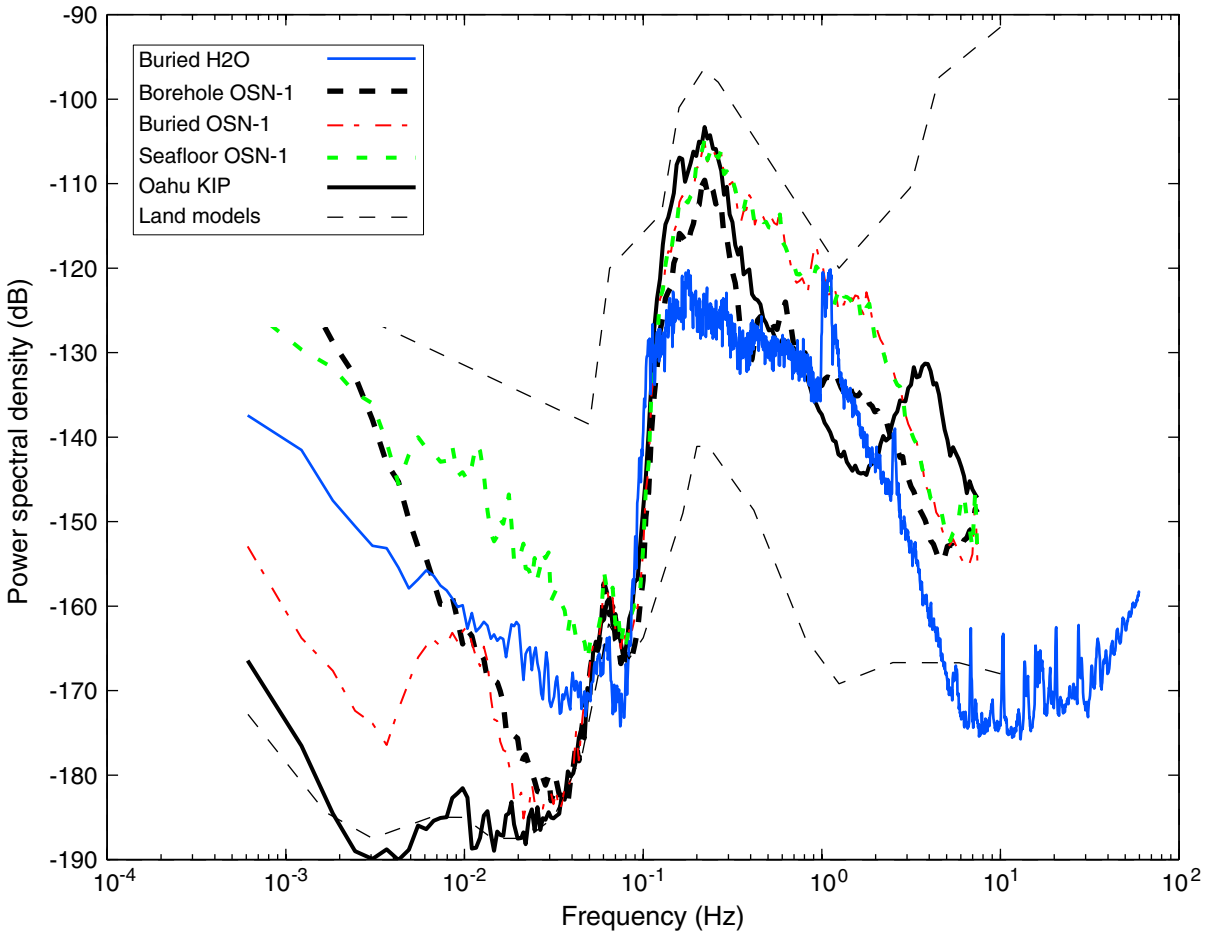

Figure F6. Horizontal component spectra from the seafloor, buried, and borehole installations at the OSN-1 (Ocean Seismic Network) are compared with the spectra from the buried installation at the H2O and from the KIP GSN station on Oahu. The sediment resonance peaks in the band 0.3 to 8 Hz are up to 35 dB louder than background levels and far exceed the microseism peak at 0.1 to 0.3 Hz. That the resonance peaks are considerably higher for horizontal components than for vertical components is consistent with the notion that these are related to shear wave resonances (or Scholte modes). Power spectral density is given in decibels relative to 1 $(m/s^2)^2$/Hz.

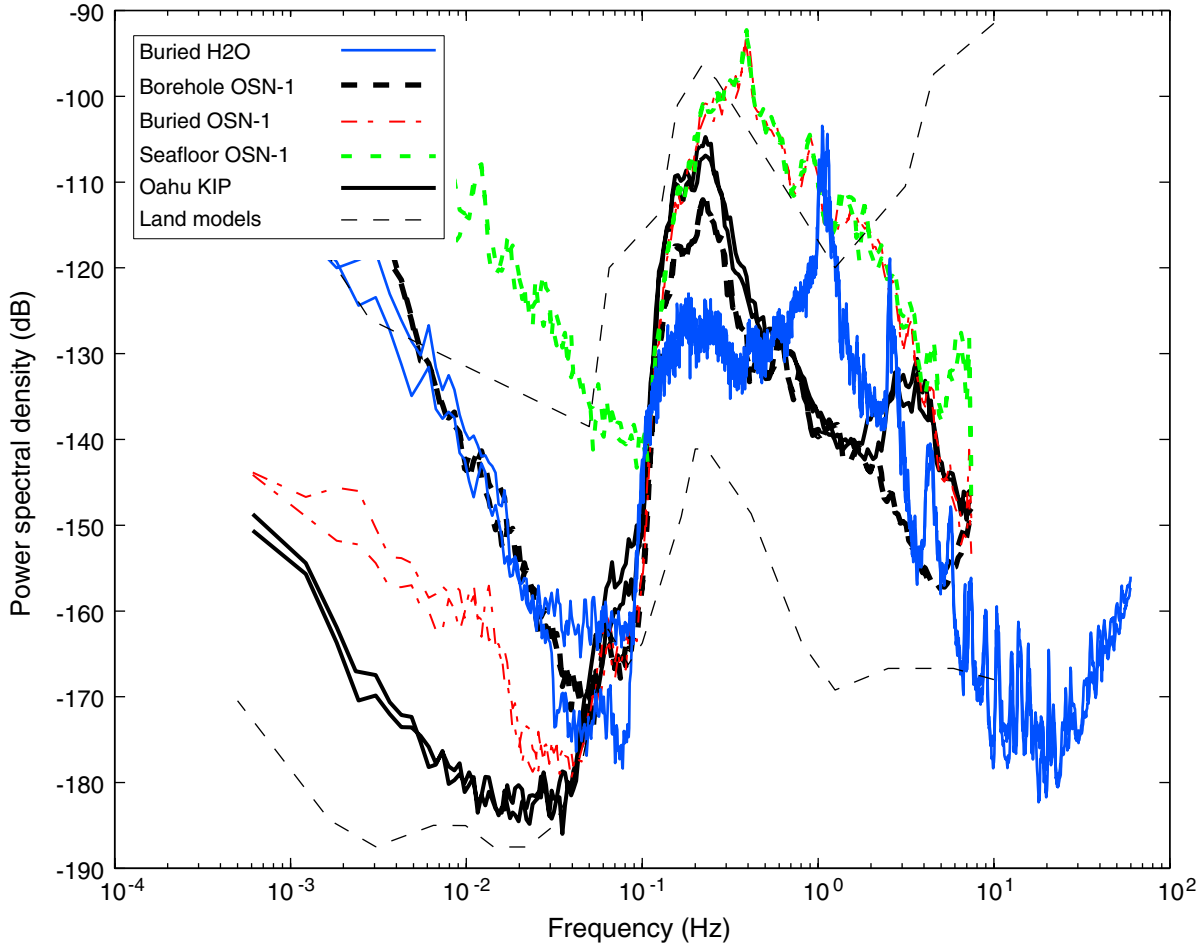

Figure F7. Leg 200 time distribution charts. Comparisons of (**A**) onsite, underway, and in-port days and (**B**) site activities.

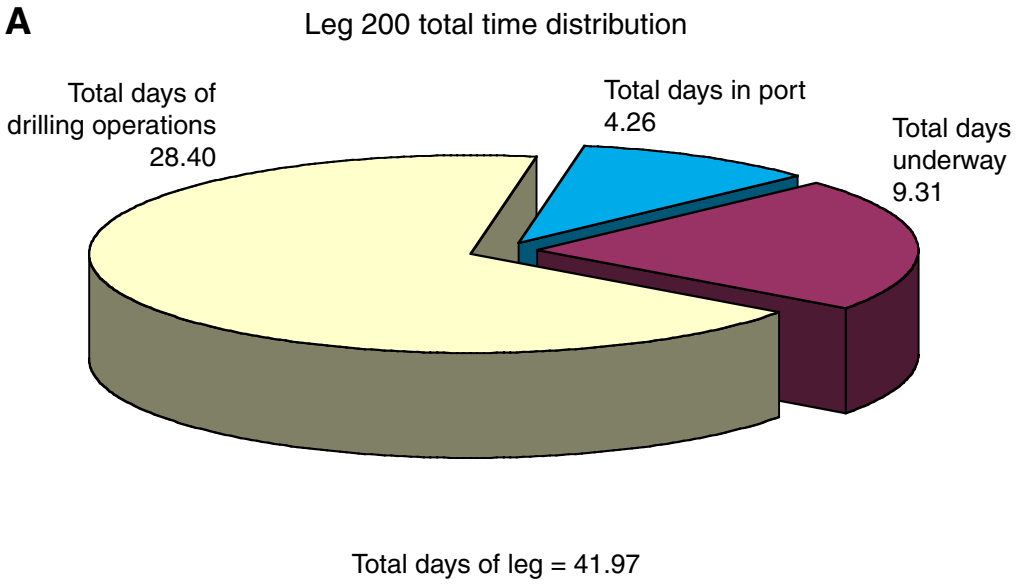

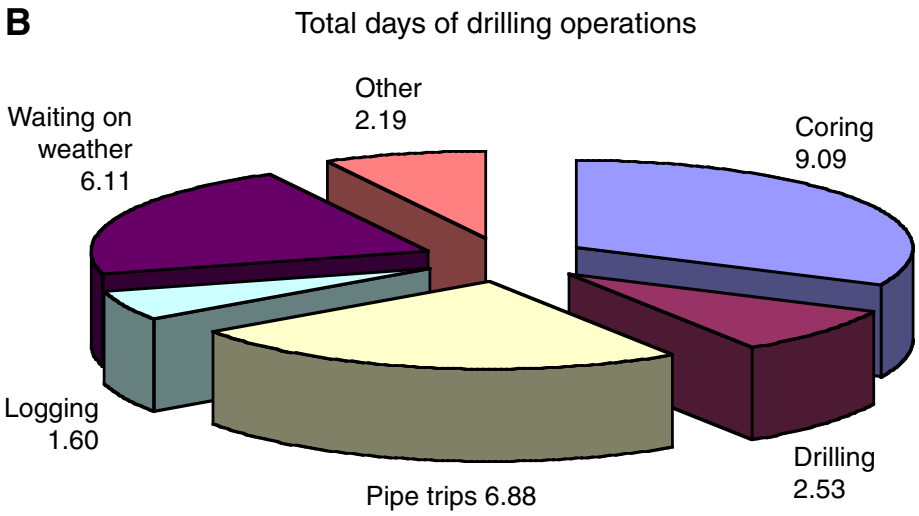

Figure F8. All drilling at the Hawaii-2 Observatory (H2O) took place at Site 1224 (proposed Site H2O-5), which is 1.48 km northeast of the junction box at the H2O. Alternate drilling sites (H2O-1 through H2O-4) that were discussed in the Leg 200 Scientific Prospectus are also shown (circles with crosses). Circles are drawn at 1, 2, and 3 km radius from the junction box. Also shown are the location of the single-channel seismic lines acquired during the site survey cruise in 1997 (dashed lines) and the track line taken by the *JOIDES Resolution* on 26 December 2001 (solid line). The echo sounder recording in Figure **F4,** p. 38, was made along this line.

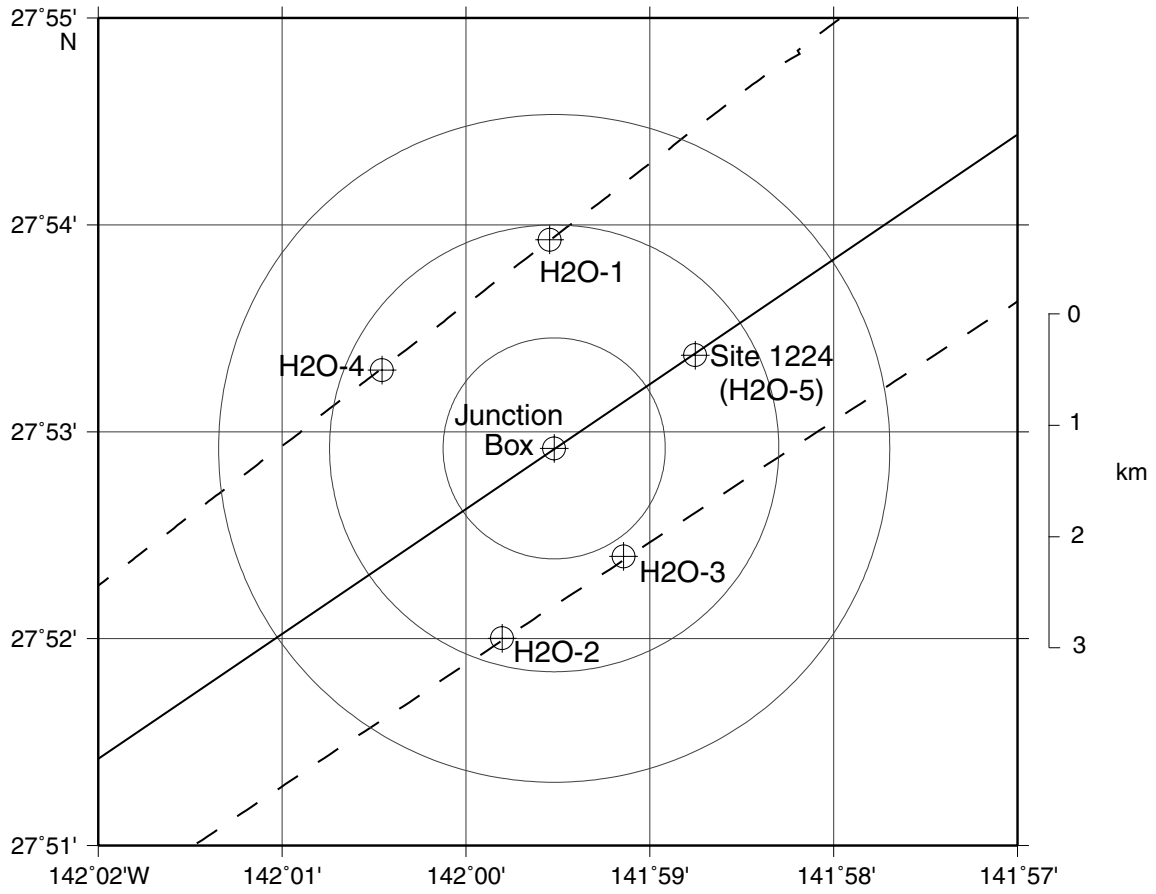

Figure F9. Summary of the critical dimensions of the reentry cone and casing deployed in Hole 1224D. On reentering the cone for the last time, it was observed that the reentry cone had settled 1.75 m below the mudline. The inside diameter (drift) of the 10¾-in casing is 9.9 in. CSG = casing, TD = total depth, ID = inner diameter, HGR = hanger. (Figure provided courtesy of Scott Pederson, Transocean Sedco Forex.)

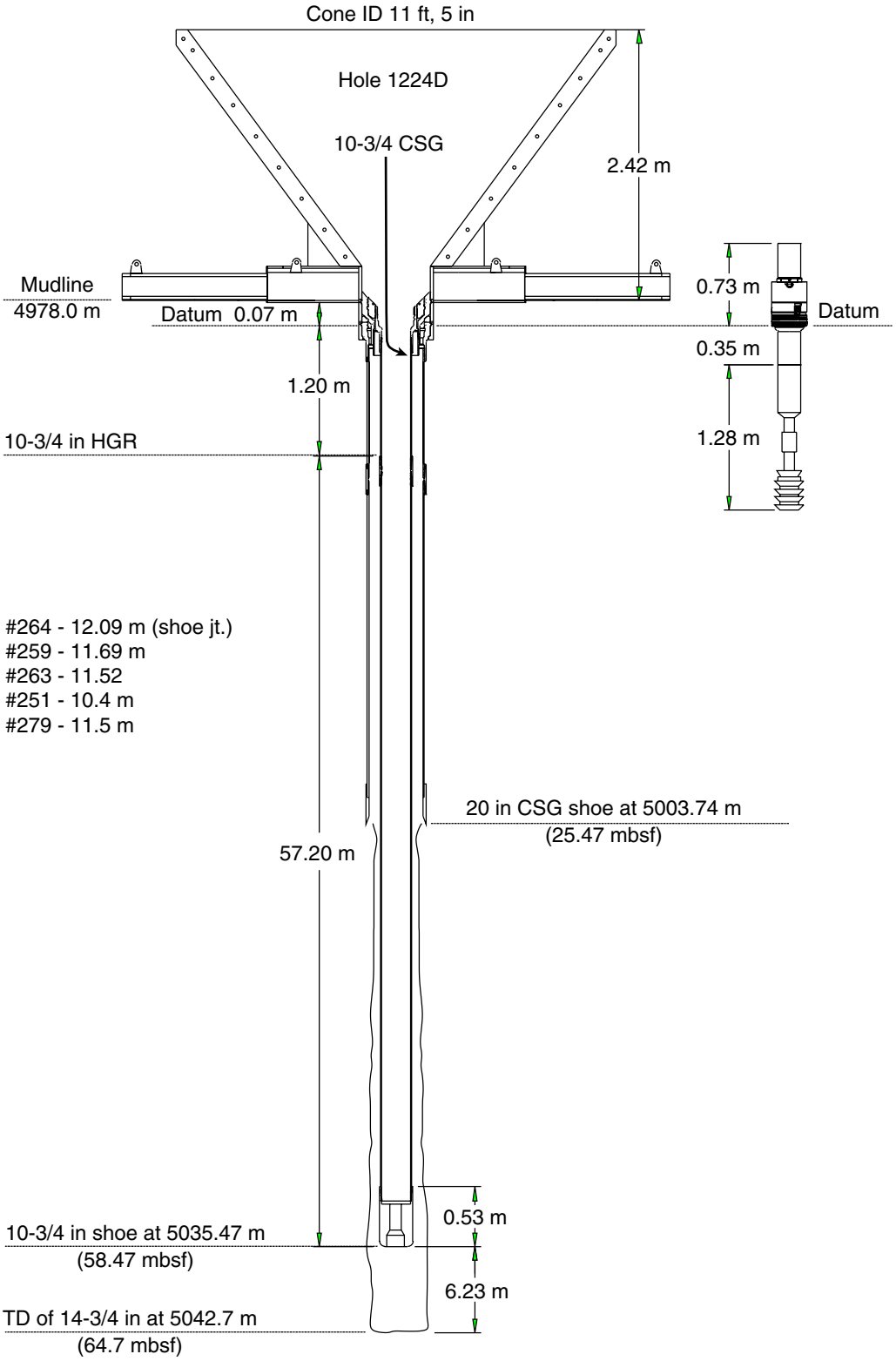

Figure F10. This photograph, taken from the video camera on the VIT sled, shows the reentry cone in Hole 1224D.

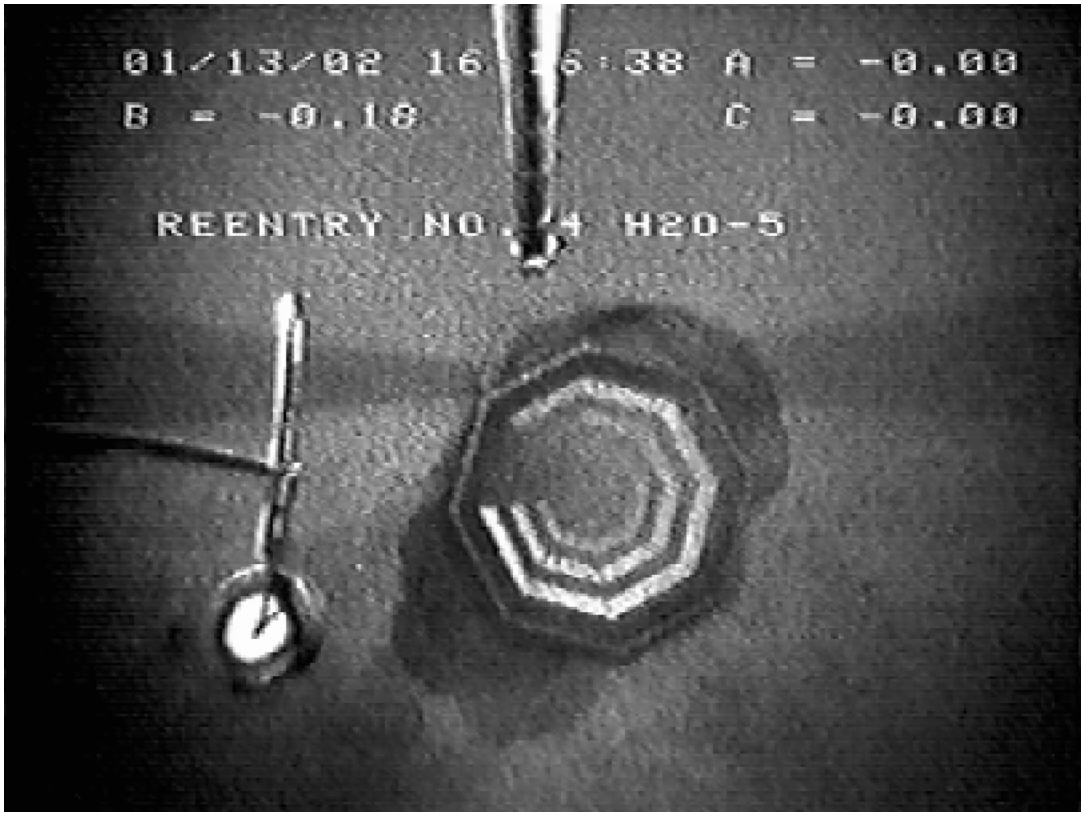

Figure F11. Summary of the critical dimensions of the free-fall funnel deployed in Hole 1224F. The throat inside diameter is 12.5 in. TD = total depth. (Figure provided courtesy of Scott Pederson, Transocean Sedco Forex.)

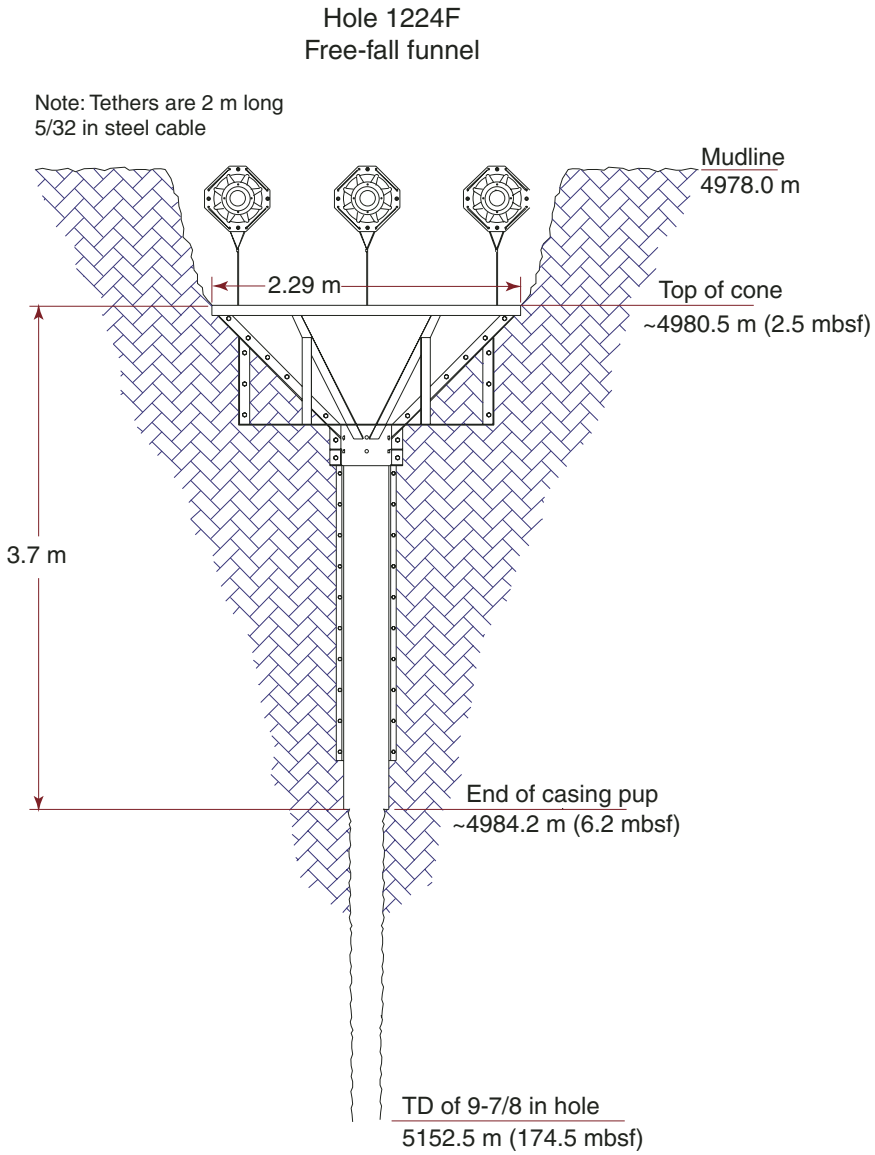

Figure F12. This photograph, taken from the video camera on the VIT sled, shows the free-fall funnel buried in the seafloor in Hole 1224F.

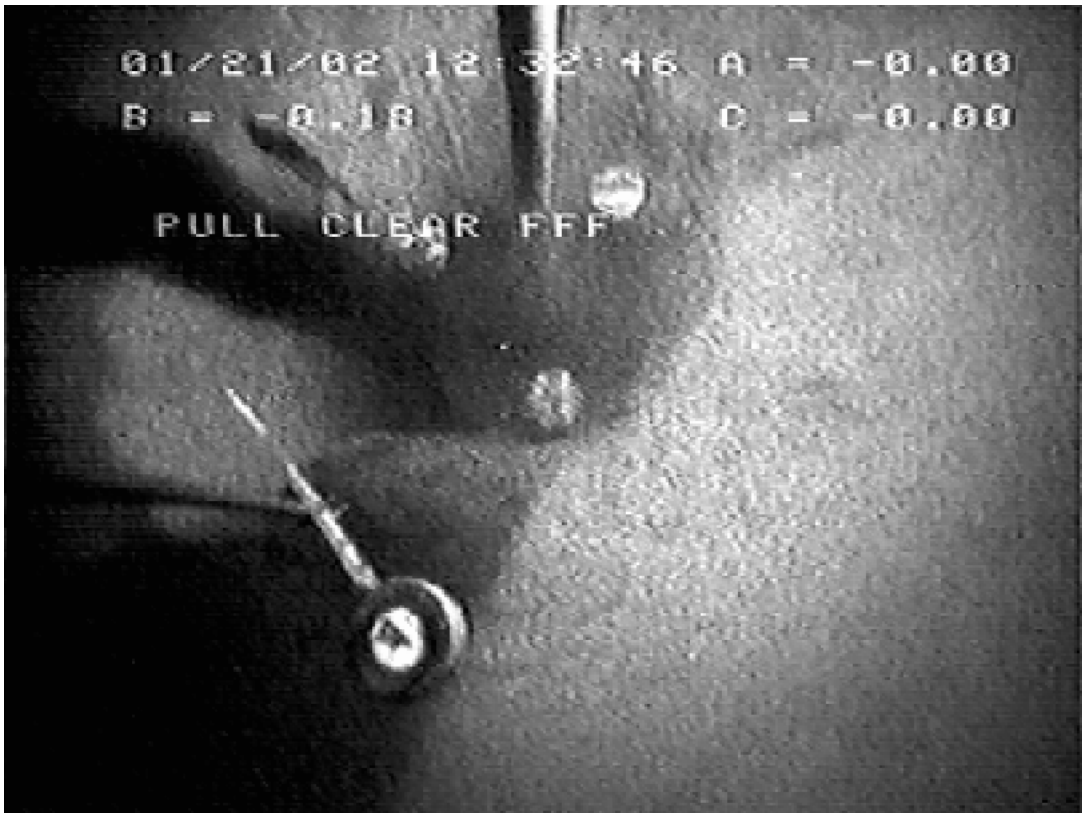

Figure F13. Coccoliths (spherical) and discoasters (star shaped) from Section 200-1224E-2R-7.

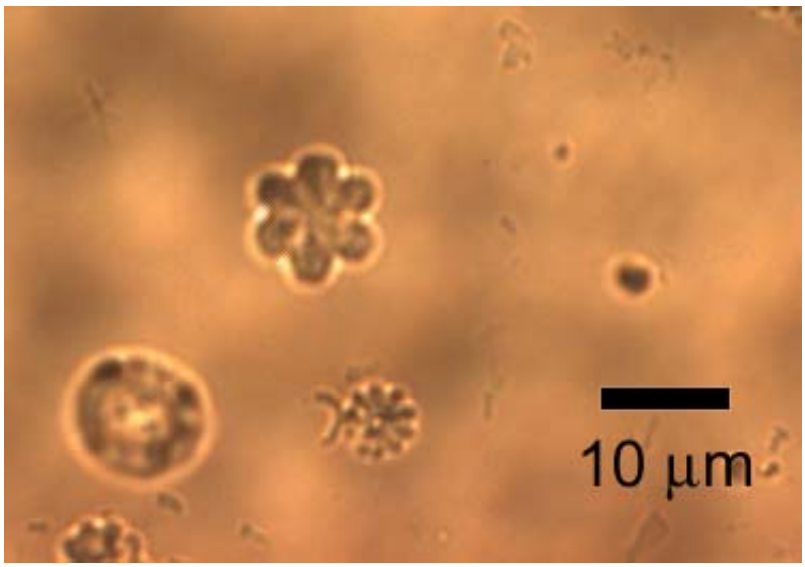

Figure F14. Lithologic summary of basalts cored at Site 1224. Basalt recovered in cores that penetrated basement are placed below the average depth estimated for the basement contact, which is 28 mbsf. Otherwise, the top of the recovered core is assumed by convention to start at the top of the cored interval. Locations of thin section samples are shown by red dots. Sediments are shown down to the presumed basement contact at 28 mbsf, but, as with the basalts, the depth of recovery is only known to lie somewhere within the cored interval and somewhere above the basalt.

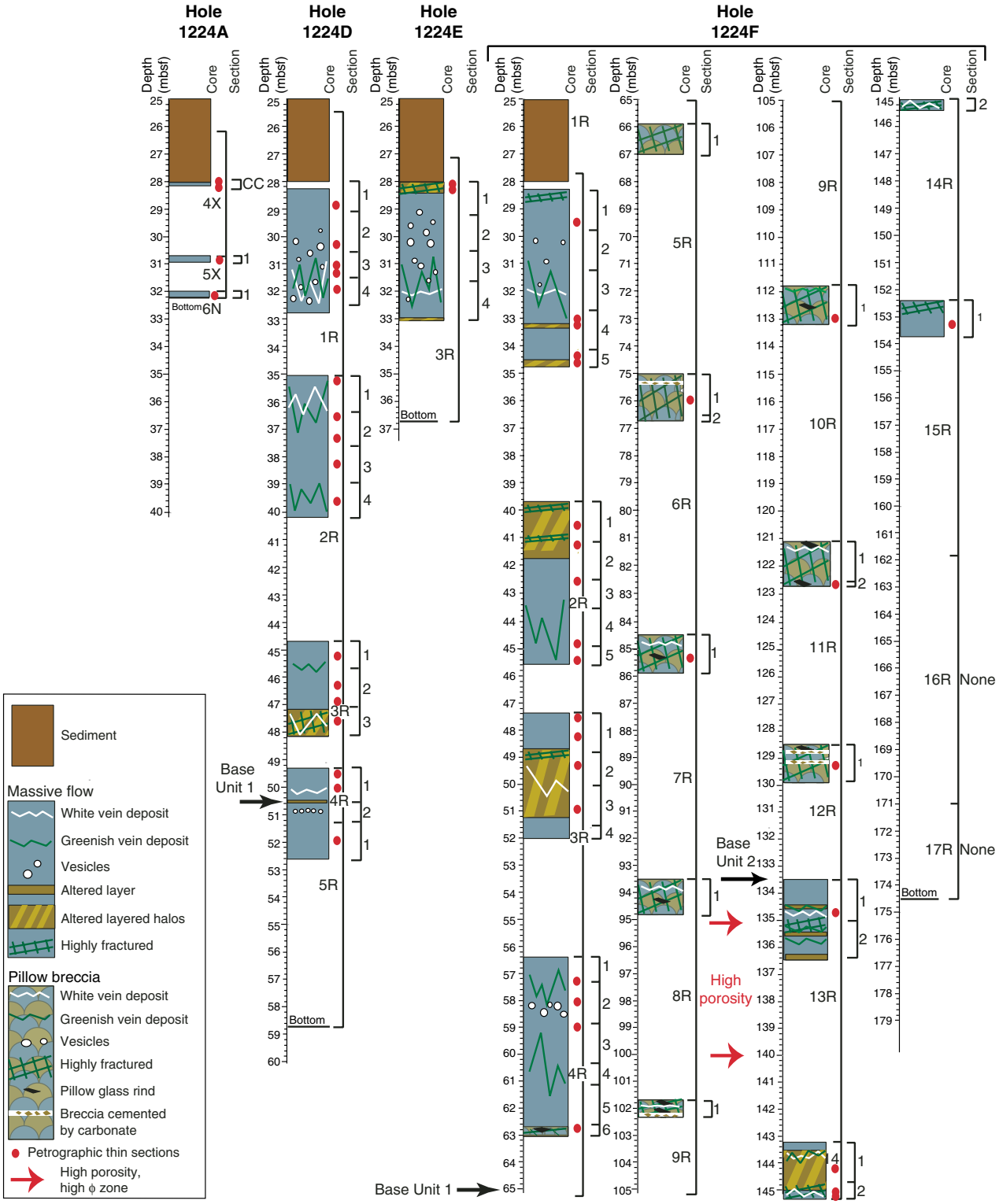

Figure F15. Flow-top hyaloclastite from lithologic Unit 2 cemented by calcite (interval 200-1224F-6R-1 [Piece 6, 29–33 cm]). Fresh glass is very dark gray; altered glass is gray; palagonitized glass is orange; and calcite is white and light gray.

Figure F16. Chemical compositions vs. depth for basalts from Hole 1224D. **A.** TiO_2. **B.** Zr. The vertical lines suggest the possible breakdown of the hole into three chemical types based on TiO_2 and three types based on Zr concentrations.

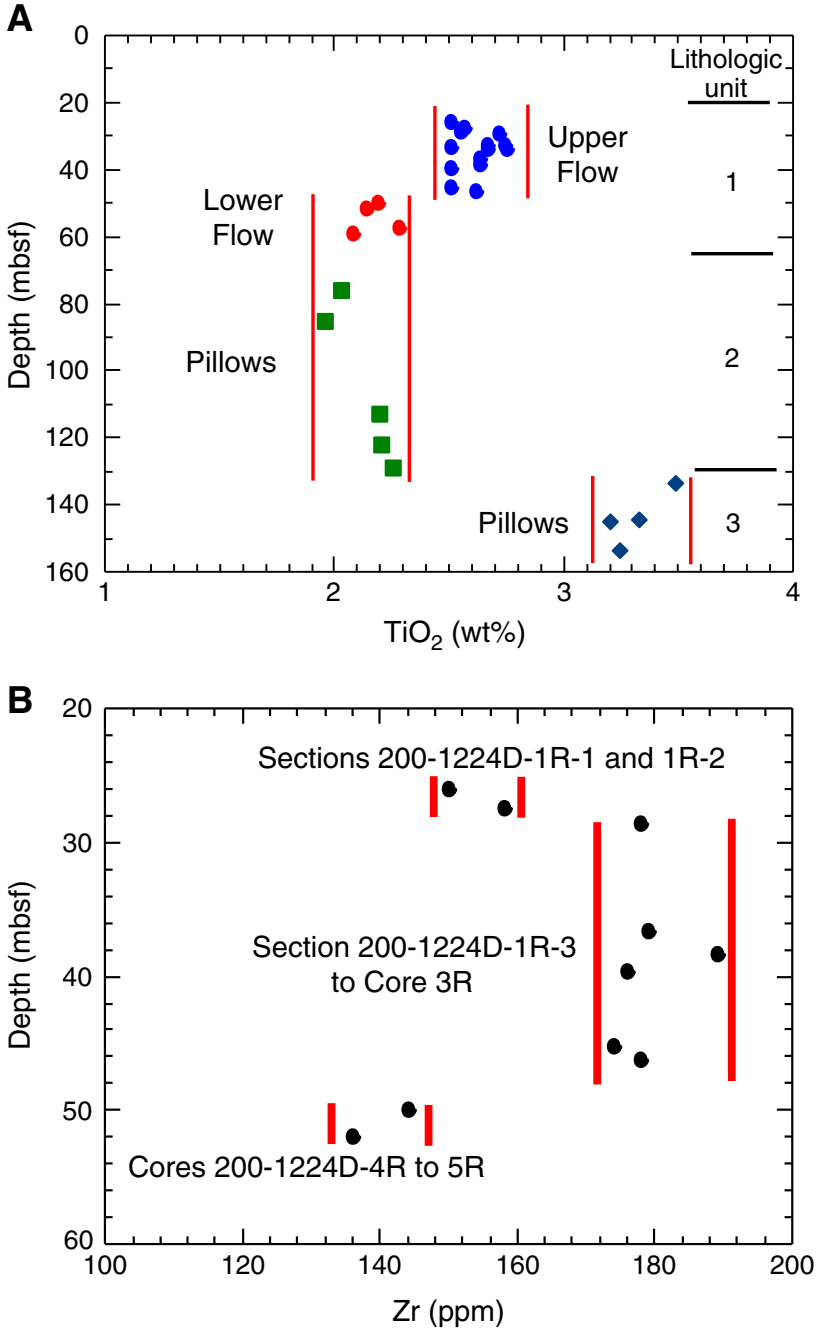

Figure F17. Sampling point and identification of the main secondary minerals in the basement section at Site 1224. Green = clay, blue = carbonate, gray = quartz, yellow = zeolite. Note that in order to minimize confusion with curated depths, the top basalt core in each hole on this figure has not been shifted to 28 mbsf as was done in Figure F14, p. 48. (Continued on next page.)

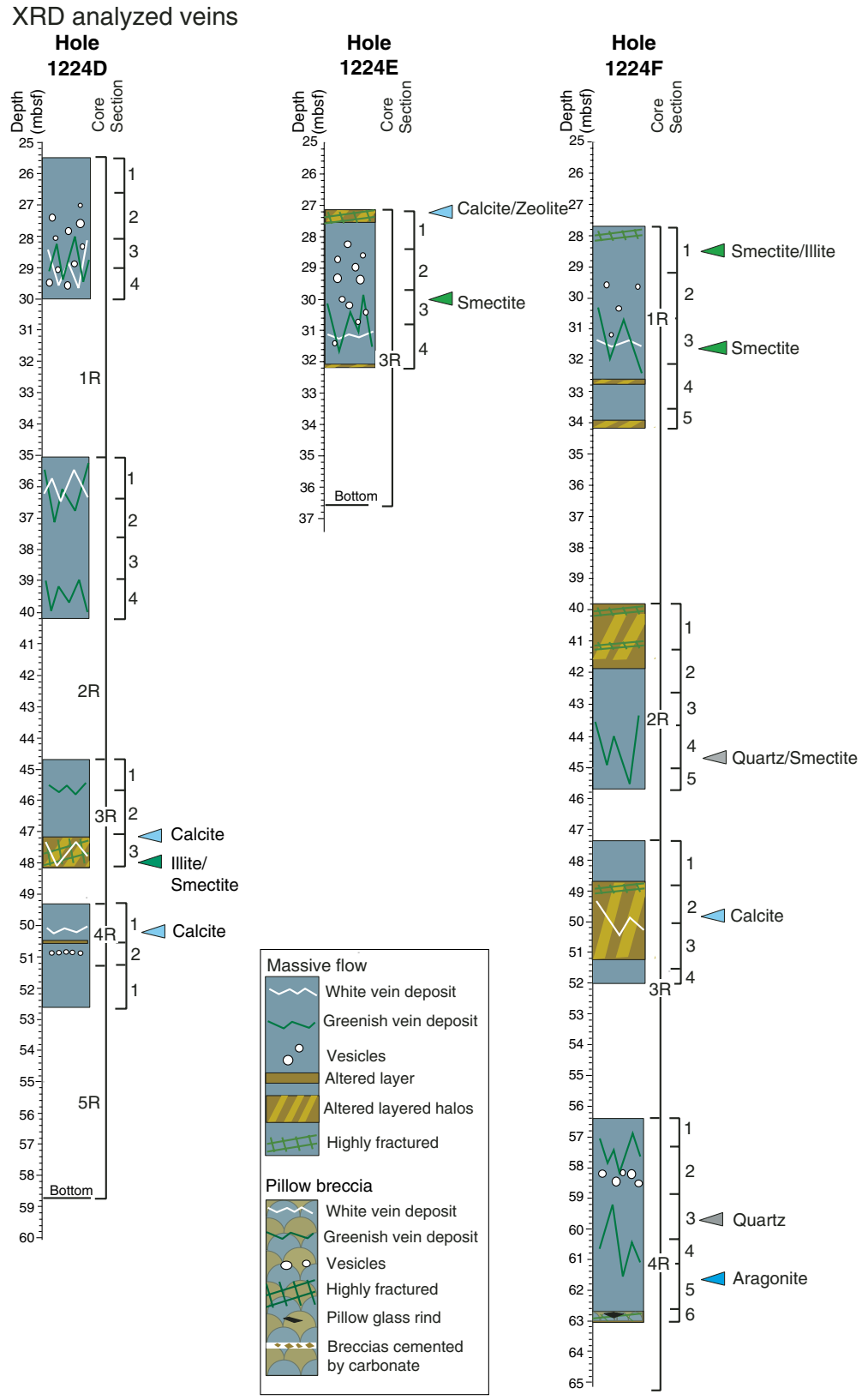

Figure F17 (continued).

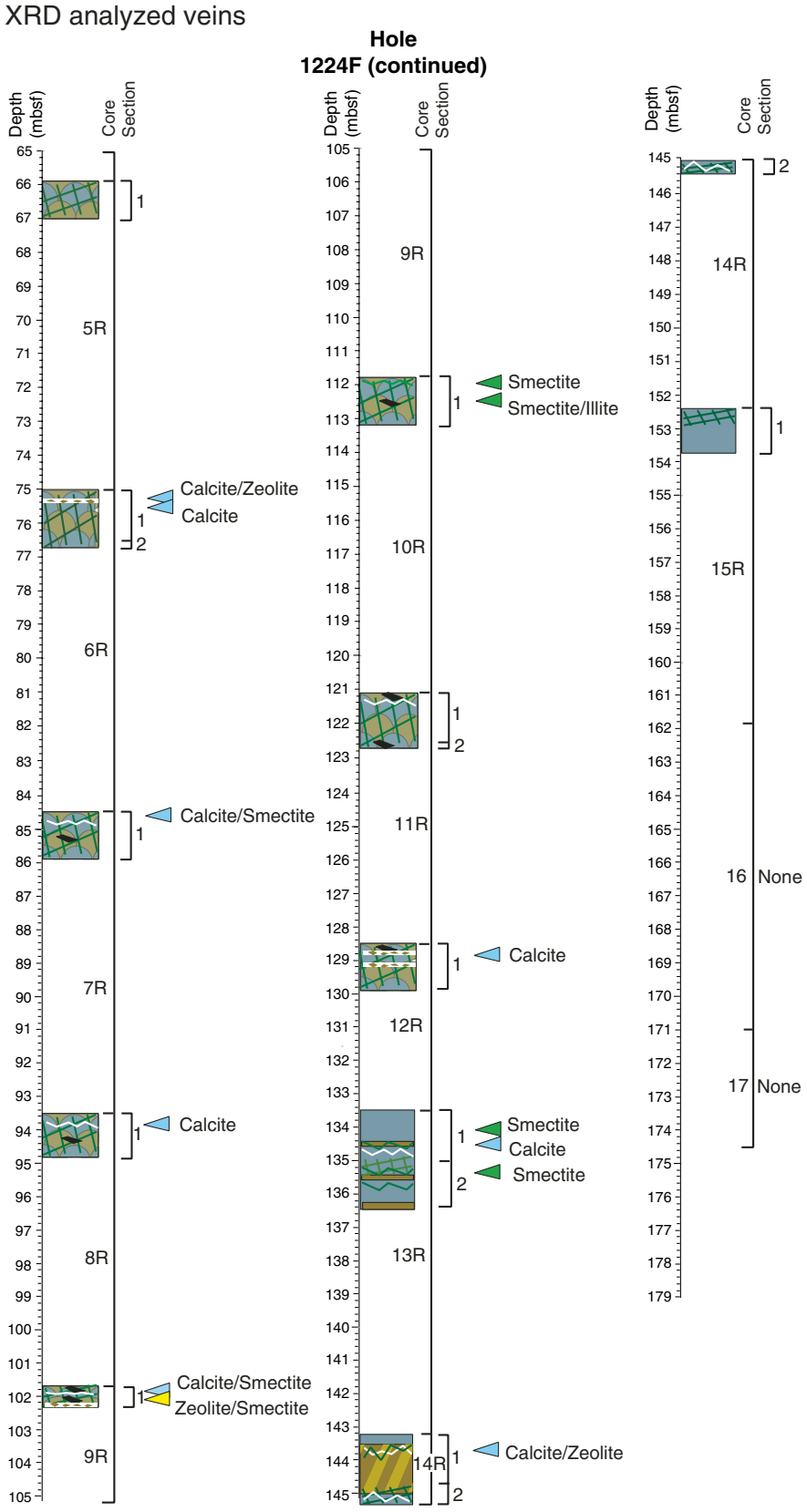

Figure F18. Photomicrograph showing bacterial cells from an upper sediment layer from a depth of 1.45 mbsf (Sample 200-1224C-1H-4, 145–150 cm). **A.** After staining with the DNA-binding fluorochrome SYBR Green I. **B.** Hybridization with the Bacteria-specific, CY3-labeled probe EUB338. Note the numerous bacteria responding to the specific hybridization, indicating the high amount of metabolically active bacteria within the sediment.

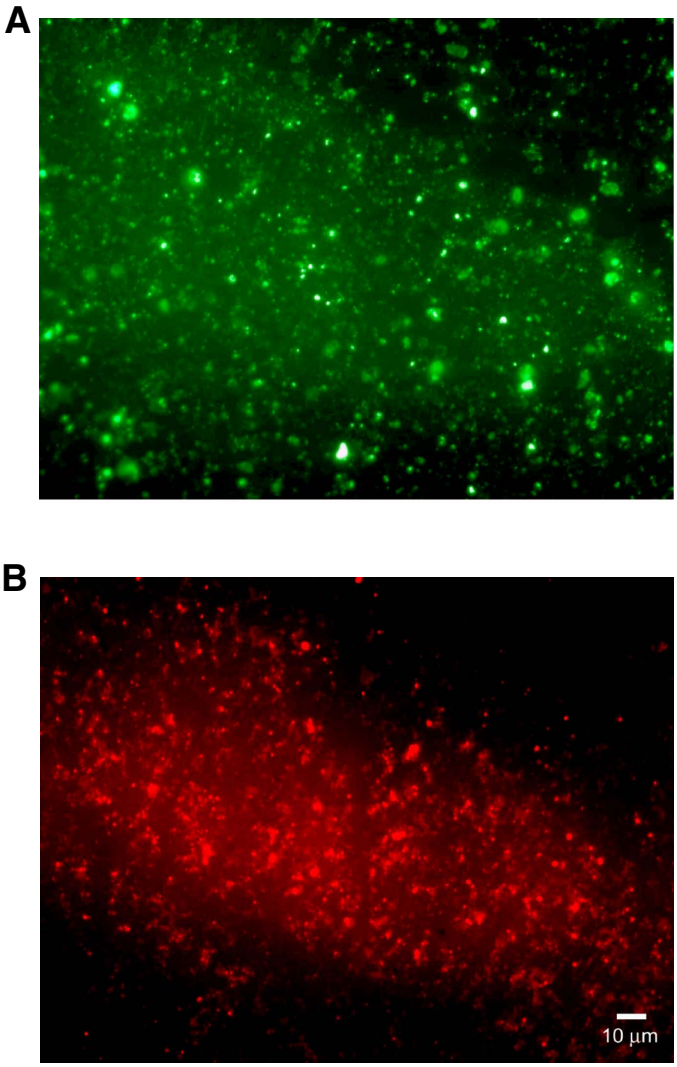

Figure F19. Fungal hyphae grown in a $CaCO_3$-filled cavity within a massive tholeiitic lava flow unit.

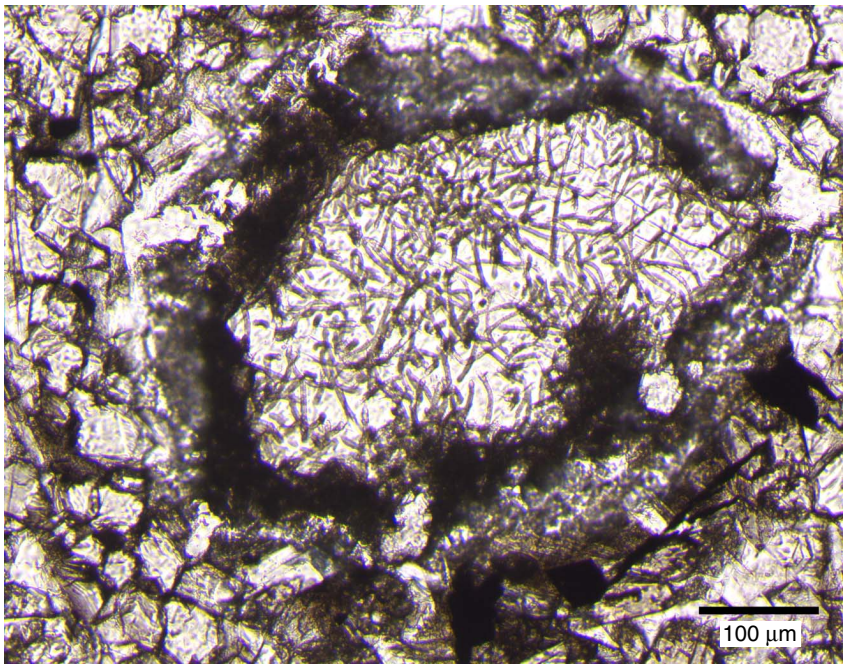

Figure F20. Compressional wave velocities vs. depth in Holes 1224D, 1224E, and 1224F. Seven depth zones are introduced, as seen on the far right. Compressional wave velocities in the three holes have similar depth dependence between 27 and 53 mbsf. Zones 1 and 2 correspond to logging Unit I (Figs. **F21,** p. 56, **F24,** p. 59); zone 3 corresponds to logging Unit II; zone 4 corresponds to logging Unit III; zones 5 and 6 correspond to logging Unit IV; and zone 7 corresponds to logging Unit V.

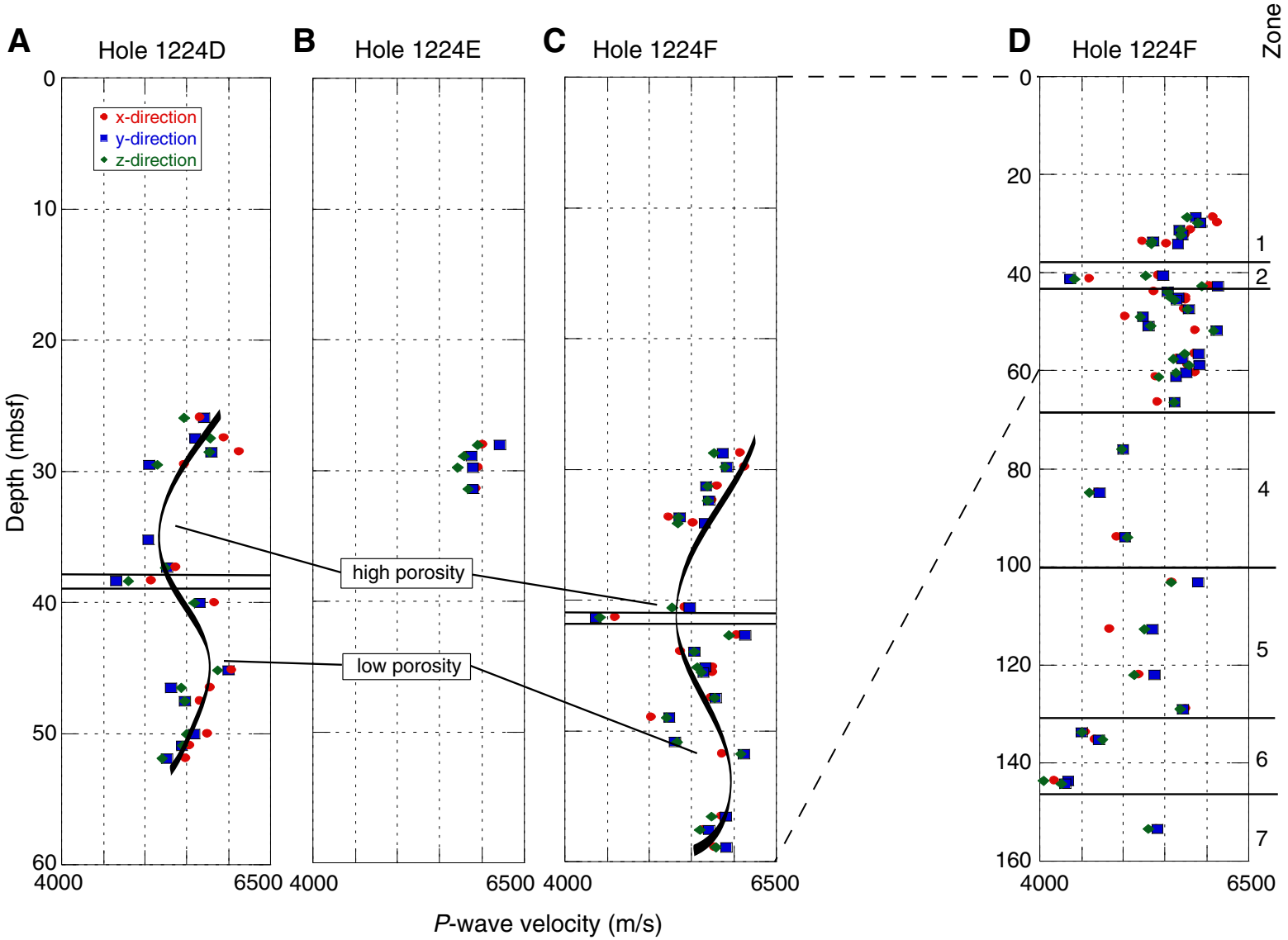

Figure F21. Composite log of the temperature, spontaneous potential (SP), and electrical resistivity logs recorded in Hole 1224F during Leg 200. Track 1: temperature. Track 2: SP. Track 3: deep induction resistivity (ILD). Track 4: spherically focused resistivity log (SFLU).

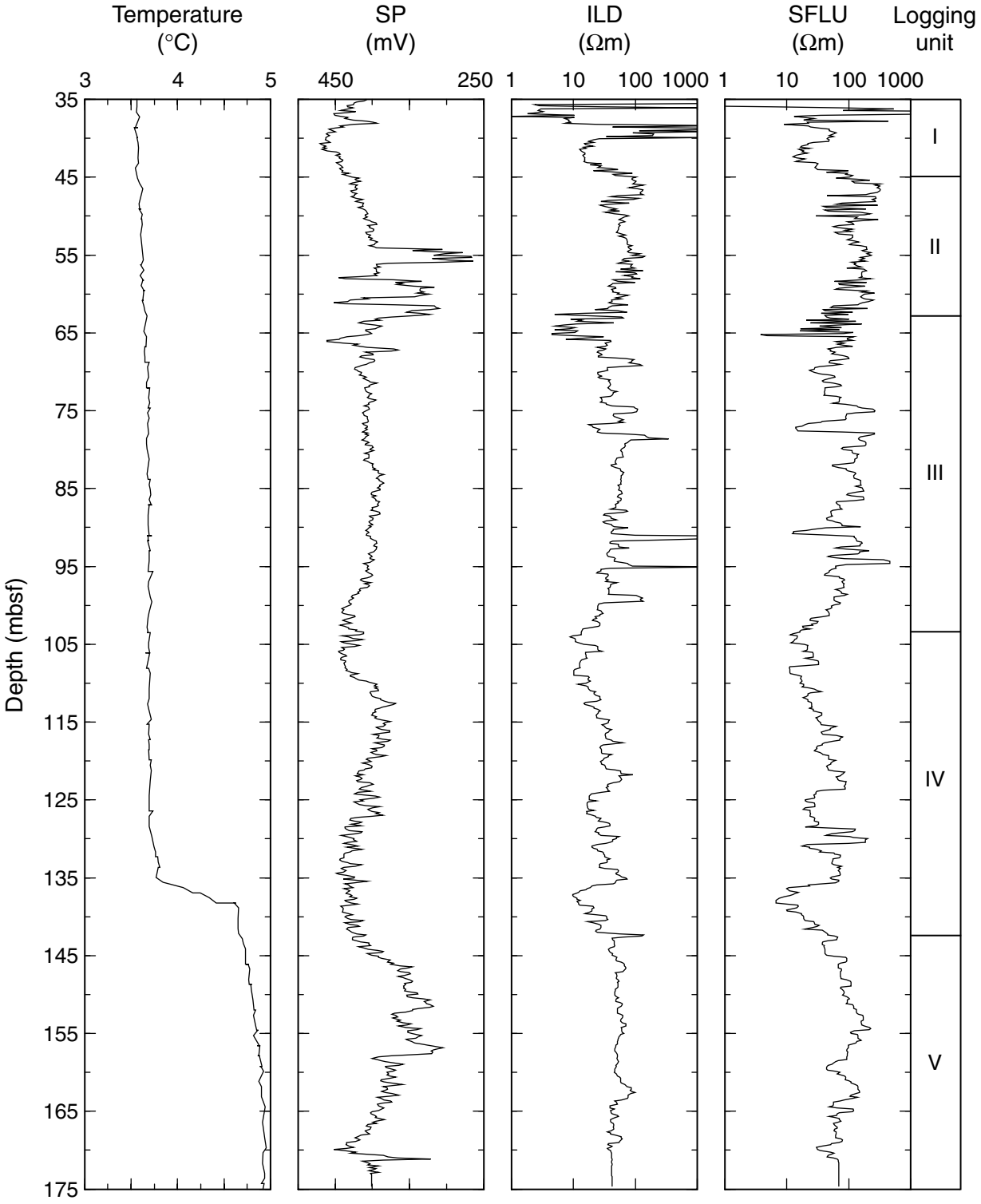

Figure F22. Logging data in Hole 1224F: caliper, resistivity, neutron porosity (NPHI), and gamma ray bulk density (RHOB). The arrows indicate the boundaries of the five logging units discussed in the text.

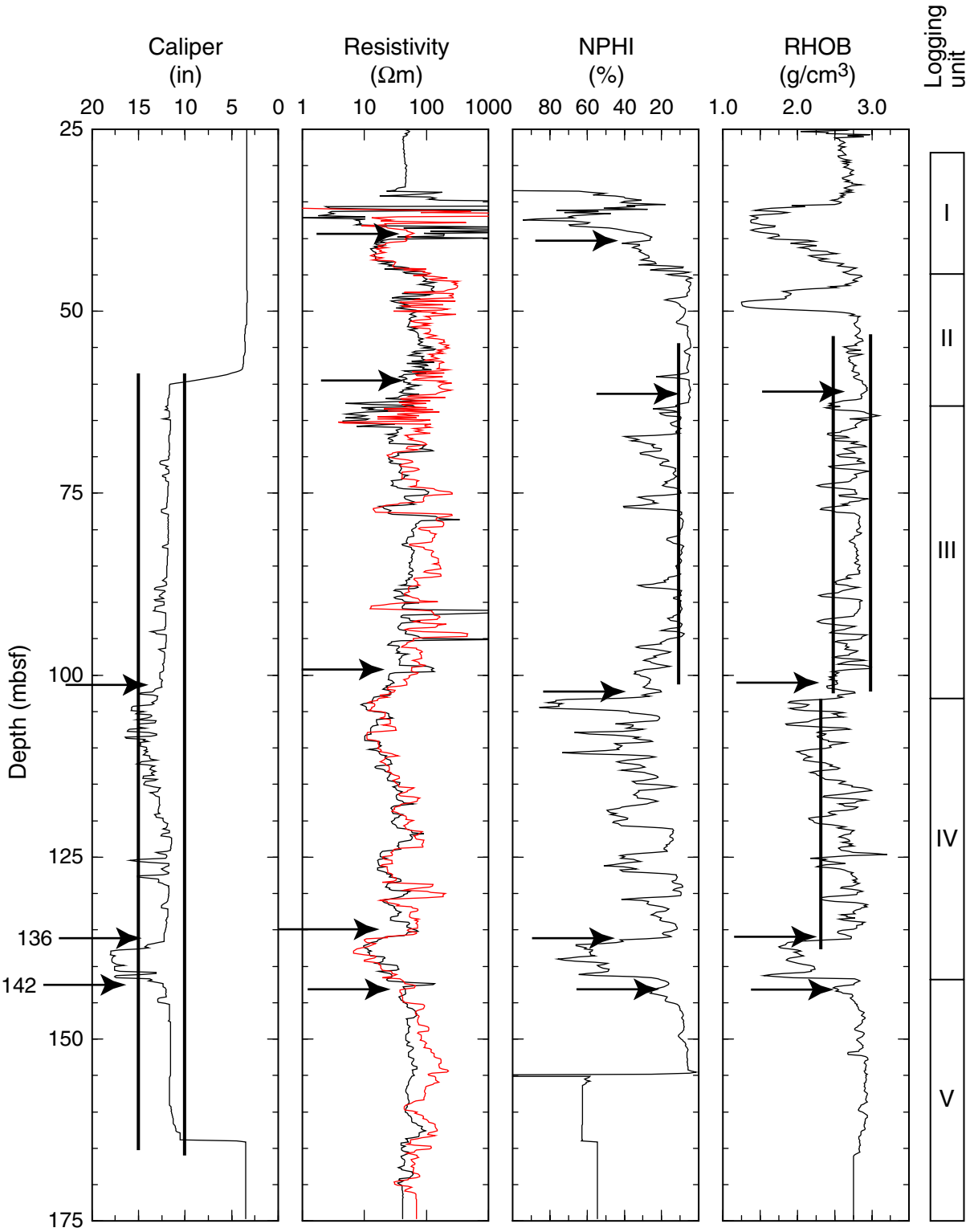

Figure F23. Installation of the reentry cone and steel casing in Hole 1224D as observed on deep-source records. This figure is shown in five sections. It is extracted from the EPC graphic recording for the period 2118 to 2220 hr on 2 January. The traveltime interval shown is ~410 ms; the light horizontal traces are spaced at 100 ms. The heavier vertical traces are 5-min marks. CHRT = casing hanger running tool. The 14-s fluctuation with an amplitude of up to 4 ms in the traveltime of the direct water wave is primarily due to the heave of the ship pulling and slackening the VIT cable. The 1- to 2-ms fluctuations in the traveltime for the reentry cone is a measure of the VIT heave plus the uncompensated heave of the drill string because the cone is rigidly linked to the ship's heave compensator by the drill string.

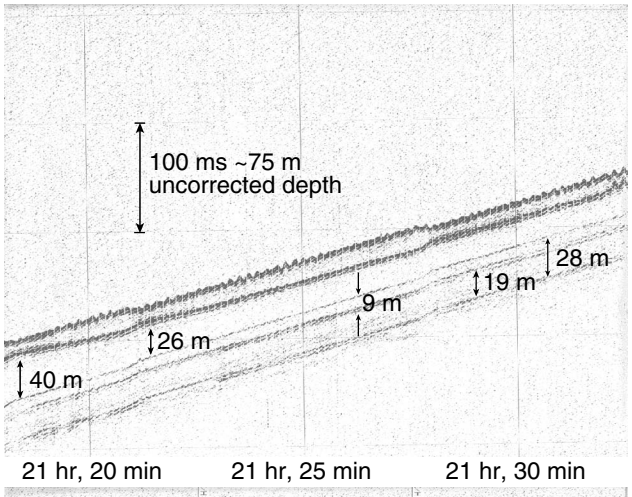

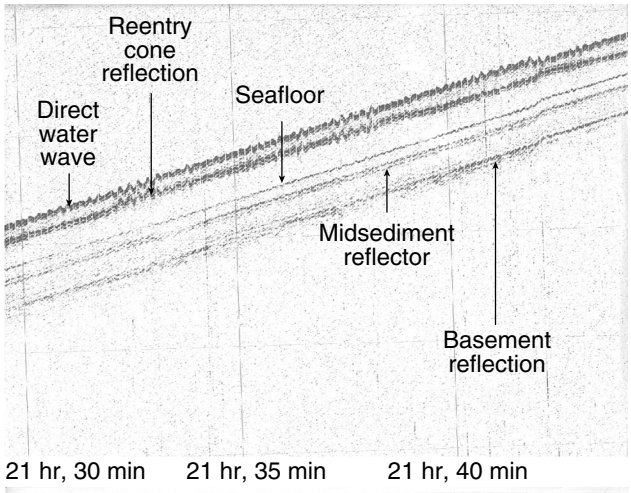

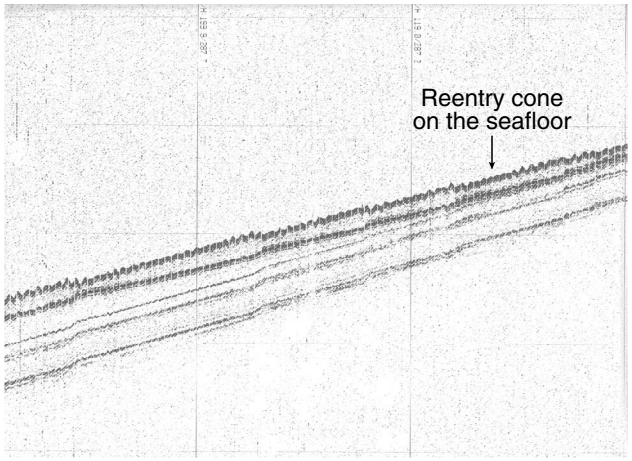

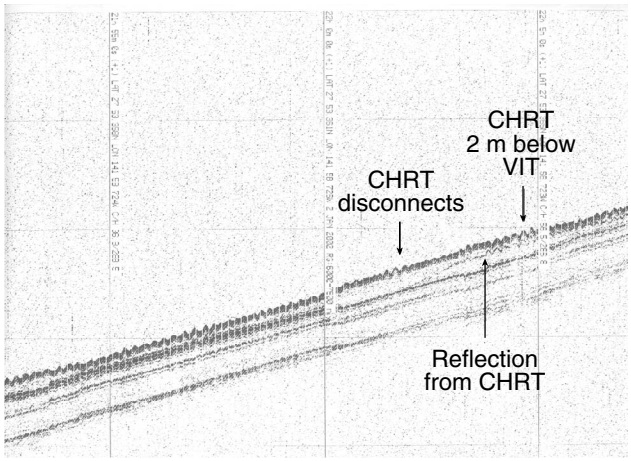

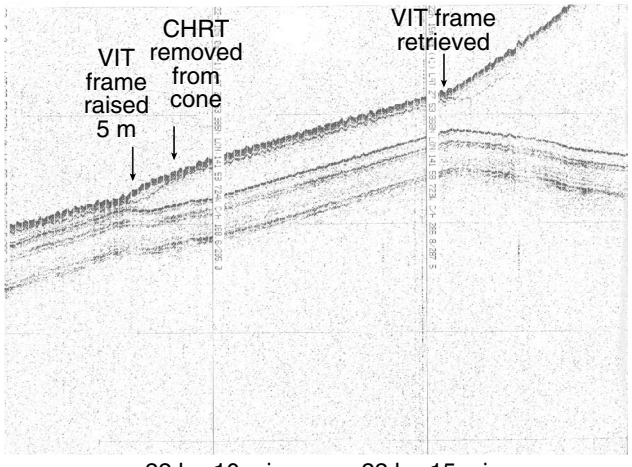

Figure F24. Tracking RMS (root-mean square) energy levels in one-octave bands is a convenient way to observe time-dependent effects in the broadband seismic data from the Hawaii-2 Observatory. The spikes around 5 and 20 hr in this figure correspond to T-phases from earthquake events. The intense activity between 10 and 15 hr can be associated with the drawworks. RMS level is given in decibels relative to a count.

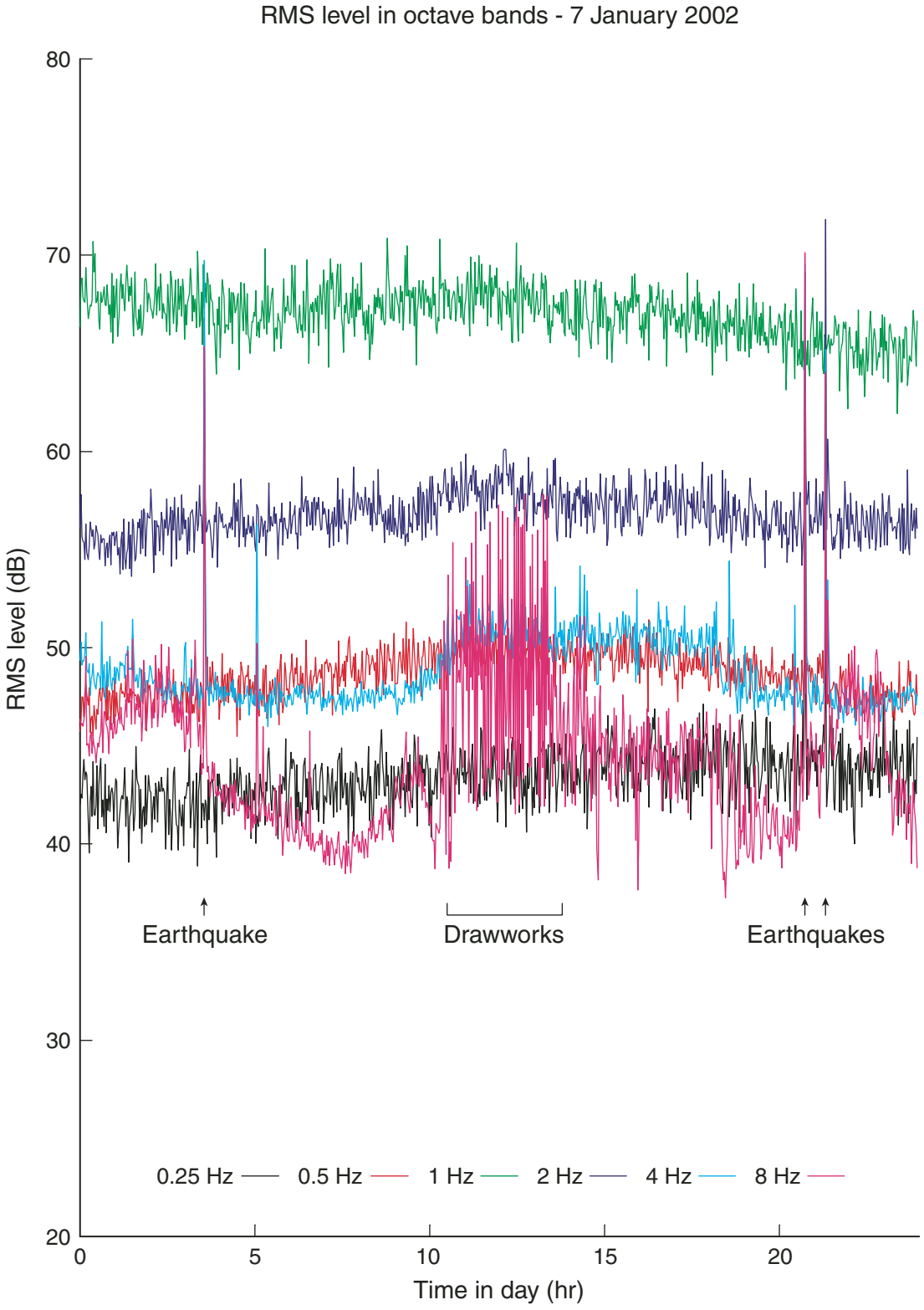

Figure F25. Location of Site 1223 and the Nuuanu Landslides. Line 12 shows the seismic reflection profile collected during the 1988 *Thomas Washington* cruise (Rees et al., 1993). The bathymetry shows that Site 1223 is near a seamount.

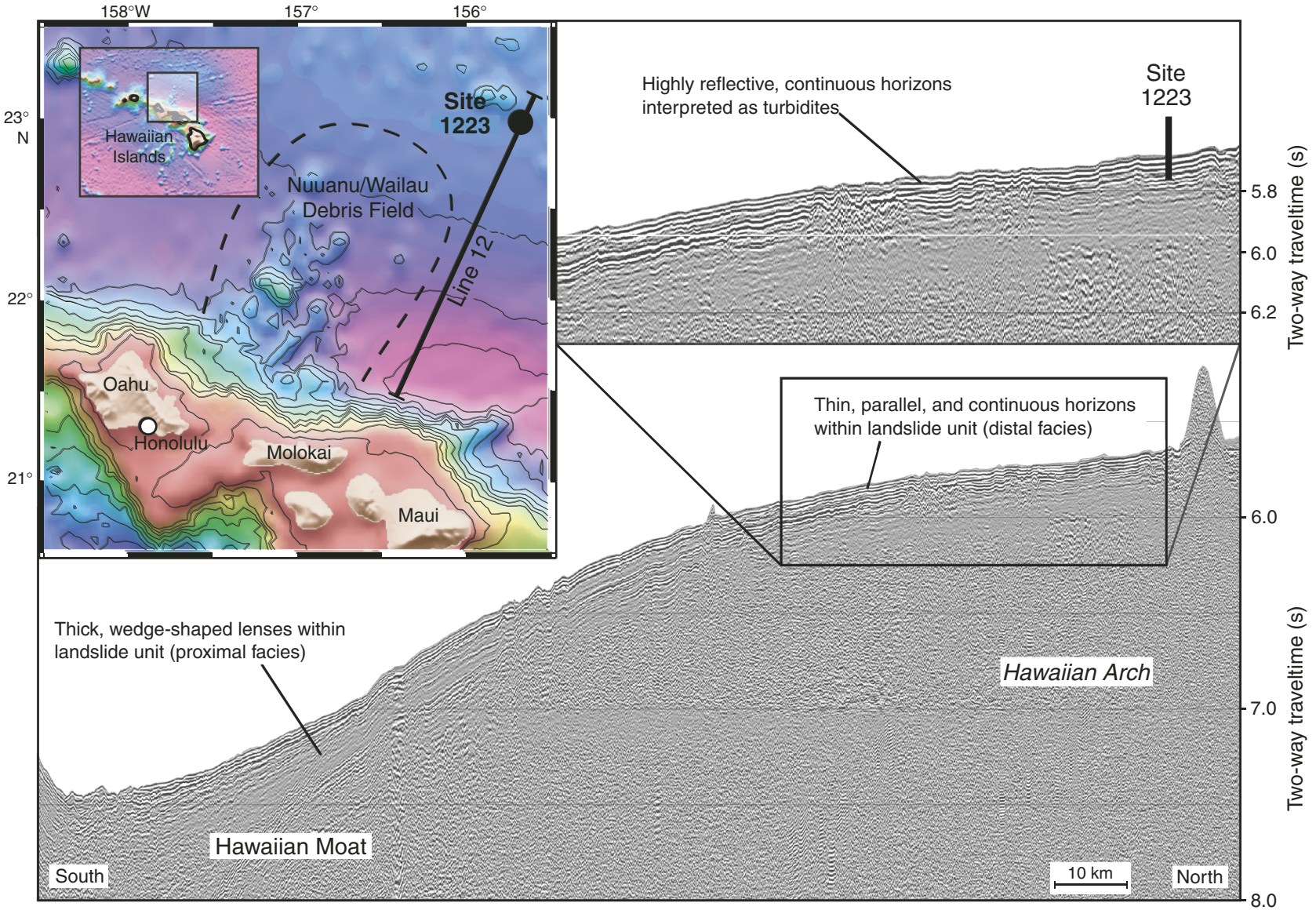

Figure F26. Lithologic units of Site 1223.

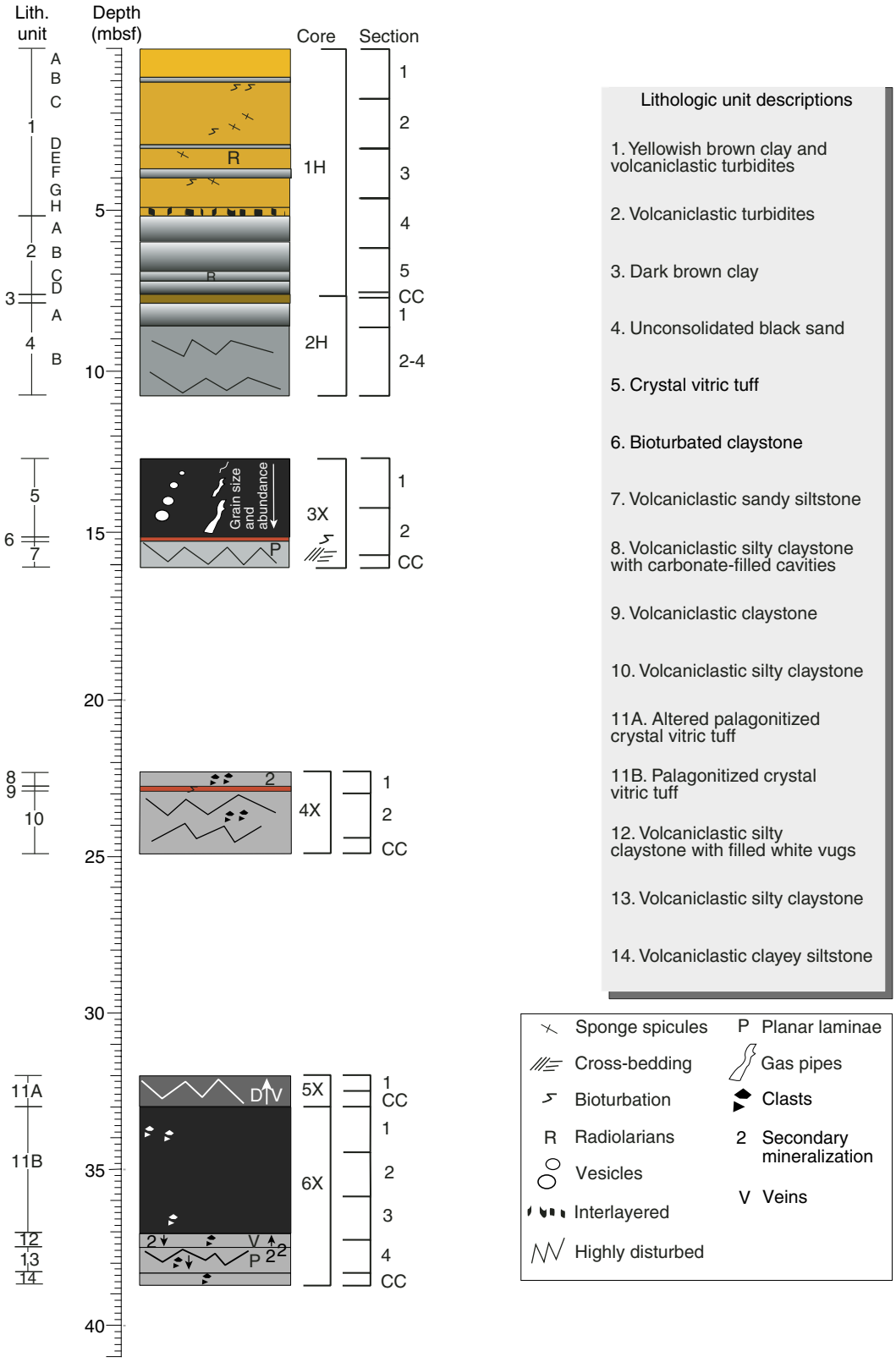

Figure F27. A–D. Schematic drawing of a landslide and the resulting directed blast eruption (from Moore and Albee, 1981).

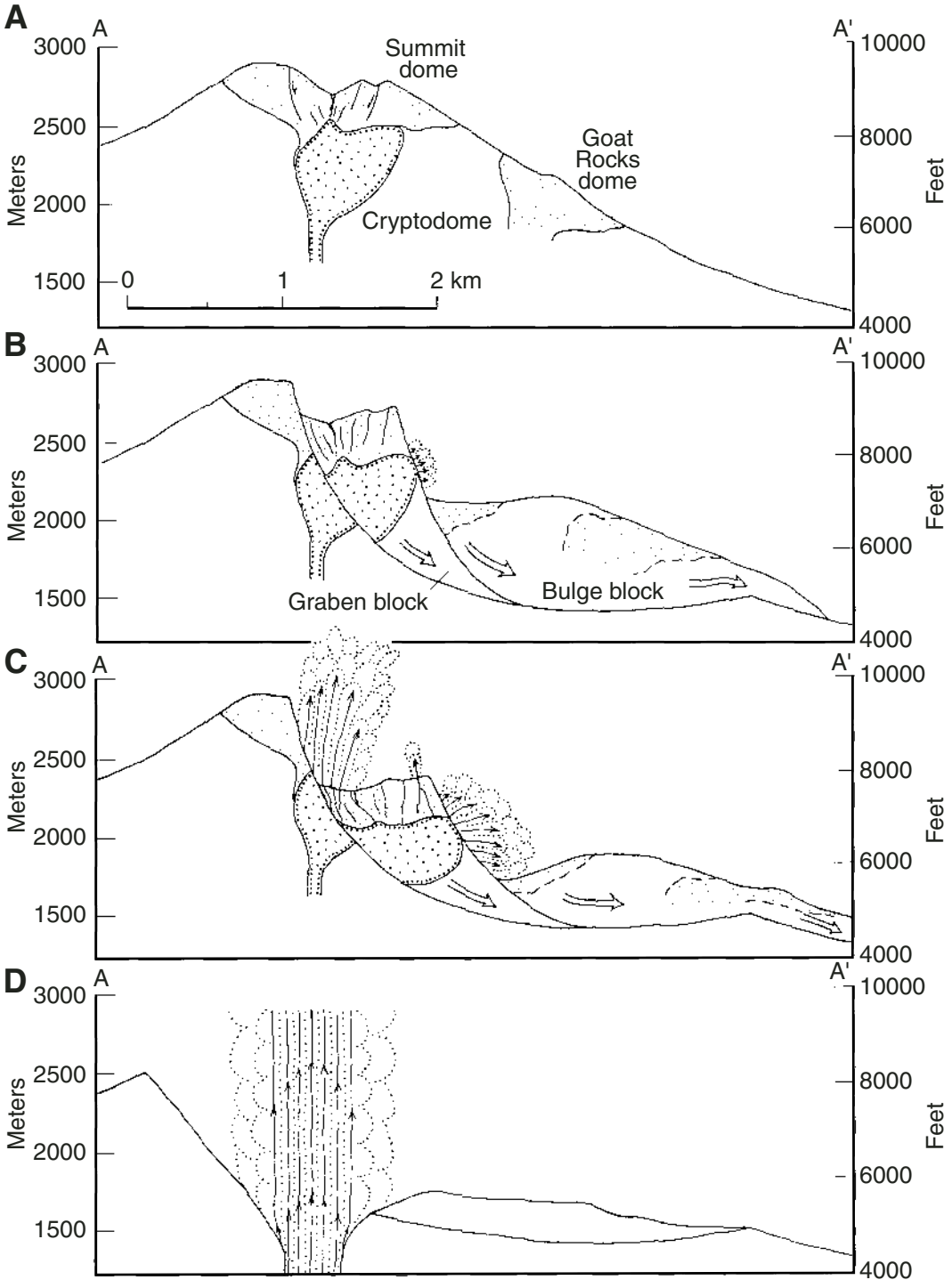

Figure F28. Major oxide discriminant diagrams. **A, C.** Al_2O_3 vs. FeO^T as Fe_2O_3. **B, D.** SiO_2 vs. Al_2O_3. Symbols distinguish vitric tuffs (red left-pointing triangles) and siltstones (gray triangles). Arrows in A and B indicate the effects of subtraction of 13 wt% olivine = Fo_{85} from a representative tuff composition. Additional symbols in A and B are large open triangles = basaltic glasses from Kilauea and Puna Ridge (Clague et al., 1995); half-solid squares = Honolulu Volcanic Series (Jackson and Wright, 1970; Clague and Frey, 1982); downward-pointing triangles = North Arch Volcanic Series (Dixon et al., 1997); blue diamonds = Hana Volcanic Series, Haleakala Volcano, Maui (Chen et al., 1991). Additional symbols in C and D are dark-green squares = high-MgO basalts from Koolau Volcano, Oahu (Frey et al., 1994); light-green right-pointing triangles = enriched mid-ocean-ridge basalt (E-MORB) (data compilation from Lamont-Doherty Earth Observatory Petrologic Database at **www.ldeo.columbia.edu/datarep/index.html** and J. Natland, P. Castillo, and Y.-L. Niu, unpubl. data)

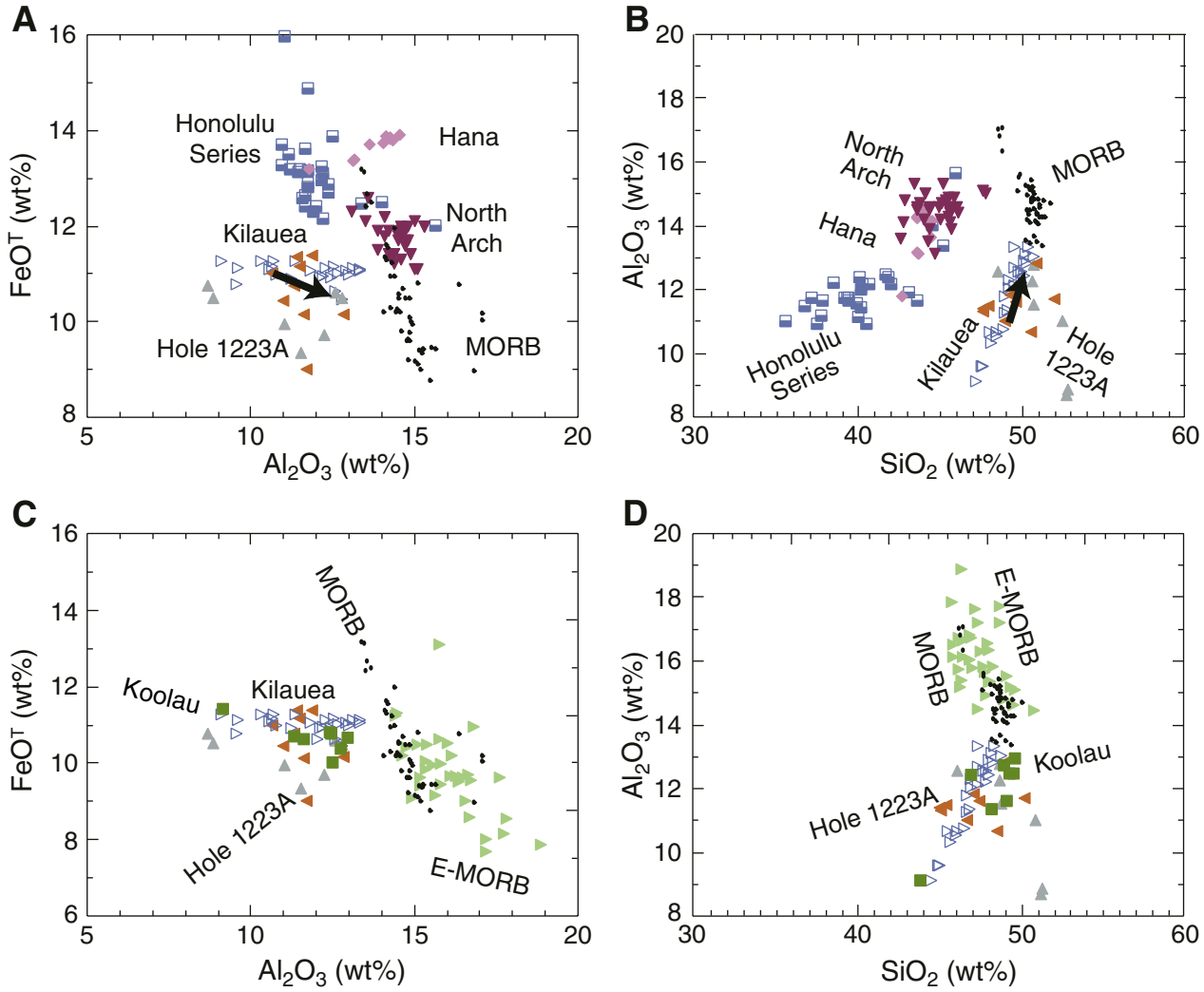

Figure F29. Ternary diagrams showing effects of addition of detrital and authigenic clays to basaltic volcaniclastic material. Inset diagrams show placement of enlarged portions of ternary diagrams on which data are plotted. **A.** CaO-Al_2O_3-K_2O (CAK) diagram. **B.** Total iron as MgO-Al_2O_3-$Fe_2O_3^T$ (MAF) diagram. Symbols distinguish vitric tuffs (red left-pointing triangles) and siltstones (gray triangles). Fields 1 and 2 distinguish vitric tuff samples having, respectively, higher proportions of detrital clay, inferred from their proportionate increase in Al_2O_3 (see the "Site 1223" chapter for discussion). Small triangles = glasses from Kilauea and Puna Ridge (Clague et al., 1995); small dots = normal mid-ocean-ridge basalt (N-MORB) glasses from the Pacific-Antarctic East Pacific Rise; large purple dots = N-MORB glass from DSDP Site 501 and three portions of its palagonitized rim (Noack et al., 1983). Fields for kaolinite (K), illite (I), and continental montmorillonite (M) are from Grim (1964). Average pelagic clay (PC) is from Cronan and Toombs (1969). The saponite nontronite (sap and non) fields (inset diagrams only) are for vein and replacement clays in basalts of DSDP Hole 504B (Honnorez et al., 1983).

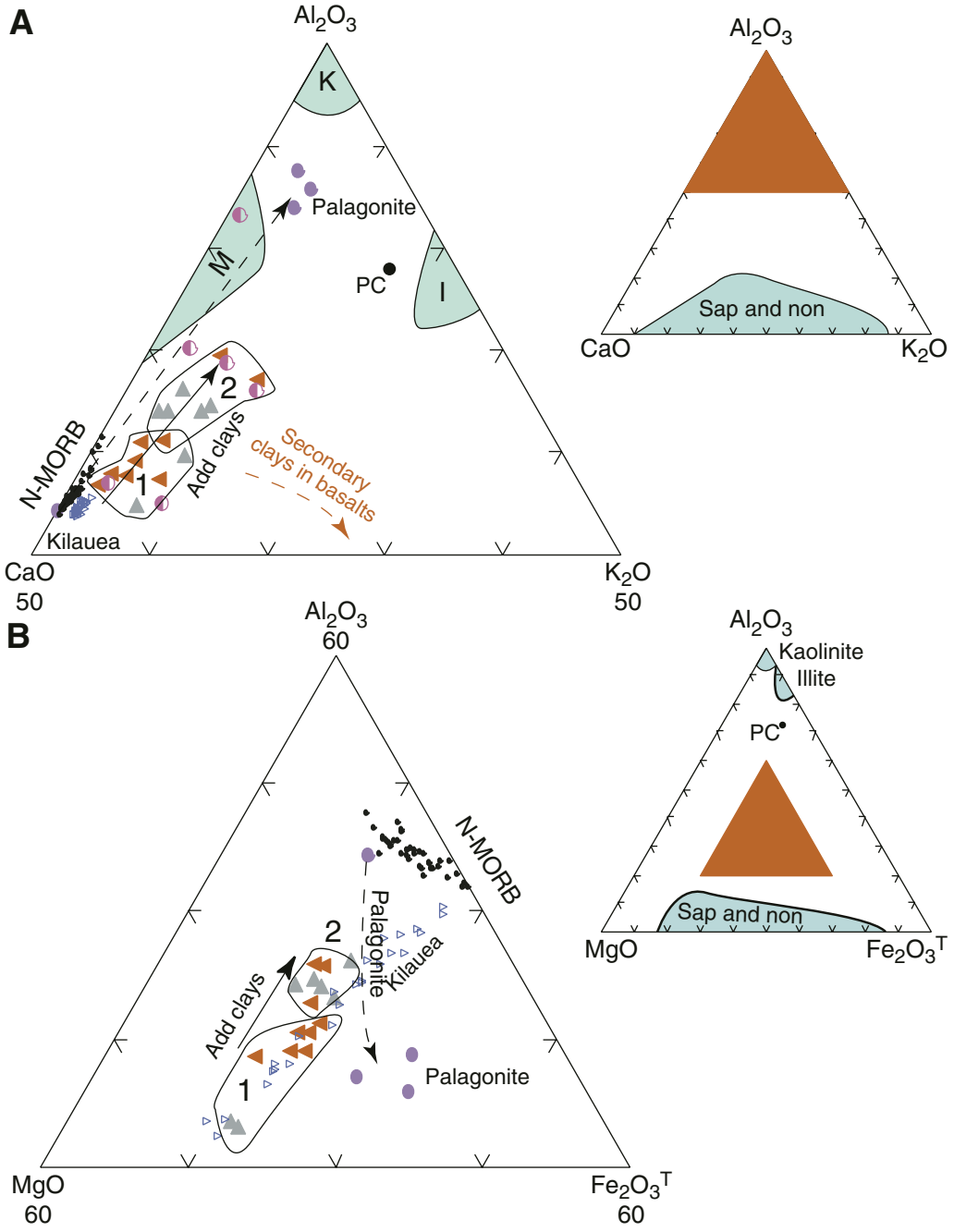

Figure F30. Comparison of analyses of samples from Hole 1223A with Kilauea-Puna Ridge and Koolau tholeiites plus normal and enriched mid-ocean-ridge basalt (MORB and E-MORB, respectively). **A.** MgO vs. SiO_2. **B.** MgO vs. Ba. **C.** MgO vs. Zr. The general effect of subtraction of olivine with 45 wt% MgO is indicated by the arrow. Symbols distinguish vitric tuffs (red left-pointing triangles) and siltstones (gray triangles). Large open triangles = basaltic glasses from Kilauea and Puna Ridge (Clague et al., 1995); dark-green squares = high-MgO basalts from Koolau Volcano, Oahu (Frey et al., 1994); light-green right-pointing triangles = E-MORB (data compilation from Lamont-Doherty Earth Observatory Petrologic Database at www.ldeo.columbia.edu/datarep/index.html and J. Natland, P. Castillo, and Y.-L. Niu, unpubl. data); small dots = normal mid-ocean-ridge basalt (N-MORB) glasses from the Pacific-Antarctic East Pacific Rise.

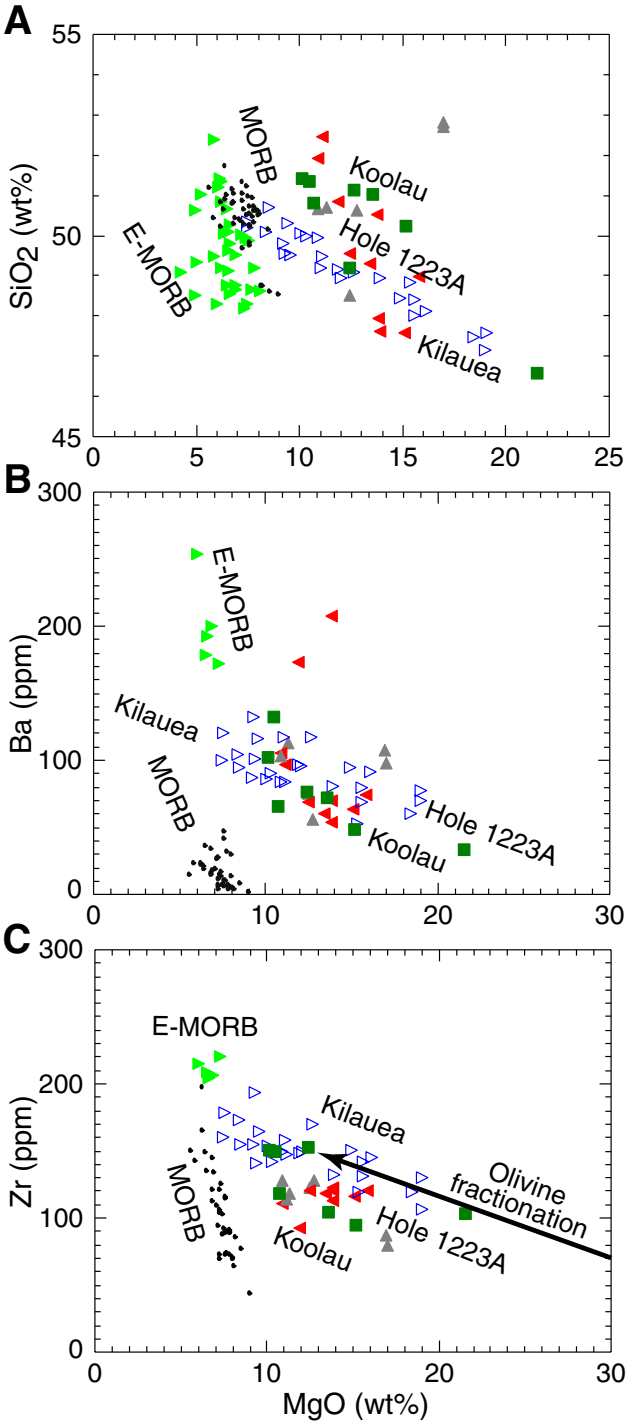

Table T1. Operations summary, Leg 200.[N1]

Hole	Latitude	Longitude	Water depth (mbsl)	Number of cores	Interval cored (m)	Core recovered (m)	Total recovery (%)	Interval drilled (m)	Total penetration (mbsf)	Time on site (hr)	Time on site (days)
1223A	22°58.410′N	155°39.259′W	4235.1	6	41.0	23.5	57.4	0	41.0	29.0	1.21
		Site 1223 totals:		6	41.0	23.5	57.4	0	41.0	42.0	1.75
1224A	27°53.369′N	141°58.754′W	4966.1	6	32.2	1.7	5.2	0	32.2	14.58	0.61
1224B	27°53.370′N	141°58.754′W	4970.4	1	0.2	0.2	100.0	0	0.2	2.25	0.09
1224C	27°53.369′N	141°58.757′W	4967.1	1	6.5	6.5	100.5	0	6.5	30.75	1.28
1224D	27°53.370′N	141°58.752′W	4967.1	5	33.5	15.6	46.7	31.2	64.7	268.90	11.20
1224E	27°53.363′N	141°58.757′W	4967.1	3	28.7	14.9	52.0	8	36.7	20.00	0.83
1224F	27°53.363′N	141°58.757′W	4967.1	17	146.8	37.7	25.7	0	174.5	176.90	7.37
		Site 1224 totals:		33	247.9	76.7	30.9	39.2	314.8	592.17	24.67
		Leg 200 totals:		39	288.9	100.2	34.7	39.2	355.8	634.17	26.42

Table T2. Summary of holes drilled in normal crust on the Pacific plate with an age <100 Ma and penetration into basement >10 m.

Leg	Hole	Age (Ma)	Latitude	Longitude	Basement penetration (m)	Sediment thickness (m)
DSDP:						
16	163	72.0	11°N	150°W	18	176
54	420	3.4	09°N	106°W	29	118
54	421	3.4	09°N	106°W	29	85
54	429	4.6	09°N	107°W	21	31
63	469*	17.0	33°N	121°W	58	391
63	470A	15.0	29°N	118°W	48	167
63	471	12.0	23°N	112°W	82	741
63	472	15.0	23°N	114°W	25	112
65	483B	1.7	23°N	109°W	157	110
92	597B	29.0	19°S	130°W	25	48
92	597C†	29.0	19°S	130°W	91	53
ODP:						
136	843B‡	95.0	19°N	159°W	71	243
200	1224D	46.3	28°N	142°W	36	29
200	1224F	46.3	28°N	142°W	145	29

Notes: * = at the foot of Patton Escarpment. † = a reentry cone was emplaced at this site. ‡ = this is the location of Hole OSN-1.

Table T3. Time distribution, Leg 200.

Activity	Time (days)
In port:	4.26
Underway (includes survey):	9.31
Drilling operations:	
Coring	9.09
Drilling	2.53
Pipe trips	6.88
Logging	1.60
Waiting on weather	6.11
Other	2.19
Total:	28.40
Total (16 Dec 2001 to 27 Jan 2002):	41.97

Table T4. Coring summary, Site 1224. (Continued on next two pages.)

Hole 1224A
Latitude: 27°53.3723′N
Longitude: 141°58.7494′W
Time on site (hr): 592.17 (0845 hr, 28 December 2001–2355 hr, 21 January 2002)
Time on hole (hr): 14.58 (1455 hr, 28 December–0530 hr, 29 December 2001)
Seafloor (drill pipe measurement from rig floor, mbrf): 4977.0
Distance between rig floor and sea level (m): 10.9
Water depth (drill pipe measurement from sea level, m): 4966.1
Total depth (drill pipe measurement from rig floor, mbrf): 5009.2
Total penetration (meters below seafloor, mbsf): 32.2
Total length of cored section (m): 32.2
Total core recovered (m): 1.67
Core recovery (%): 5.19
Total number of cores: 6

Hole 1224B
Latitude: 27°53.3690′N
Longitude: 141°58.7538′W
Time on hole (hr): 2.25 (0530 hr, 29 December–0745 hr, 29 December 2001)
Seafloor (drill pipe measurement from rig floor, mbrf): 4981.3
Distance between rig floor and sea level (m): 10.9
Water depth (drill pipe measurement from sea level, m): 4970.4
Total depth (drill pipe measurement from rig floor, mbrf): 4981.5
Total penetration (meters below seafloor, mbsf): 0.2
Total length of cored section (m): 0.2
Total core recovered (m): 0.20
Core recovery (%): 100.0
Total number of cores: 1

Hole 1224C
Latitude: 27°53.369′N
Longitude: 141°58.7571′W
Time on hole (hr): 30.75 (0745 hr, 29 December–1430 hr, 30 December 2001)
Seafloor (drill pipe measurement from rig floor, mbrf): 4978.0
Distance between rig floor and sea level (m): 10.9
Water depth (drill pipe measurement from sea level, m): 4967.1
Total depth (drill pipe measurement from rig floor, mbrf): 4984.5
Total penetration (meters below seafloor, mbsf): 6.5
Total length of cored section (m): 6.5
Total core recovered (m): 6.53
Core recovery (%): 100.46
Total number of cores: 1

Hole 1224D
Latitude: 27°53.3699′N
Longitude: 141°58.7525′W
Time on hole (hr): 268.9 (1220 hr, 2 January–1815 hr, 13 January 2002)
Seafloor (drill pipe measurement from rig floor, mbrf): 4978.0
Distance between rig floor and sea level (m): 10.9
Water depth (drill pipe measurement from sea level, m): 4967.1
Total depth (drill pipe measurement from rig floor, mbrf): 5042.7
Total penetration (meters below seafloor, mbsf): 64.7
Total length of cored section (m): 33.5
Total length of drilled intervals (m): 31.2
Total core recovered (m): 15.65
Core recovery (%): 46.72
Total number of cores: 5
Total number of drilled intervals: 2

Hole 1224E
Latitude: 27°53.3627′N
Longitude: 141°58.7568′W
Time on hole (hr): 20 (1900 hr, 13 January–1500 hr, 14 January 2002)
Seafloor (drill pipe measurement from rig floor, mbrf): 4978.0
Distance between rig floor and sea level (m): 10.9
Water depth (drill pipe measurement from sea level, m): 4967.1
Total depth (drill pipe measurement from rig floor, mbrf): 5014.7
Total penetration (meters below seafloor, mbsf): 36.7
Total length of cored section (m): 28.7
Total length of drilled intervals (m): 8.0
Total core recovered (m): 14.91
Core recovery (%): 51.95
Total number of cores: 3
Total number of drilled intervals: 1

Table T4 (continued).

Hole 1224F
Latitude: 27°53.3634′N
Longitude: 141°58.7567′W
Time on hole (hr): 176.9 (1500 hr, 14 January–2355 hr, 21 January 2002)
Seafloor (drill pipe measurement from rig floor, mbrf): 4978.0
Distance between rig floor and sea level (m): 10.9
Water depth (drill pipe measurement from sea level, m): 4967.1
Total depth (drill pipe measurement from rig floor, mbrf): 5152.5
Total penetration (meters below seafloor, mbsf): 174.5
Total length of cored section (m): 146.8
Total core recovered (m): 37.7
Core recovery (%): 25.68
Total number of cores: 17

Core	Date	Local time (hr)	Depth (mbsf) Top	Depth (mbsf) Bottom	Length (m) Cored	Length (m) Recovered	Recovered (%)
200-1224A-							
1X	28 Dec 2001	1610	0.0	6.0	6.0	0.00	0.00
2X	28 Dec 2001	1720	6.0	15.6	9.6	0.02	0.21
3X	28 Dec 2001	1835	15.6	25.2	9.6	0.01	0.10
4X	28 Dec 2001	2210	25.2	30.7	5.5	1.24	22.55
5X	29 Dec 2001	0105	30.7	32.0	1.3	0.18	13.85
6N	29 Dec 2001	0430	32.0	32.2	0.2	0.22	110.00
			Cored totals:		32.2	1.67	5.19
200-1224B-							
1H	29 Dec 2001	0725	0.0	0.2	0.2	0.20	100.00
			Cored total:		0.2	0.20	100.00
200-1224C-							
1H	29 Dec 2001	0850	0.0	6.5	6.5	6.53	100.46
			Cored total:		6.5	6.53	100.46
200-1224D-							
			*****Drilled from 0.0 to 25.5 mbsf*****				
1R	4 Jan 2002	0530	25.5	35.1	9.6	4.15	43.23
2R	4 Jan 2002	1710	35.1	44.7	9.6	4.81	50.10
3R	5 Jan 2002	0025	44.7	49.3	4.6	3.30	71.74
4R	5 Jan 2002	0555	49.3	51.3	2.0	1.99	99.50
5R	6 Jan 2002	0100	51.3	59.0	7.7	1.40	18.18
			*****Drilled from 59.0 to 64.7 mbsf*****				
			Cored totals:		33.5	15.65	46.72
			Drilled totals:		31.2		
			Total:		64.7		
200-1224E-							
			*****Drilled from 0.0 to 8.0 mbsf*****				
1R	13 Jan 2002	2005	8.0	17.5	9.5	1.03	10.84
2R	13 Jan 2002	2110	17.5	27.1	9.6	9.49	98.85
3R	14 Jan 2002	1505	27.1	36.7	9.6	4.39	45.73
			Cored totals:		28.7	14.91	51.95
			Drilled total:		8.0		
			Total:		36.7		
200-1224F-							
1R	15 Jan 2002	0455	27.7	39.7	12.0	6.13	51.08
2R	15 Jan 2002	0930	39.7	47.3	7.6	5.32	70.00
3R	15 Jan 2002	2125	47.3	56.4	9.1	4.13	45.38
4R	16 Jan 2002	0650	56.4	65.9	9.5	6.20	65.26
5R	16 Jan 2002	1225	65.9	75.0	9.1	0.95	10.44
6R	16 Jan 2002	2035	75.0	84.5	9.5	1.50	15.79
7R	17 Jan 2002	0240	84.5	93.5	9.0	1.20	13.33
8R	17 Jan 2002	0750	93.5	102.7	9.2	1.31	14.24
9R	17 Jan 2002	1225	102.7	111.8	9.1	0.60	6.59
10R	17 Jan 2002	1645	111.8	121.1	9.3	1.40	15.05
11R	17 Jan 2002	2315	121.1	128.5	7.4	1.71	23.11
12R	18 Jan 2002	1130	128.5	133.5	5.0	1.20	24.00
13R	18 Jan 2002	1505	133.5	143.2	9.7	2.73	28.14

Table T4 (continued).

Core	Date	Local time (hr)	Depth (mbsf)		Length (m)		Recovered (%)
			Top	Bottom	Cored	Recovered	
14R	19 Jan 2002	0300	143.2	152.4	9.2	2.02	21.96
15R	19 Jan 2002	1045	152.4	161.8	9.4	1.30	13.83
16R	19 Jan 2002	1700	161.8	171.0	9.2	0.00	0.00
17R	19 Jan 2002	2250	171.0	174.5	3.5	0.00	0.00
			Cored totals:		146.8	37.70	25.68

Table T5. Coring summary, Site 1223.

Hole 1223A
Latitude: 22°58.4095′N
Longitude: 155°39.2590′W
Time on site (hr): 42 (0730 hr, 21 December–0130 hr, 23 December 2001)
Time on hole (hr): 29 (2030 hr, 21 December–0130 hr, 23 December, 2001)
Seafloor (drill pipe measurement from rig floor, mbrf): 4245.8
Distance between rig floor and sea level (m): 10.7
Water depth (drill pipe measurement from sea level, m): 4235.1
Total depth (drill pipe measurement from rig floor, mbrf): 4286.8
Total penetration (meters below seafloor, mbsf): 41
Total length of cored section (m): 41.0
Total core recovered (m): 23.54
Core recovery (%): 57.4
Total number of cores: 6

Core	Date (Dec 2001)	Local time (hr)	Depth (mbsf) Top	Depth (mbsf) Bottom	Length (m) Cored	Length (m) Recovered	Recovered (%)
200-1223A-							
1H	21	2055	0.0	7.7	7.7	7.79	101.2
2H	21	2225	7.7	12.7	5.0	3.08	61.6
3X	22	0515	12.7	22.3	9.6	3.34	34.8
4X	22	0915	22.3	32.0	9.7	2.62	27.0
5X	22	1115	32.0	33.0	1.0	1.01	101.0
6X	22	1700	33.0	41.0	8.0	5.70	71.2
				Cored totals:	41.0	23.54	57.4

CHAPTER NOTE*

N1. 27 October 2004—After this chapter was published, an error was found in Table T1. The hole location longitudes were erroneously listed as east rather than west.

*Dates reflect file corrections or revisions.